NTNU – Trondheim
Norwegian University of
Science and Technology

Adiabatic compressed air energy storage

Eirik Mørkved Helsingen

Master of Energy and Environmental Engineering
Submission date: June 2015
Supervisor: Lars Olof Nord, EPT

Norwegian University of Science and Technology
Department of Energy and Process Engineering

NTNU
Norwegian University
of Science and Technology

Department of Energy
and Process Engineering

EPT-M-2015-32

MASTER THESIS

for

student Eirik Mørkved Helsingen

Spring 2015

Adiabatic compressed air energy storage

Background and objective

With growing renewable energy electrical power generation on the European electrical grid, the flexibility of the grid is of importance to handle changes in wind or solar power. One solution to this is to store energy during times of low electricity demand and high renewable energy availability for use in periods of high demand on the grid. Of the many energy storage options, compressed air energy storage (CAES) stands out as one of the more interesting. The technology becomes more attractive if, in addition to storing pressure, the heat from the compression can be stored. This could eliminate the need for supplying a fuel during the expansion phase. This is called adiabatic compressed air energy storage (ACAES) since no external heat would be added to the cycle. Another option could be to store the heat from compression *and* add heat by combustion.

The overall objective of the Master's thesis is to make a detailed process model of an ACAES plant and subsequently simulate the process and generate results such as round-trip efficiency.

The following tasks are to be considered:

1. Literature study on adiabatic compressed air energy storage
2. Evaluation and decision of ACAES cycle configuration(s) to be studied.
3. Build-up of process model of the selected cycle(s) and simulation of the process.
4. Comparison of the ACAES cycle to a reference CAES cycle.
5. Sensitivity analysis.

Within 14 days of receiving the written text on the master thesis, the candidate shall submit a research plan for his project to the department.

When the thesis is evaluated, emphasis is put on processing of the results, and that they are presented in tabular and/or graphic form in a clear manner, and that they are analyzed carefully.

The thesis should be formulated as a research report in English with summary, conclusion, literature references, table of contents etc. During the preparation of the text, the candidate should make an effort to produce a well-structured and easily readable report. In order to ease the evaluation of the thesis, it is important that the cross-references are correct. In the making of the report, strong emphasis should be placed on both a thorough discussion of the results and an orderly presentation.

The candidate is requested to initiate and keep close contact with his/her academic supervisor(s) throughout the working period. The candidate must follow the rules and regulations of NTNU as well as passive directions given by the Department of Energy and Process Engineering.

Risk assessment of the candidate's work shall be carried out according to the department's procedures. The risk assessment must be documented and included as part of the final report. Events related to the candidate's work adversely affecting the health, safety or security, must be documented and included as part of the final report. If the documentation on risk assessment represents a large number of pages, the full version is to be submitted electronically to the supervisor and an excerpt is included in the report.

Pursuant to "Regulations concerning the supplementary provisions to the technology study program/Master of Science" at NTNU §20, the Department reserves the permission to utilize all the results and data for teaching and research purposes as well as in future publications.

The final report is to be submitted digitally in DAIM. Based on an agreement with the supervisor, the final report and other material and documents may be given to the supervisor in digital format.

☐ Work to be done in lab (Water power lab, Fluids engineering lab, Thermal engineering lab)
☐ Field work

Department of Energy and Process Engineering, 14. January 2015

Olav Bolland
Department Head

Lars Nord
Academic Supervisor

Preface

I would like to thank my supervisor, Lars Olof Nord, for always being available, helpful and interested when I came knocking on his door for advice.

Trondheim, June 2015

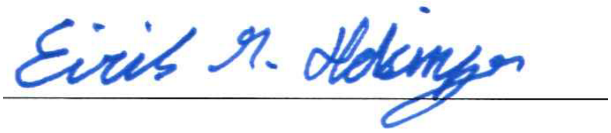

Eirik Mørkved Helsingen

Adiabatic compressed air energy storage

Eirik Mørkved Helsingen

Abstract

An increasing amount of intermittent renewable energy sources are being introduced to the European electrical grid. This results in difficulties to maintain and ensure a reliable and steady electricity supply. Energy storage can be used to balance the fluctuations caused by the renewable electricity sources, and thus allow the electricity generation to follow demand. As of today there are two facilities for compressed air energy storage (CAES) in the world, one in Huntorf (Germany) and one in McIntosh (USA). These power plants are diabatic and require supply of fuel. An alternative to diabatic CAES can be adiabatic storage where the need of fuel falls away.

The main objective of this thesis is to model and simulate an adiabatic CAES cycle in order to calculate and analyse the round-trip efficiency. The purpose is to assess whether an adiabatic configuration can be a good option for energy storage.

The adiabatic model was built and simulated using the process-modelling program EBSILON®Professional. It was simulated over a full cycle consisting of; 7.8 hours charging period with constant power, 12 hours storage and 2.3 hours with constant power generation. The model was simulated using both real and ideal component values. Effects of changing compressor and gas efficiencies were investigated, and a sensitivity analysis was performed. The adiabatic model was also compared with two reference models, based on the existing diabatic power plants.

The calculated round-trip efficiency for the real configuration was 55.4 %. Using the ideal configuration the efficiency reached as high as 71.2 %, which corresponds well with the values known from the literature. For the real configuration caused a 3 % change in compressor and gas turbine efficiency a 5 % change in round-trip efficiency. The sensitivity analysis showed that gas turbine and compressor operation at powers different than design had strong impact on the round-trip efficiency. Ambient air temperature, thermal storage tank temperature and intercooler outlet temperatures also made considerable changes to the round-trip efficiency. The efficiencies calculated for the diabatic CAES reference models were 44 % for the Huntorf model and 51.3 % for the McIntosh model. These values are close to the real power plant efficiencies of 42 % and 54 % respectfully.

The most important result from this work is the adiabatic CAES model round-trip efficiency of 55.4 %. This is of the same magnitude as the real McIntosh power plant efficiency. For an adiabatic CAES power plant is there however no fuel consumption and accordingly no cost of fuel or greenhouse gas emissions. It is therefore believed that the simulated adiabatic CAES model could be a viable option for energy storage in a future intermittent electrical system.

Adiabatisk komprimering av luft for energilagring

Eirik Mørkved Helsingen

Sammendrag

Utfordringen med å opprettholde en pålitelig og stabil kraftforsyning i Europa øker i takt med den voksende mengden fluktuerende fornybare energikilder introdusert til strømnettet. Energilagring kan brukes til å balansere svingningene forårsaket av de fornybare kildene, og dermed kan strømproduksjonen i større grad følge etterspørselen. Per i dag finnes det to anlegg for komprimering av luft for energilagring, et i Huntorf (Tyskland) og et i McIntosh (USA). Disse er begge diabatiske og trenger tilførsel av brensel. Et alternativ til diabatisk lagring kan være adiabatisk lagring der behovet for brensel faller bort.

Hensikten med denne oppgaven er å modellere og simulere en syklus for adiabatisk komprimering av luft for energilagring for å kunne beregne og analysere den totale virkningsgraden. Målet er å vurdere om en adiabatisk konfigurasjon kan være et godt alternativ for energilagring.

Modellen ble bygget og simulert ved hjelp av prosess-simuleringsverktøyet EBSILON®Professional. Den adiabatiske modellen ble simulert over en full syklus bestående av 7.8 timer kompresjon ved konstant kraftforbruk, 12 timer lagring og 2.3 timer ekspansjon ved konstant kraftgenerering. Modellen ble simulert med både reelle og ideelle komponentverdier. Virkningen av å endre kompressorenes og gassturbinenes virkningsgrader ble undersøkt, og en sensitivitetsanalyse ble gjennomført. Den adiabatiske modellen ble også sammenliknet med to referansemodeller, basert på de to diabatiske kraftverkene.

Med reelle komponentverdier ble den totale virkningsgraden av den adiabatiske modellen beregnet til 55.4 %. Ved bruk av ideelle verdier steg den totale virkningsgraden til 71.2 %, som samsvarer godt med den verdien som brukes i litteraturen. For den reelle modellen førte en endring i kompressor- og turbinvirkningsgrad på 3 % til en endring på 5 % i den totale virkningsgraden. Sensitivitetsanalysen viste at drift av kompressorer og gassturbin med kraftnivåer utenfor designområdet, hadde en stor innflytelse på den totale virkningsgraden. Omgivelsestemperaturen, den termiske lagringstemperaturen og mellomkjølernes utløpstemperatur hadde også en betydelig innvirkning på den totale virkningsgraden. Virkningsgraden beregnet for referansemodellene var 44 % for Huntorf og 51.3 % for McIntosh. Dette er nære de virkelige virkningsgradene til disse kraftverkene på henholdsvis 42 % og 54 %.

Det viktigste resultatet fra denne oppgaven er den totale virkningsgraden på 55.4 % oppnådd for den adiabatiske modellen. Dette er av samme størrelsesorden som for McIntosh-modellen, men i motsetning til den diabatiske modellen trenger ikke den adiabatiske modellen brensel for å produsere kraft, følgelig har den heller ingen kostnader for brensel eller klimagassutslipp. Adiabatisk komprimering av luft kan således være et konkurransedyktig og bra alternativ for energilagring i et fremtidig intermitterende elektrisk system.

Contents

Abstract ii
Sammendrag iii
Nomenclature viii
Acronyms xi

List of Figures **xiii**

List of Tables **xv**

1 Introduction **1**
1.1 Background 1
1.2 Objective 2
1.3 Outline 2
1.4 Risk assessment 2
1.5 Contribution 2
1.6 Limitation of work 3

2 The future of the European electrical grid **4**
2.1 Carbon dioxide allowances 5
2.2 The European electrical grid - today 5
2.3 The European electrical grid - tomorrow 7
2.4 Market 9

3 Compressed air energy storage - CAES **11**
3.1 Diabatic compressed air energy storage 11
3.2 Compressed air storage 13
3.2.1 Salt cavern 13
3.2.2 Hard rock cavern 13
3.2.3 Porous rock cavern 14
3.3 Adiabatic compressed air energy storage 14
3.3.1 The ADELE project 15
3.3.2 The ALACAES project 15
3.4 Isothermal compressed air energy storage 16
3.4.1 SutstainX 16
3.4.2 LightSale 17

3.5 Thermal energy storage - TES . . . 17
3.5.1 Sensible heat storage . . . 18
3.5.2 Latent heat storage . . . 19
3.5.3 Active and passive thermal storage . . . 20

4 Other energy storage technologies 21
4.1 Mechanical energy storage . . . 23
4.1.1 Pumped hydro storage - PHS . . . 23
4.1.2 Flywheel . . . 24
4.2 Chemical energy storage . . . 25
4.2.1 Hydrogen . . . 25
4.2.2 Methane . . . 26
4.3 Electro-chemical energy storage (batteries) . . . 27
4.3.1 Lithium-ion battery . . . 27
4.3.2 Sodium-sulfur battery . . . 27
4.3.3 Flow battery . . . 27
4.4 Electrical energy storage . . . 28
4.4.1 Superconducting magnetic energy storage – SMES . . . 28
4.4.2 Supercapacitor . . . 29
4.5 Summary of different storage technologies . . . 30

5 Thermodynamics 33
5.1 The first law of thermodynamics . . . 33
5.2 The second law of thermodynamics . . . 34
5.2.1 Irreversible and reversible processes . . . 35
5.2.2 Entropy and the entropy rate balance . . . 35
5.2.3 Isentropic efficiencies . . . 36
5.3 Ideal gas and polytropic process . . . 37
5.3.1 The ideal gas model . . . 37
5.3.2 Polytropic process . . . 37
5.3.3 Polytropic efficiency . . . 39
5.3.4 Real gas behavior . . . 39
5.4 Ideal gas turbine cycle . . . 40
5.5 CAES Evaluation Criteria . . . 42

6 Components 44
6.1 Compressor . . . 44
6.1.1 Radial versus axial . . . 44
6.1.2 Compressor characteristics . . . 44
6.2 Gas turbine . . . 46
6.2.1 Radial versus axial . . . 46
6.2.2 Turbine characteristics . . . 46
6.3 Thermal storage tank . . . 47

6.3.1 Heat transfer mechanisms . . . 47
6.3.2 Thermal losses . . . 47
6.4 Heat exchanger . . . 49
6.5 Combustion chamber . . . 49
6.5.1 Stability limits . . . 49
6.5.2 Emissions . . . 50
6.5.3 Heating values . . . 51
6.6 Pumps . . . 52
6.6.1 Pump characteristics . . . 52

7 EBSILON®Professional and model setup 54
7.1 Introduction to EBSILON®Professional . . . 54
7.2 Design and off-design . . . 55
7.3 Possibilities and limitations in EBSILON®Professional . . . 55
7.4 General assumptions . . . 56
7.5 Huntorf reference model . . . 58
7.6 McIntosh reference model . . . 62
7.7 ACAES model . . . 65
7.8 Code . . . 70

8 Results 72
8.1 Results - Huntorf reference model . . . 72
8.1.1 Transient operation of the Huntorf model . . . 73
8.2 Results - McIntosh reference model . . . 75
8.2.1 Transient operation of the McIntosh model . . . 75
8.3 Results - the ACAES model . . . 78
8.3.1 Transient operation of the ACAES model . . . 79
8.4 Sensitivity analysis . . . 85
8.4.1 Ambient conditions . . . 85
8.4.2 Thermal storages . . . 86
8.4.3 Power consumption and generation . . . 87
8.4.4 Intercoolers outlet temperature . . . 88
8.4.5 Summary of sensitivity analysis . . . 89

9 Discussion 91
9.1 Discussion of the reference models . . . 91
9.1.1 Round-trip efficiency and other key parameters . . . 91
9.1.2 Carbon emissions . . . 92
9.1.3 Waste heat . . . 93
9.1.4 The effect of local off-design . . . 93
9.2 Discussion of the ACAES model . . . 94
9.2.1 Round-trip efficiency . . . 94
9.2.2 Power consumption and generation . . . 94

9.2.3 Thermal efficiency 95
9.2.4 Storage tanks assumptions 96
9.2.5 Other key values 97
9.3 Summary of discussions 98

10 Conclusions & further work **99**

Bibliography **101**

Appendix A ACAES model ebsScript code **108**

Nomenclature

Symbols

Symbol	*Unit*	*Description*
A	$[m^2]$	area
C	[m/s]	velocity
C_xH_y	[-]	hydrocarbon
c_p	[J/kg K]	specific heat at constant pressure
c_V	[J/kg K]	specific heat at constant volume
H	[J/kg]	polytropic head
h	$[W/m^2K]$	convection heat transfer coefficient
h	[J/kg]	enthalpy per unit of mass
$\bar{h}_{RP}$	[J/mol fuel]	enthalpy of combustion per mole
k	$[W/m^2]$	thermal conductivity
k	[-]	ratio of specific heats, c_p/c_V
KE	[J]	kinetic energy
m	[kg]	mass
$\dot{m}$	[kg/s]	mass flow rate
n	[-]	polytropic constant
PE	[J]	potental energy
p	[bar]	pressure
Q	[J]	heat transfer
$\dot{Q}$	[W]	heat transfer rate
R	[m/W]	thermal resistance
S	[J/k]	entropy
s	[J/kg K]	entropy per unit of mass
T	[K]	temperature
t	[s]	time
U	$[W/m^2K]$	overall heat transfer coefficient
U	[J]	internal energy, or
u	[J/kg]	internal energy per unit of mass
V	$[m^3]$	volume
v	$[m^3/kg]$	specific volume
W	[J]	work
$\dot{W}$	[W]	rate of work, or power
z	[m]	elevation

Greek Letters

Symbol	*Description*
Δ	change
ϵ	emissivity
η	efficiency
Π	Allowance price

Subscripts

Symbol	*Description*
C	cold
c	compressor
$cond$	conduction
$conv$	convection
cv	control volume
el	electric
f	fuel
$\frac{int}{rev}$	internal reversible
gen	generator
H	hot
i	inlet, or mixture component
is	isentropic
j	number of components present in mixture
kin	kinetic
lm	log mean
max	maximum
$mech$	mechanical
o	outlet
P	products
p	polytropic
pot	potential
R	reactants
rad	radiation
sys	system
T	temperature
t	turbine
tot	total
v	specific volume
w	wall
$1,2,3$	different states of a system, different location

Constants

Symbol	*Description*	*Value*
g	gravitational acceleration	9.82 [m/s^2]
σ	Stephan-Boltzmann constant	$5.67 \cdot 10^{-8}$ $[W/m^2K^4]$
$\Re$	universal gas constant	8.314 [J/mol K]

Acronyms

AC Alternating Current

ACEAS Adiabatic Compressed Air Energy Storage

BBC Brown Boveri & Cie

CAES Compressed Air Energy Storage

CES Chemical Energy Storage

DC Direct Current

DCAES Diabatic Compressed Air Energy Storage

EEX European Energy Exchange

ER Energy Rate

EU European Union

EU ETS European Union Emission Trading System

GHG Greenhouse Gas

HP High Pressure

HR Heat Rate

ICAES Isothermal Compressed Air Energy Storage

LP Low Pressure

n.a not available, or not applicable

OP operational

PCM Phase Changing Material

PHS Pumped Hydro Storage

REFPROF Reference Fluid Thermodynamic and Transport Properties

R&D Research and Development

rpm Revolutions per minute

SMES Superconducting Magnetic Energy Storage

TES Thermal Energy Storage

UHC Unburned Hydrocarbon

VID Verein Deutscher Ingenieure

VPP Virtual Power Plant

List of Figures

2.1 Renewable energy share in gross final energy consumption, EU-28 from 2004-2030 . . . 4
2.2 Transportation of electricity . . . 6
2.3 Price and volume of electricity generated 31/3-2014 in Germany . . . 6
2.4 Net electricity generation in Europe 1980-2011 . . . 7
2.5 Percentage of the net electricity generation in Europe 2011 . . . 8
2.6 The grid of the future . . . 8

3.1 CAES power plant . . . 12
3.2 Salt deposits in Europe . . . 14
3.3 Sketch of an ACAES power plant . . . 15
3.4 LightSale Energy ICAES consept . . . 16
3.5 Principle of TES operation . . . 17

4.1 Energy storage technology maturity . . . 21
4.2 Global installed grid-connected electricity storage capacity . . . 22
4.3 Pumped hydro storage . . . 23
4.4 Sectional view of flywheel . . . 24
4.5 Electrolysis - Hydrogen from water . . . 26
4.6 Schematic of a flow battery . . . 28
4.7 Schematic of a superconducting magnetic energy storage system . . . 29
4.8 Schematic of a supercapacitor . . . 30
4.9 Sketch of generation time and power output . . . 32

5.1 P-v diagram of a polytropic process . . . 38
5.2 Joule-Brayton cycle . . . 41

6.1 Axial compressor characteristics . . . 45
6.2 Gas turbine characteristics . . . 46
6.3 Thermal storage tank heat transfer mechanisms . . . 48
6.4 Combustion stability limits . . . 50
6.5 Pollution from combustion . . . 51
6.6 Centrifugal pump performance curve . . . 53

7.1 Huntorf model . . . 61

7.2 McIntosh model 64
7.3 ACAES model 69
7.4 Flowchart of ebsScript code 71

8.1 Results from Huntorf CAES power plant model 74
8.2 Results from McIntosh CAES power plant model 77
8.4 Change in air storage mass and pressure over operation 80
8.5 Changes of thermal storage mass and temperatures during operation 81
8.6 Changes of hot thermal storage mass and temperatures during operation . . . 82
8.7 Outlet temperatures of air preheater and gas turbine 82
8.8 Plots of energy transfers 84
8.9 Change of ambient air temperature 85
8.10 Change of initial temperatures in hot and cold thermal storage 86
8.11 Change of specific heat loss coefficient of cold and hot tank 87
8.12 Change of compression and expansion power consumption/generation 88
8.13 Change in intercooler air outlet temperature 88
8.14 Percentage change of all analyzed parameters 90

List of Tables

3.1 Solid sensible heat storage mediums 18
3.2 Liquid sensible heat storage mediums 19
3.3 Commercial PCM materials 20

4.1 Usage of energy storage technologies in the electrical grid 22
4.2 Summarization of different storage technologies 30

7.1 General assumptions 57
7.2 Assumptions, Huntorf CAES power plant model 58
7.3 Known data, Huntorf CAES power plant 59
7.4 Assumptions, McIntosh CAES power plant model 62
7.5 Known data, McIntosh CAES power plant 63
7.6 Heat transfer fluids available in EBSILON®Professional[i] 65
7.7 Assumptions, ACAES power plant model 67

8.1 Results, Huntorf model 72
8.2 Results, McIntosh model 75
8.3 Results, ACAES model 78
8.4 Different compressor and turbine efficiencies 79

Chapter 1

Introduction

1.1 Background

Today, fossil fuels account for more than 80% of the global energy consumption [1]. And with the increasing population and demand of higher quality of life the power consumption rises. The preferred energy carrier in everyday life is electricity, due to its versatility and simplicity. In many ways is it the corner stone of our modern society. However, the known fossil fuel reserves used to generate electricity are becoming more and more scarce, and it is estimated that the proven reserves of coal will last around 100 years[2] and the conventional oil around 45 years [3].

The large amount of electricity generated from fossil fuels, also poses a threat to the environment, as an increased level of CO_2 and other pollutants can make greenhouse effect stronger, and result in a global warming effect. The International Energy Agency (IEA) stated in World energy outlook 2012 [4] that no more than a third of the proven fossil fuel reserves can be consumed in order for the world to stay below the 2°C goal. In the United Nations (UN) report on climate change stated the Intergovernmental Panel on Climate Change working group 1: *"Continued emissions of greenhouse gases will cause further warming and changes in all components of the climate system. Limiting climate change will require substantial and sustained reductions of greenhouse gas emissions."* [2].

It is rather evident that the worlds reserves of fossil fuel will not last for ever and independent of the 2°C goal a transition towards other energy sources are needed. The other and "new" energy source, the renewable energy, is the answer. However, renewable energy power production have a tendency to fluctuate, being dependant on the availability of the resources utilized, i.e. wind, solar, tide, wave. This implies difficulties for a society used to a continuous and reliable source of power. One of the key factors for integrating renewable energy sources into today's power market is energy storage.

There are several types of storage technologies, all with different functions and usability. One of the most promising large scale energy storage technologies are compressed air energy storage (CAES). There are three main concepts of CAES power plants, diabatic, adiabatic and isothermal CAES. Diabatic CAES is the oldest technology and today there are currently two DCAES power plants in operation. The DCAES power plants need external heat during

the expansion phase. This heat is added from combusting a fuel. The topic of this thesis is adiabatic compressed air energy storage (ACAES). It is called adiabatic CAES as it stores the compression heat for reuse during the expansion phase, thus eliminating the need of external heat. As of today is there no ACAES power plant in operation, but two power plants are however under planning.

1.2 Objective

The purpose of this work is to build and simulate a detailed process model of an ACAES design and calculate its round-trip efficiency. The model will be compared with two reference models, which are based upon known designs of the two existing DCAES power plants. The main objective is to find out if ACAES can be a good alternative for energy storage.

1.3 Outline

The report is divided into 10 chapters. Chapter 2 gives an introduction to the European electrical grid, how it might change in the future and how energy is traded. Chapter 3 gives an introduction to adiabatic and other compressed air energy storage systems. In Chapter 4 are other energy storage technologies presented. A summary of all the storage technologies is given in Section 4.5. Chapter 5 and 6 introduces the basic thermodynamic principle needed to understand the operation of diabatic and adiabatic CAES power plants. The simulation tool, model layouts and the model assumptions is presented in Chapter 7. Results of the simulations and sensitivity is presented in Chapter 8, followed by discussion in Chapter 9. Finally, in Chapter 10, is a conclusion given together with further work.

1.4 Risk assessment

There has been no practical work during the making of this report or any other activities that could affect the health, safety or security. Hence have no risk assessment been carried out.

1.5 Contribution

The main contributions from this work were:

- Process simulations of two diabatic CAES and one adiabatic CAES power plant designs.
- Calculation and evaluation of round-trip efficiency for an adiabatic CAES design.
- Literature study on energy storage technologies.

1.6 Limitation of work

- All simulations have been performed quasi-dynamic, neglecting fast changing dynamic effects.
- The electricity price, which is the deciding criteria for adiabatic compressed air energy storage operation, is not considered during the simulations. For the reference models, the natural gas price is not considered.
- The simulation does not count for reduced performance at start-up and shut-down.
- Simulations were based on assumed values from similar power plants and other studies, since no real data for adiabatic CAES is available.

Chapter 2

The future of the European electrical grid

One of the major objectives of the European Union (EU) is to achieve a competitive low carbon economy by 2050, thus reducing the overall greenhouse gas (GHG) emissions by at least 80 % below 1990 levels and keeping the global temperature increase below 2°C[5]. Milestones have been derived from the 2050 objective at 2020, 2030 and 2040 with a GHG reduction at 20 %, 40 % and 60 % respectfully. Some of the framework to reach these milestones has been created. To reach the 2020 milestone the European Union has as goal to increase the share of renewable power generation to 20 % [5].

In October 2014 the European Union announced their climate and energy policy framework towards 2030. This framework included a domestic reduction of GHG by 40 % compared to 1990 levels and a minimum share of renewable power generation of 27 % [6]. Figure 2.1 shows a rough estimate of the future renewable share in gross energy consumption towards both 2020 (blue solid line) and 2030 (green solid line). The dotted line is a linear interpolation based on the actual values from 2004 to 2012 shown in red. The Figure shows that if the continued growth has a slope equal to the average from 2004 to 2012, both the goal for 2020 and 2030 would be achieved.

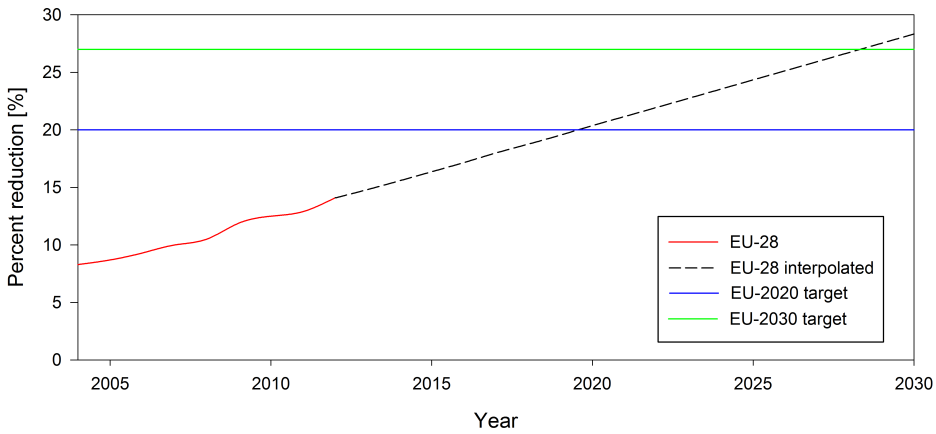

Figure 2.1: Renewable energy share in gross final energy consumption, EU-28 from 2004-2030 [i]

[i] Based on data from [7]

2.1 Carbon dioxide allowances

Allowances of carbon dioxide are the main measure used by the European Union to reach their climate change goal. By placing a value on emission one hope to make greenhouse gas emission part of European companies agenda. One allowance grants the user the right to emit one tonne of CO_2, or the equivalent amount of the more potent greenhouse gases NO_2 and perfluorocarbons. It can only be used once. Today all the 28 EU member states operates with the EU Emission Trading System (EU ETS) plus Norway, Iceland and Lichtenstein [8].

It is mandatory for all power and heat generators, energy intensive industry and aviation to use allowances. The cap for overall volume greenhouse gas emitted is reduced every year, and allowances are distributed to countries and companies. If a company require any extra allowances it needs to buy more or draw on their credit. Companies are also allowed to invest in certain types of emission-saving projects around the world instead of buying extra quotas. However, if a company do not use all of its allowances, they can sell them to other companies. The end result is a flexible market allowing companies to choose the most cost efficient way to reduce their emissions [8]. Since the allowances can be traded on the open market is the price constantly changing. From February to May 2015 have the price on the Global Environmental Exchange varied from 6.36 to 7.66 €/tonne CO_2 [9].

2.2 The European electrical grid - today

As Figure 2.2 illustrates, is the transmission of electrical power one directed with a power flow from the producer to the consumers. The electrical power is generated from large central power plants and converted to high voltage before it is put out on a high voltage long range transmission system. High voltage is used to minimize the transmission losses. The electricity is then transported to a medium and a low voltage distribution system. Typically the industry is using the electricity with medium voltage while households uses low voltage [10].

Historically the grid of today can be seen as a result of access to natural resources, geography and economy. Power plants are usually built close to the natural resources (coal, hydro etc.). The electrical grid then carries the power to where it is needed, usually far away from the power plant. The transmission and distribution is run by a natural monopoly due to the expenses of construction. It also does not make sense to build more transmission system when one is enough. To avoid abuse of power is the network strictly regulated by the authorities [10].

Supply and demand of electricity typically vary throughout the day. Figure 2.3 shows the volume produced and the price of electricity on the 31. of March 2014 in Germany. In Figure 2.3a it can be seen that the highest volumes of electricity is during the middle of the day, and in Figure 2.3b that the price has one peak in the morning and another in the afternoon. Comparing the two plots one can see that the increase in volume in the areas around 05.00-10.00 and 19.00-22.00 correlate with a rapid increase in price. These are the typical periods for people to wake up in the morning to go to work and for making dinner in the afternoon. The

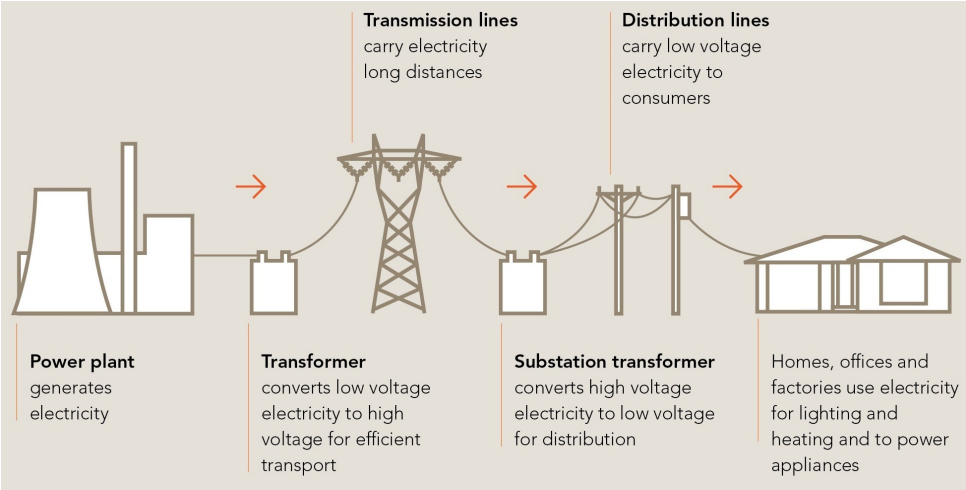

Figure 2.2: Transportation of electricity [ii]

[ii]Source, EEX:http://eex.gov.au/files/2012/01/AEMO-Transport-of-Electricity_High-Res.jpg

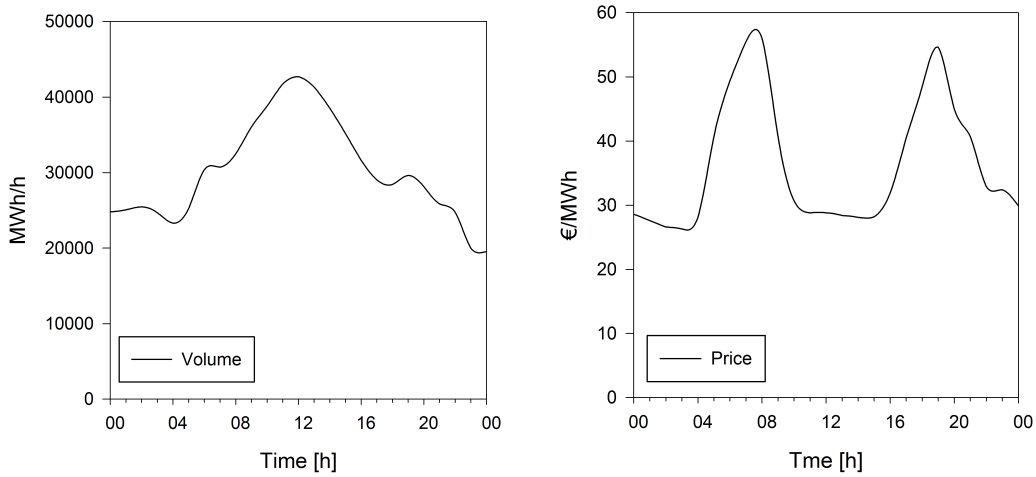

(a) Volume (b) Price

Figure 2.3: Price and volume of electricity generated 31/3-2014 in Germany [iii]

[iii]Based on data from [11]

reason for the high prices in these time periods are the sudden changes in power demand taking place, which in turn requires faster power units that typically are more expensive to operate. The periodic change in electricity price with the time of day can be utilized to store energy. When energy is abundant and cheap it is bought and stored, later when the price is higher and energy is scarce the energy is sold. This is called time shifting, and is one of the fundamental driving forces behind large scale energy storage power plants.

2.3 The European electrical grid - tomorrow

The development of renewable energy sources in the European net electricity generation can be seen in Figure 2.4. The volume of renewable energy sources in the European energy mix is increasing from around 500 billion kWh to a little less than 1000 billion kWh from 1980 to 2011. With an increasing share of intermittent renewable generation (i.e. wind and solar) the possibility to have a dynamic and fast changing grid becomes more and more important. Figure 2.5 shows the share of different energy sources in the European net electricity generation in 2011.

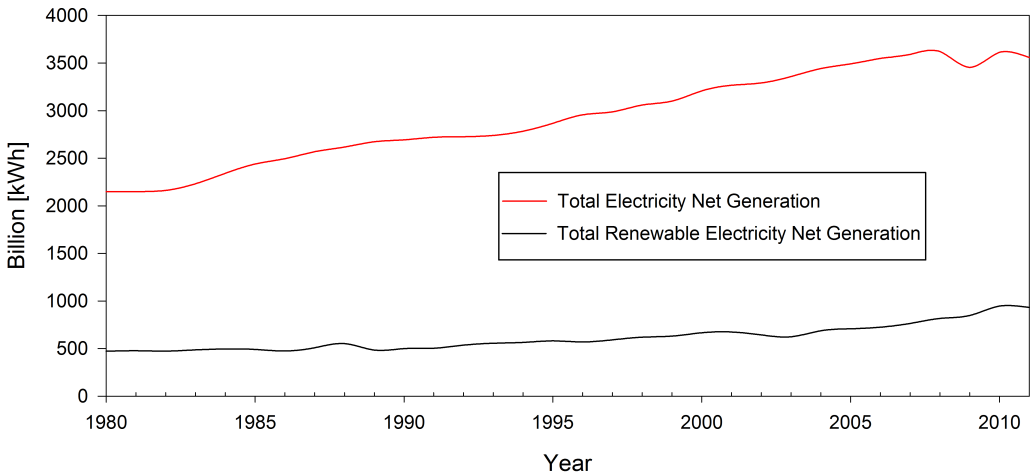

Figure 2.4: Net electricity generation in Europe 1980-2011[iv]

[iv]Based on data from U.S. Energy Information Administration [12]

As mentioned above does the need of a fast changing and dynamic grid becomes increasingly important with the increase of intermittent power generation. Research done in Germany, Spain and Denmark shows that when the share of intermittent generation exceeds 20-25 % it needs to be restricted during periods of low consumption to avoid reactive power, frequency and voltage disturbances[13]. This example illuminate the main challenge for the future grid; to find an economical and efficient way of integrating the increasing renewable power generation while maintaining a secure and reliable supply [14].

There is uncertainty regarding the final development of the European electrical grid and a large part it is associated with the composition of the primary energy mixture. It is clear that a shared vision is desirable to create and implement new standards. The key features needed to achieve this are: Flexibility, Accessibility, Reliability and Economy. In the term flexible lies the understanding that the grid needs to be able to adapt to changes, in both usage and technology, while still fulfilling the customer's needs. It needs to be accessible to all users and producers, and assure a high quality and security of supply. And it need to stimulate economic growth through providing innovation, efficiency and fairness in competition [10].

Figure 2.6 illustrates how the grid of the future, also called Smart Grid, could operate. Smart Grids utilizes advancement in metering, control units, storage and communication

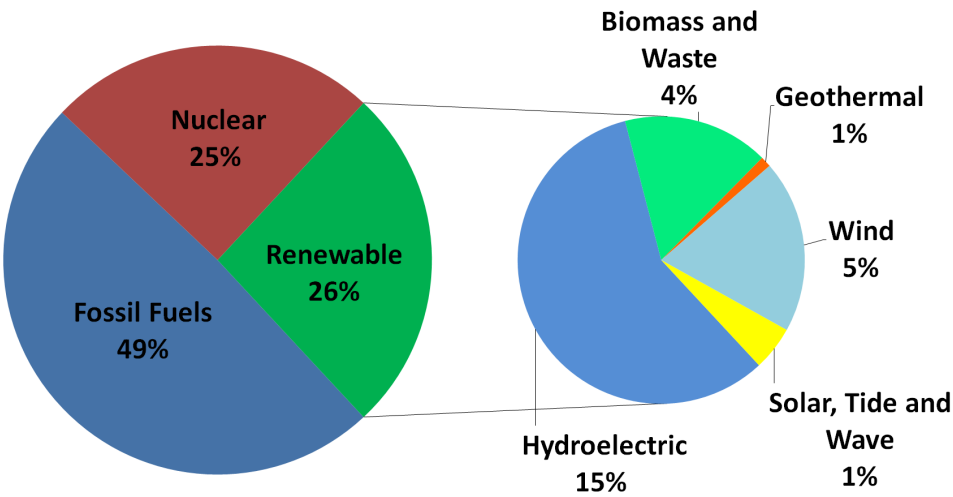

Figure 2.5: Percentage of the net electricity generation in Europe 2011[v]

[v]Based on data from U.S. Energy Information Administration [12]

technologies. The different units of the grid communicate with each other and are able to control power flows in a flexible manner through advanced communication technology. Power is generated centrally and distributed, and the flow of electricity is bi-directional. Bi-directional electricity transfer provides the power consumer with the opportunity to generate and transfer electricity back to the grid [10].

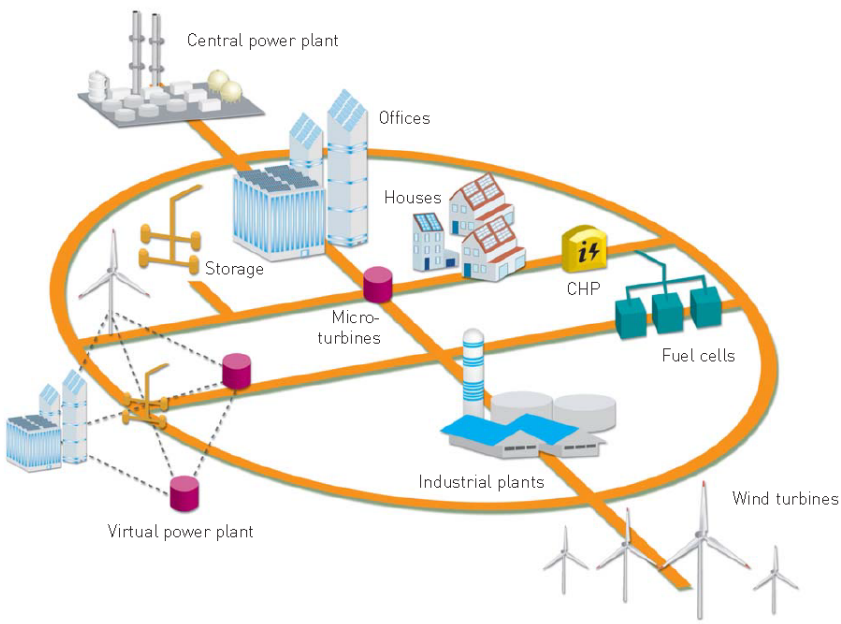

Figure 2.6: The grid of the future [vi]

[vi]Source: [10]

If a renewable energy source stops generating power over a longer period of time, i.e. there is no wind to operate the wind turbines, standby capacity is needed. This extra capacity could be supplied from an energy storage technology, operating with energy stored

at a previous time when energy was abundant. Typically this would be controlled from a virtual power plant (VPP). A virtual power plant is a control unit that enables a cost efficient integration of distributed energy resources and it is a necessity in a decentralized energy system. Some parameters used by the VPP for regulation can be; needed power output, storage reserve, price etc.[15].

2.4 Market

Power in Europe today is traded at different energy exchange, for example at Noorpool and The European Energy Exchange (EEX). There are two different markets depending on the type of contract that is needed, the spot market and the derivatives market. The spot market operates on two levels, with an intra-day market and a day-ahead market. On the day-ahead market power is traded for the following day, using a blind auction procedure, every day all year in hour and block contracts. The activity on this market sets the reference price for the PHELIX-day base, which is the reference price of the European wholesale market. On the intra-day market power is bought on the same day as it is used. Trading and pricing is continuous and are allowed until 45 minutes before the power is used. The derivatives market allows transaction at a specific time agreed upon in advance. This market is typically used to optimize production or consumption over a longer period of time, and it is possible to hedge against price change for up to six years in advance [16].

It is clear that with a fundamental change of how electricity is generated and distributed, there will also be a change in how it is traded. In Germany there has been a change in energy policy and turnaround due to the growing share of renewable energy. The effect can be seen on the EEX where planning and trading takes place at shorter periods of time [17].

EEX highlights in their paper on energy policy cornerstones [17] what they believe to be the key factors for a successful development of the new market. The energy market needs a long term reliable political framework. This is in particular important for investment decisions. The energy policy needs to be formed with a European perspective, creating opportunities for large scale transmission and balancing of power across borders. Equal opportunities should be offered for all participants in a transparent market. Prices are then regulated by supply and demand, awarding cost efficiency and innovation [17].

Subsidisation of renewable energy will in the future still be necessary, but should in the future be reduced over time. This allows price to be decision making for operation. Renewable energy producers can offer guaranty of origin, utilizing the willingness of people to pay extra for green power. This would also strengthen the transparency of the marked and lower the need of government subsidisation [17].

The European emissions trading system needs to be strengthened, giving a stronger incentive to invest in technologies with low GHG emissions. Today there is a surplus of allowances, partially because of the financial crisis causing an emission reduction, making carbon low technology less profitable. An inclusion of new sectors to the emission trading system, as well as countries and regions, will further strengthen integration of renewable power [17].

Capacity mechanism, where power generators are paid to have standby volumes of energy, should only be used as a last resort. No one knows the effect of a fully integrated renewable power market, and focus should be on exploiting other options such as energy storage. Integration of demand side management will also give the consumer the choice to adjust their demands after the market conditions. This could also reduce the need of fossil fuels used in capacity mechanisms [17].

Chapter 3

Compressed air energy storage - CAES

Compressed Air Energy Storage (CAES) is of today the only suitable option for energy storage with a power output on the same scale as pumped hydro storage (PHS), i.e. 100-1000 MW [18]. The only CAES power plants currently in operation is diabatic CAES. This section aims to present the different types of CAES power plants; diabatic, adiabatic and isothermal. The final section of this chapter introduces thermal energy storage, which is a vital part of any adiabatic CAES system configuration.

The main components of a CAES power plant are[19]:

- Multistage compressor train
- Underground or above ground air storage
- Expander train
- Motors and generators
- Piping and fittings
- Control system.

Another vital requirement for any CAES power plant is a system that can handle the compression heat. For diabatic CAES is the compression heat removed by intercoolers and an aftercooler. This is done to reduce the power needed for compression and to reduce the required storage volume. The heat however is not saved, and must be supplied in the expander train in the form of fuel. For adiabatic CAES and isothermal CAES is the compression heat stored and reused in the expander train. The heat is then either removed during compression or after and stored as sensible heat in a thermal energy storage unit (TES).

3.1 Diabatic compressed air energy storage

The basic principle of a CAES power plant can be seen in Figure 3.1. A typical plant compress air to 45 to 70 bar[18]. The air is cooled down to near ambient temperature and stored, either

above ground in tanks or underground in caves or old reservoirs. When power is needed, the compressed air is released from the storage unit and mixed with natural gas in a combustion chamber. The warm exhaust gas expands through a gas turbine connected to a generator and generates power. The reason for mixing the compressed air with natural gas is to increase the temperature and thus increasing the efficiency [18, 20, 21, 22]. When natural gas combustion is used together with the compressed air, it is called diabatic CAES (DCAES)[23].

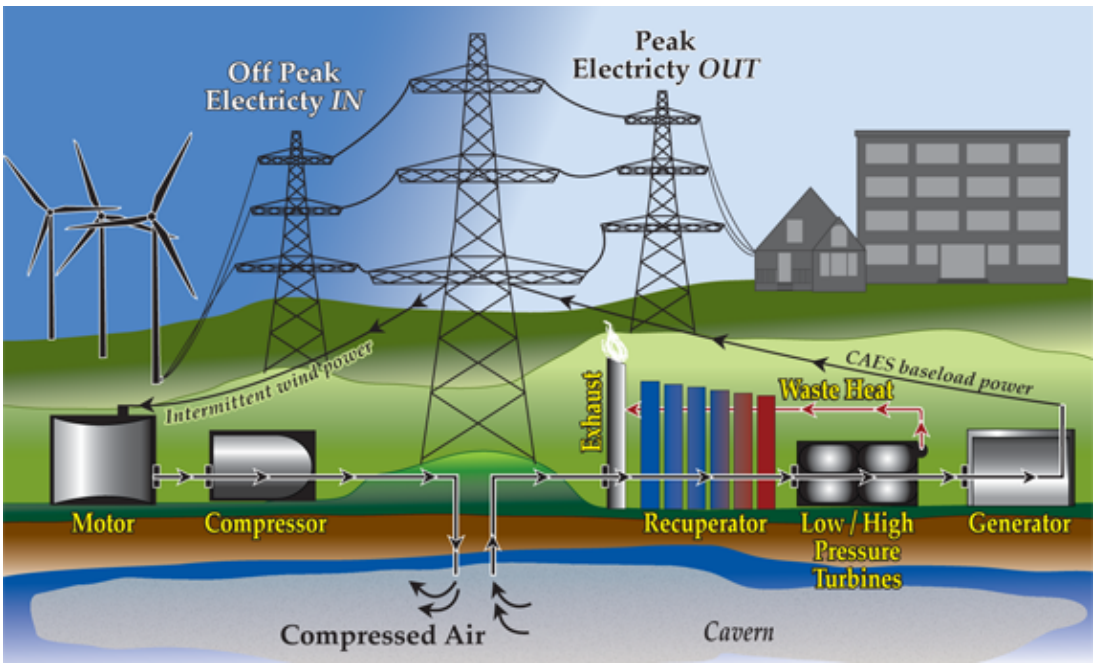

Figure 3.1: CAES power plant [i]

[i]Source, WindSoHy: `http://windsohy.com/images/stories/caes_illustration_final.png`, Accessed October 2014

Today there are two large scale DCAES plants in operation. One plant lies in McIntosh (1991), USA and the other lies in Huntorf (1978), Germany. The McIntosh plant has a capacity of 2860 MWh (110 MW for 26 hours), while the Huntorf plant has 870 MWh (290 MW for 3 hours) capacity. They both use old salt caverns for air storage [20, 18], with volume of 555000 m^3 and 300000 m^3 respectfully. The round-trip efficiency of the McIntosh plant is 54 % and for the Huntorf plant it is around 42 % [24, 25]. The initial investment cost lies in the area of 500-1500 USD/kW [26]. Both power plants are used for time shift, frequency regulation and spinning reserve capacity. They can also both be used for black-starts [18, 19].

The main difference between the two plants is the fact that the McIntosh plant uses a recuperator after the turbine to heat the cold storage air with the hotter exhaust gas before it enters the combustion chamber[27]. This reduces the fuel consumption with about 22-25 % [24] and is the major reason for the big difference in round-trip efficiency of the two plants.

Some of the advantages with DCAES is the fast start up time, long life span, large power capacity and fast ramp up time (uses 3 minutes to get to 50 % capacity)[23]. They provide significant energy storage at low cost at a high degree of flexibility for operations. When operated at 20 % of maximum load, the heat rate is 80 % of the nominal heat rate at maximum

load. Conventional fuel based power plants such as gas turbines have a poor part load efficiency in comparison [19]. DCAES power plants can also be designed for the specific site conditions such as off-peak energy price, fuel cost, capital cost of construction and type of storage. The combustor can also be designed for different types of fuel such as natural gas, biogas, oil and hydrogen [19]. Both the Huntorf and McIntosh DCAES power plant uses natural gas as heat source and thus emits CO_2. The natural gas consumption is however 68 % less than for a natural gas combustion turbine based on heat rates[27], and the DCAES plant can be CO_2-free if biogas or hydrogen is used as heat source instead. The loss of the compression heat also lowers the efficiency of the plant. For further development of CAES systems, these are the key objectives to solve.

3.2 Compressed air storage

As mentioned, compressed air can both be stored underground and over ground. Underground storage is cost efficient for large installations, but it can be hard to find suitable locations. Over ground storage on the other hand, can be done in pressure containers, tanks and pipes. An advantage with over ground storage is the possibility to place the CAES plant where it is needed, as an alternative to upgrading transmission lines[20]. Naturally an over ground installation would need more isolation, to be able to handle higher seasonable and daily temperature variation. Due to the need of isolation, over ground storage is also believed to be five times more expensive than underground storage and with a smaller storage capacity[18]. The size of over ground CAES plants are thought to be between 10-30 MW for 4-6 hours [20].

There are three main types of caverns suitable for underground storage of compressed air; salt, hard rock and porous caverns[28]. In general must the storage cavity be deep enough underground to allow safe operation of high pressure cycles, and the cavity must be dense to prevent air from leakage [19].

3.2.1 Salt cavern

Salt cavern pressurised air storage is the most viable option today for large scale storage. The construction cost is relatively low (2-10 $/kWh), due to the technique of solution mining. Solution mining consists of dissolving salt from the strata using water or another liquid, creating large cavities of the desired shape and size. Salt walls have a high elastoplasticity, allowing them to withstand high pressure cycles with low degradation, resulting in a low risk of air leakage. Both the Huntorf and McIntosh CAES power plant uses salt wall caverns for storage [28]. Figure 3.2 shows the salt deposits in Europe.

3.2.2 Hard rock cavern

The hard rock cavern have a higher construction cost than salt caverns, around 30 $/kWh. The construction cost can be significantly lowered by using existing mines, but suitable lo-

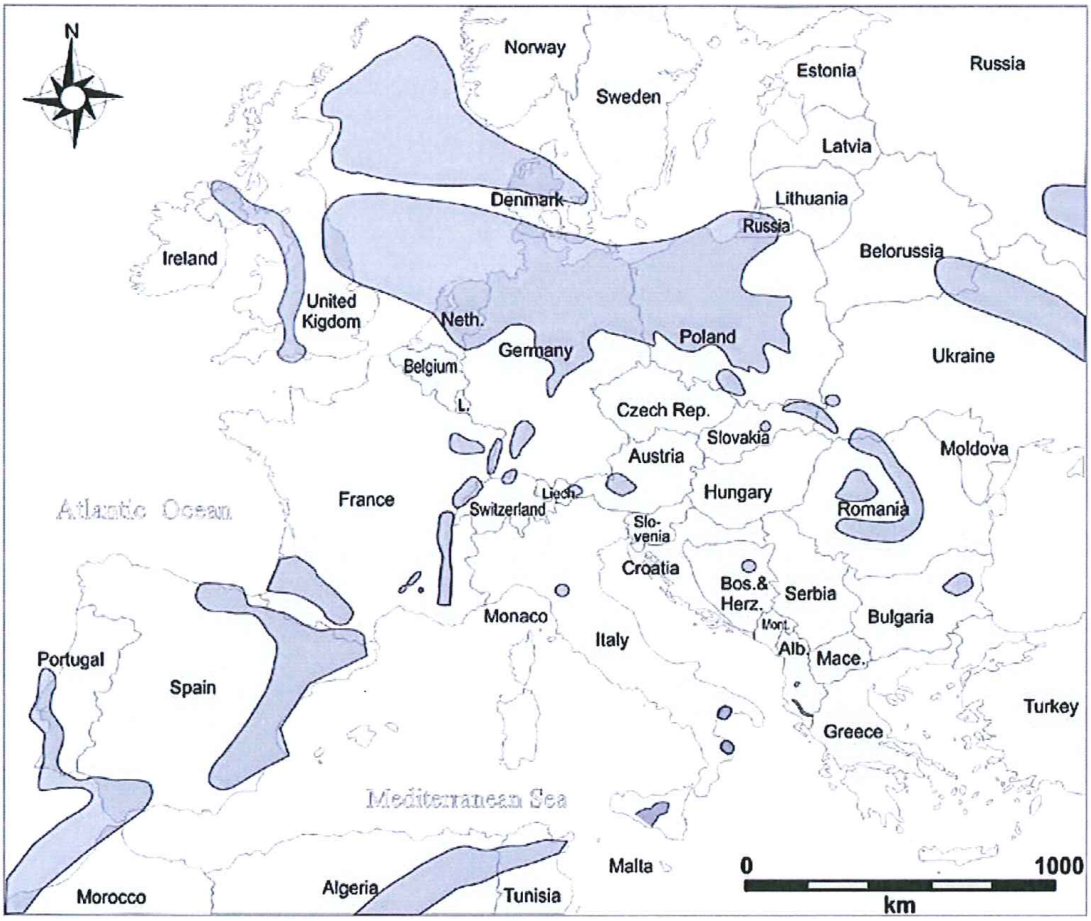

Figure 3.2: Salt deposits in Europe [ii]

[ii] Source: [29]

cations are scarce. The storage depth varies from 300 to 1500 meters below the surface [28].

3.2.3 Porous rock cavern

The porous rock cavern have the lowest estimated construction cost of all, around 0.10 $/kWh. Despite the low construction cost, porous rock formations have some challenges. The rock may not contain minerals that react rapidly with oxygen, leading to a consumption of the stored air. It must provide a sufficient storage volume and it need to be permeable enough to allow the required airflow rates [19].

3.3 Adiabatic compressed air energy storage

The main difference between Adiabatic CAES (ACEAS) and DCAES is the fact that ACAES do not need fuel to heat the expanding air. Instead it stores and reuse the heat generated during the compression. The heat is transferred from the warm air to a storage medium through a downstream cooler. The storage medium could be a solid, a fluid or molten salt. When power is needed, the air is reheated with the stored compression heat [23]. A sketch of an

ACAES power plant is shown in Figure 7.3. There are currently two ACAES projects under planning; the ADELE project in Germany and the ALACAES project in Switzerland[21, 30].

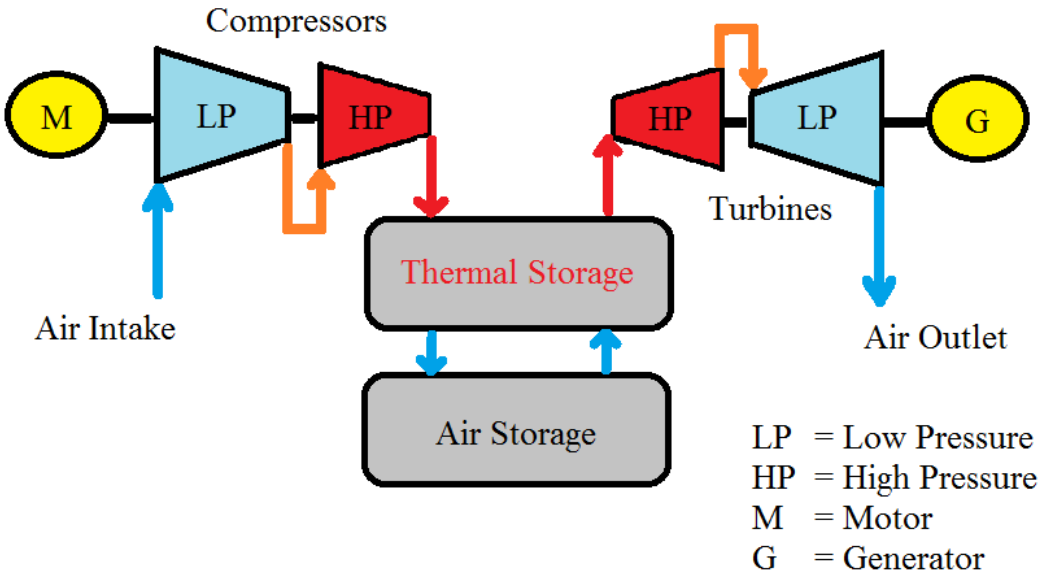

Figure 3.3: Sketch of an ACAES power plant

3.3.1 The ADELE project

In the case of the ADELE project, it might have a demo plant operational as early as 2016. The project aims for a storage capacity of 1000 MWh with a power output of 300 MW [21]. Air is compressed to a total of 100 bar and a temperature of around 600°C. The air is then let through a 40 meter high pressurized container, with a bed of stones and ceramic bricks as head storage medium. The cold air, at around 50°C, is stored separately [18, 21].

The round-trip efficiency of the ADELE power plant is believed to be around 70 %[21]. This is a lot higher than traditional DCAES, and it uses no fuel, so there are no CO_2 emissions. This makes ACAES competitive with PHS. However, the initial cost goes up, due to the need of a heat exchanger and a heat storage device[23]. There are still many uncertainties around the behaviour of the compressor, the insulation and the heat storage medium at such high temperatures and pressure [21].

3.3.2 The ALACAES project

The ALACAES project aims to have a 1 MW test plant ready by 2017. The pilot plant is constructed under the Swiss Alps, using old tunnels and caverns. Air is compressed from 70 to 100 bars and stored in a pressurised container. The compression heat is stored, through direct heat transfer, in packed bed of rocks placed in a concrete container able to operate with temperatures up to 800°C. The round-trip efficiency is estimated to be 72 % and the thermal efficiency 95 %. It have a ramping time less than 5 minutes and have black start

capabilities[30]. By placing the entire power plant inside the mountain, the visible environmental footprint of the power plant is reduced. Placing the plant in already existing hard rock caverns also make an easy access for constructions compared to salt caverns. Experience with turbomachinery inside mountain is also plentiful from hydropower plants. The thermal storage is also safe as rock is being used as medium, since there are no chemical instabilities or corrosive materials involved [30].

3.4 Isothermal compressed air energy storage

Isothermal CAES (ICAES) works by compressing and expanding air at near constant and close to ambient temperature, thus reducing the work of the compressor [20]. Two companies developing technology for ICAES are SustainX and LightSale. The round-trip efficiency of an ICAES power plant can reach around 80 %. Estimated capital cost for an ICAES system is 1000-1500 €/kW. Life time is expected around 30 years, with 15000 cycles. The deployment time is a few minutes and typical power output around 5kW [23]. The basic idea for ICAES system can be seen in Figure 3.4.

Both the SustainX and LightSale designs use pneumatic cylinders. One of the advantages with this technology is the fact that the same unit is used for both compression and expansion and thus reducing the investment costs. However, the technology is still immature and expensive to scale to a large power supply[18].

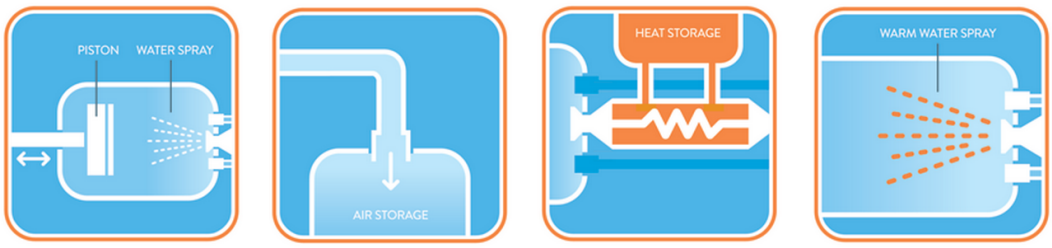

Figure 3.4: LightSale Energy ICAES consept [iii]

[iii] Source: [31]

3.4.1 SutstainX

The technology developed by SustainX is based on technology known from the naval diesel reciprocating engine industry. One 1.5 MW test facility have been constructed in 2013. In the SustainX design the compression heat is stored in water based foam sprayed into the compression cylinder. The operating pressure range is from atmospheric pressure to around 200 bar. During expansion is the compression cycle reversed [32].

The SustainX plant can go from cold start to full power in less than 60 seconds. It can switch from charge mode to discharge mode in 5 seconds, and it has a charge/discharge

ratio of 1.333. One of the biggest challenges is however to increase a relatively low round-trip efficiency of 55 %. Capital costs lies in the area of 2.400-3000 $/kW [32].

3.4.2 LightSale

LightSale Energy uses a modified compressor rather than a conventional compressor from the naval industry. They use spray of water and not foam to extract the compression heat. So far have no test facility been build, but their goal is to reach a high round-trip efficiency of 70 %. Capital costs is expected to be 500$/kW [32].

3.5 Thermal energy storage - TES

According to World Energy Outlook [4] one third of the final global energy demand was utilized by households in 2010. A lot of this energy was used for heating and cooling applications. One way of making heating and cooling of buildings and industrial processes more efficient, and thus reducing the amount of energy from fossil fuels consumed, is to store thermal energy in form of heat or cold when it is abundant for reuse later when it is scarce. This is the working principle of thermal energy storage (TES) and it can be seen graphically in Figure 3.5. Some of the benefits from storing thermal energy can be increased efficiency of the process, reduced capacity need and operational flexibility [33, 34].

There are many different ways of storing thermal energy and for different applications. Heat can be stored over longer periods of time, such as weeks and months (long term storage), or it can be stored for days or hours (short term storage). The methods and materials used depend on the temperature available and the temperature needed for later. In this section will two types of thermal energy storage be described; latent and sensible storage [33]. Two different concepts will also be presented, active and passive storage.

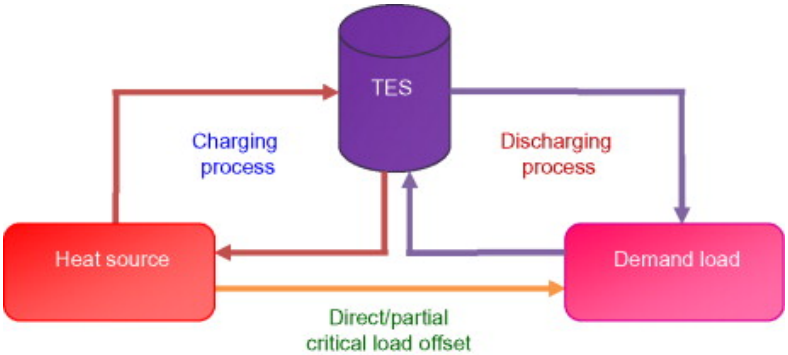

Figure 3.5: Principle of TES operation [iv]

[iv] Source: [34]

3.5.1 Sensible heat storage

Sensible heat storage works by storing thermal energy in a medium by raising (or lowering) the temperature of the medium. So the temperature increases and the medium becomes hot to touch. The energy stored in a sensible medium is proportional to the heat capacity, the difference in charge and discharge temperature, and to the mas of medium [35]. There are two main types of material used for sensible storage, solids and liquids. In general liquids have a higher specific heat capacity, a higher energy density and lower self-discharge rate than solids. However the risk of leakage of storage material is lower and the lifespan is higher for solid materials [34].

The temperature range of solids and liquids also differs extensively. For low to medium temperature range, or in between 0 and 100°C, water is a well suited storage medium[35]. For temperatures above 100°C thermal oils are a good medium, and for temperatures over 600°C are solids such as concrete and ceramic suited [34]. According to IEA-ETSAP and IRENA [36] is the round-trip efficiency of a sensible TES in the area of 50 to 90 %.

Sensible storage materials are defined as materials where no change in phase takes place over the temperature range of the storage process. The materials need to have a good thermal capacity. The heat transfer rate when charging and discharging is often quite fast [37]. A selection of sensible thermal storage mediums can be seen in Table 3.1 and 3.2.

Table 3.1: Solid sensible heat storage mediums[v]

Storage medium	**Temperature**		**Average density (kg/m^3)**	**Average heat conductivity (W/mK)**	**Average heat capacity (kJ/kgK)**	**Volume specific heat capacity (kWh_t/m^3)**	**Media cost pr. kg (US$/kg)**	**Media cost pr. kg (US$/$kWh_t$)**
	Cold (°C)	**Hot (°C)**						
Reinforced concrete	200	400	2200	1.5	0.85	100	0.05	1
NaCl (solid)	200	500	2160	7	0.85	150	0.15	1.5
Cast iron	200	400	7200	37	0.56	160	1	32
Sillica fire bricks	200	700	1820	1.5	1	150	1	7
Magnesia fire bricks	200	1200	3000	5	1.15	600	2	6

[v]Source: [37]

Table 3.2: Liquid sensible heat storage mediums[vi]

Storage medium	Temperature		Average density (kg/m^3)	Average heat conductivity (W/mK)	Average heat capacity (kJ/kgK)	Volume specific heat capacity (kWh_t/m^3)	Media cost pr. kg (US$/kg)	Media cost pr. kg (US$/$kWh_t$)
	Cold (°C)	Hot (°C)						
Mineral oil	200	300	770	0.12	2.6	55	0.3	4.2
Synthetic oil	250	350	900	0.11	2.3	57	3	43
Silicon oil	300	400	900	0.1	2.1	52	5	80
Nitrite salts	250	450	1825	0.57	1.5	152	1	12
Nitrate salts	265	565	1870	0.52	1.6	250	0.5	3.7
Carbonate salts	450	850	2100	2	1.8	430	2.4	11
Liquid sodium	270	530	850	71	1.3	80	2	21

3.5.2 Latent heat storage

When a material changes its aggregate state, from gas to liquid or liquid to solid, energy is released. For the opposite reaction energy is required. These processes can be utilized to store energy [35]. The materials used to store the energy latently are called phase changing materials (PCM). When a substance changes its aggregate state, it does so at a constant temperature. PCMs have the ability to store and thus release large amount of thermal energy in their phase changing area [34]. According to IEA-ETSAP and IRENA [36] is the round-trip efficiency of a PCM TES in the area of 75-95 %.

When choosing a PCM for latent storage some considerations must be taken. It needs a high latent heat with a phase change that lies in the appropriate temperature area. It must be available, not too expensive, non-toxic and not flammable [35]. Some of the advantages with PCMs for latent heat storage compared to sensible heat storage mediums are the lower mass required for same amount of energy stored, meaning a lower volume needed. The energy is also stored at close to constant temperature which all together gives lower losses to the surroundings [33]. Table 3.3 shows some commercial available PCM:

[vi]Source: [37]

Table 3.3: Commercial PCM materials [vii]

Name	Type	Manufacturer	Phase change temperature (°C)	Density (kg/m^3)	Latent heat (kJ/kg)	Latent heat (MJ/m^3)	Specific heat (kJ/kgK)	Thermal conductivity (W/mK)
RT110	Paraffin	Rubitherm	112	n.a.	213	n.a.	n.a.	n.a.
E117	Inorganic	EPS	117	1450	169	245	2.61	0.7
A164	Organic	EPS	164	1500	306	459	n.a.	n.a.

3.5.3 Active and passive thermal storage

In an active thermal storage system is the thermal storage medium circulating through the heat exchangers, transferring heat by forced convection. In a passive thermal storage system is a heat transfer fluid used to charge/discharge heat to a stationary storage medium [37].

Active storage system can further be classified into direct and indirect storage. In an active direct storage system there is one heat transfer fluid that also serves as storage medium. For an active indirect storage system, there are two heat transfer fluids, where one serves as the heat medium [37].

[vii] Source: [37]

Chapter 4

Other energy storage technologies

In the following section some of the most common and most promising technologies for energy storage will be presented. Figure 4.1 shows how far the different storage technologies discussed in this section have been developed. It is quite clear that pumped hydro storage is the most mature technology and also the one with the lowest risk times capital cost.

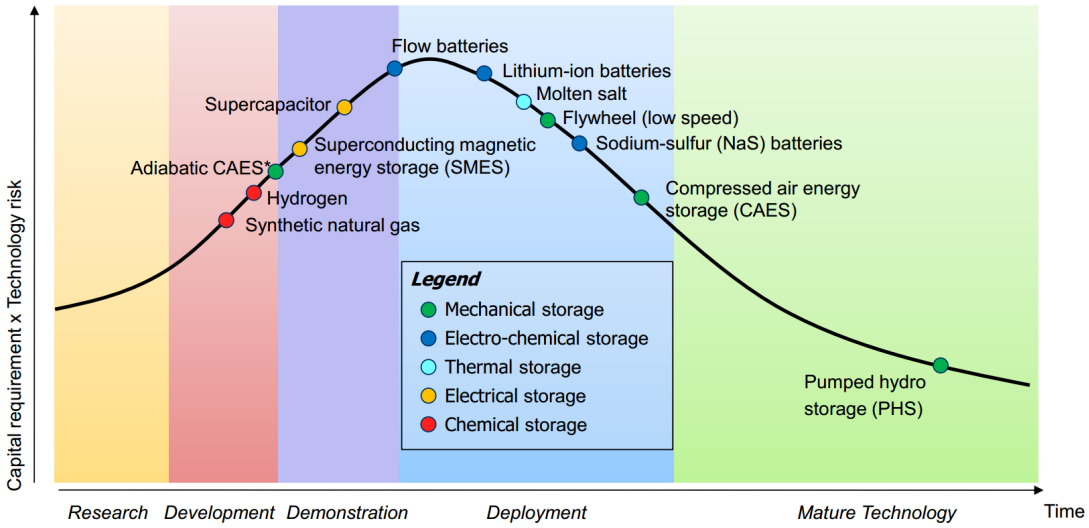

Figure 4.1: Energy storage technology maturity [i]

[i] Source: [38]

The total installed storage capacity in the world can be seen in Figure 4.2. Pumped hydro, being the most mature technology, naturally have the largest installed capacity. Compressed air energy storage, closely followed by sodium-sulphur batteries, has less than 1 % of the installed capacity. It is expected that the more immature technologies will take a higher percentage of the installed capacity in the future. Some even have the potential to compete with pumped hydro in the long run.

The way the different storage technologies function, their storage period and the usage of their power output, differ from technology to technology. Storage can be from minutes to hours, hour to days and from days to several months. Some of the most common ways of using the energy storage technology [26] are presented in Table 4.1:

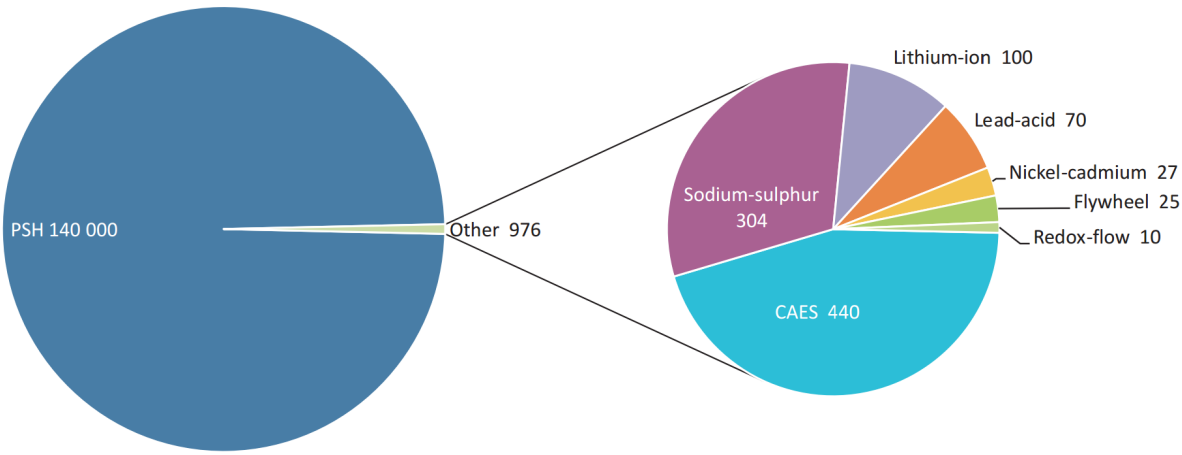

Figure 4.2: Global installed grid-connected electricity storage capacity [ii]

[ii] PSH is used in this figure instead of PHS which is used in the rest of the report. Source: [26]

Table 4.1: Usage of energy storage technologies in the electrical grid

Usage	
Frequency regulation	Continuously balancing of shifting demands within a time frame of milliseconds to 15 minutes
Load following	Continuously balancing of shifting demands within a time frame of 15 minutes to a day
Voltage support	Maintaining the voltage level in transmission and distribution within a secure and stable range
Black start	The capability of restarting without pulling electricity from the grid
Spinning reserve	The reserve capacity to compensate for rapid unexpected loss in generation, typically less than 15 minutes
Non-spinning reserve	The reserve capacity to compensate for unexpected loss in generation larger than 15 minutes
Time shifting	The ability to store energy when price is low and discharge when price is high
Peak shaving	The ability to control own energy usage in peak hours to reduce cost

4.1 Mechanical energy storage

Mechanical energy storage is a way of storing energy by means of a mechanical process, such as rotation [39]. The methods introduced in this section are Pumped Hydro Storage and Flywheel Energy Storage. Compressed air energy storage, presented in Chapter 3 is also categorized as mechanical energy storage, even though DCAES utilizes chemical energy in the form of fuel, and ACAES uses TES.

4.1.1 Pumped hydro storage - PHS

Pumped Hydro Storage is a long term storage technology. Of the different types of storage technologies it is also the most mature and the only one that are commercially proven today. Worldwide there are more than 300 plants operating [20], providing more than 95 % of the current storage capacity[23].

A pumped hydro power plant stores energy by pumping water from a lower reservoir up to a higher reservoir. Thus transforming electrical energy, via mechanical energy, to potential energy, see Figure 4.3. The effect delivered is proportional to the mass flow and head of the system, and the round-trip efficiency lies in between 70-85 % [18]. Typically the power output lies in the area of 100-1000 MW, with a timespan of hours to days [40]. Losses due to evaporation are in general small over longer periods of time due to supply from rain to the reservoir.

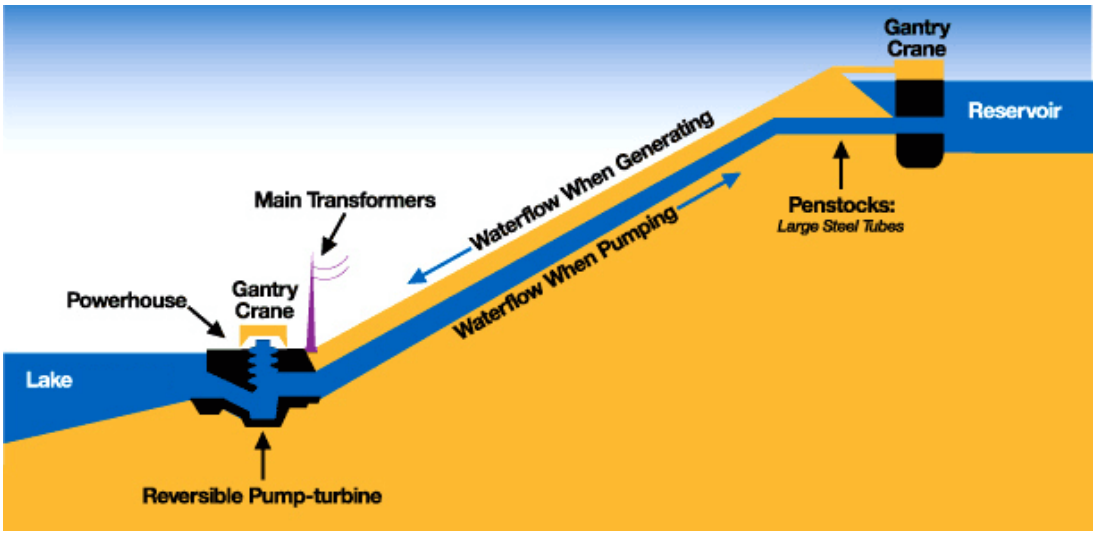

Figure 4.3: Pumped hydro storage [iii]

[iii]Source: https://www.consumersenergy.com/uploadedImages/CEWEB/OUR_COMPANY/Electricity/Pumped_Storage/how-the-ludington-pumped-storage-facility-works.gif?n=2055

There are several advantages with PHS. One is the high round-trip efficiency and another is the long expected lifespan of the power plant. Normally one would calculate with a lifespan of 50 to 100 years for a PHS plant. The storage capacity is only limited by the size of and height difference between the reservoirs, which in turn is limited by the location. The start-up time varies between a couple of seconds (on standby) to 10 minutes if completely shut

off [18]. Another advantage with PHS is the flexible operating range, both on and off peak production, with a stable frequency and voltage. PHS can be used for frequency control, non-spinning reserve and time-shifting as well as load following[24].

Some of the disadvantages with PHS are the long construction time and the high investment cost, which lies in between 500 to 4600 US/kW [26]. However, the maintenance and operation costs are low. Another disadvantage would be the low energy density of water. As mentioned the power output is proportional to the mass flow and head of the system. If the head is low, the volumes of the reservoirs have to be huge to be able to generate the same amount of power. Also, geographical suitable locations for PHS are getting fewer as a result of PHS being an old and favourable storage technology. Another disadvantage would be the environmental influence of rapidly changing water levels through emptying and filling the reservoirs.

4.1.2 Flywheel

A flywheel is a rotating wheel or disk that can store electrical energy as kinetic energy. The storage is done by a motor that accelerates the disk by applying a mechanical torque. When discharging the energy the motor acts as a generator[20]. The amount of energy that can be stored is proportional to the mass of the flywheel and square to the angular velocity [23, 41], but is restricted by the tensile strength of the materials used to create the disk. They are used for short term energy storage. Flywheels is nothing new historically, they have been used for centuries to regulate different type of equipment. Just recently have flywheels been rediscovered as a mean to store electrical energy[41]. Figure 4.4 shows a side-cut view of a flywheel.

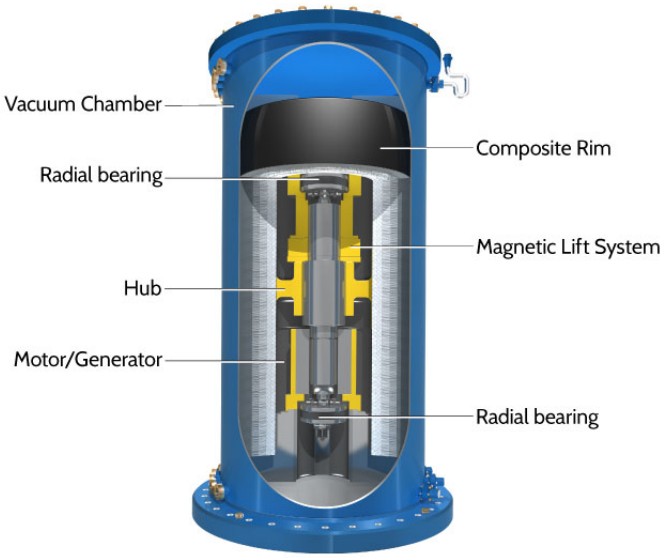

Figure 4.4: Sectional view of flywheel [iv]

[iv] Source, Beacon Power: `http://beaconpower.com/carbon-fiber-flywheels`, Accessed October 2014

Some of the advantages of a flywheel are the fast response time (less than a second)[23],

the high power density, long lifetime, low life cycle cost, high number of discharge cycles and a high round-trip efficiency of 80-85 % [20]. Due to the fast response time, flywheels are often used to regulate the frequency of fluctuating sources i.e. wind turbines. The major disadvantage is the high loss of energy for storage over longer periods of time caused by bearing friction and windage. These losses are minimized by applying a superconducting magnetic bearing system, that levitates the rotor, and to evacuate the operating chamber to create a working vacuum[42]. The power output typically lies between a few kW to 1200 kW for a couple of hours to a few seconds respectively[23]. The investment cost of a flywheel lies around 130 - 500 USD/kW[26].

4.2 Chemical energy storage

There are many forms of chemical energy etorage (CES). In this section energy storage in hydrogen and chemical production of other fuels from hydrogen will be presented. Another chemical energy storage such as batteries, will be dealt with in the section electrochemical energy storage 4.3.

4.2.1 Hydrogen

Hydrogen as an energy carrier is very versatile. It can be burned in an internal combustion engine or turbine, thus replace traditional fossil fuels, or it can be burned in a fuel cell where the efficiency is a lot higher. The drawback with fuel cells is the degree of the hydrogen gas purity required for the longevity of the fuel cells.

There are many ways to produce hydrogen gas, H_2. It can be produced from natural gas, heavy oils, biological materials and coal [41]. These ways of producing hydrogen make up 96 % of today's production. Another, and one of the simplest ways of producing hydrogen, is through electrolysis. Water molecules are split into H_2 and O_2 by using electrical energy [43]. A simple schematic of the electrolysis process can be seen in Figure 4.5.

Hydrogen production through electrolysis is the method of interest when it comes to energy storage. This produces hydrogen gas of high purity. For a low temperature electrolysis process the efficiency lays around 56-73 % [42]. One of the challenges with the electrolysis process is to find a way to make it operate efficiently on an intermittent power supply. Another challenge is the cost which lies in the area of 1000-2000USD/kW [43].

The hydrogen produced can be cooled down and stored as a liquid, pressurized and stored in caverns, stored in chemical compounds or in metallic hybrids. One of the key challenges with storage is the low volumetric energy density for hydrogen. A low volumetric energy density means a large storage container. For large scale and long term storage, underground caverns seem to be the most attractive option. Firstly, the large storage structure is already there. Secondly, the diffusion losses due to the small size of hydrogen, is assumed small because water in pores surrounding the cavern seals the hydrogen inside [41]. Long term storage in caverns will probably result in a diffusion loss around 1-3 % a year[43]. Typical range of power output is in the area of a few MW to 500 MW[23]. The round-trip efficiency

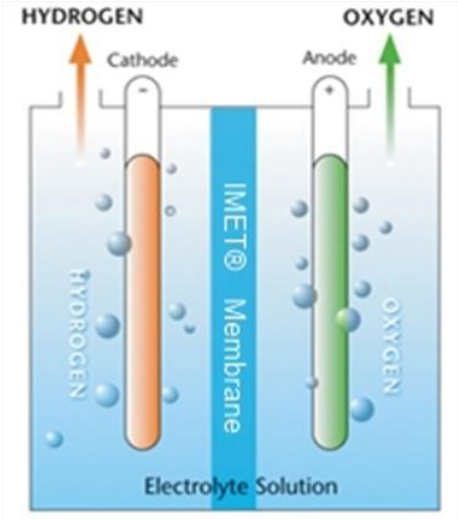

Figure 4.5: Electrolysis - Hydrogen from water [v]

[v] Source, hydrogenics: `http://www.hydrogenics.com/technology-resources/hydrogen-technology/electrolysis`, accessed October 2014

of hydrogen storage is in between 20-45 % [20].

4.2.2 Methane

Methane gas is another possible way of chemically storing energy. It can be produced through a reaction called Sabatier's reaction. This is a two-step reaction where carbon dioxide reacts with hydrogen gas, creating carbon monoxide and water. The carbon monoxide then reacts with more hydrogen gas creating methane gas and more water. The overall reaction is: $CO_{2(g)} + 4H_{2(g)} \Leftrightarrow CH_{4(g)} + 2H_2O_{(l)}$ The reaction takes place at temperatures between 200 and 750°C, with an efficiency of 70-85 % [23]. The round-trip efficiency from hydrogen production are in the area of 20-30 % [41].

Although the round-trip efficiency of synthesized methane is lower than for hydrogen, it might be a viable way of storing energy. One way of storing and transporting methane is by liquefaction. This is expensive, but methane has a higher energy density than hydrogen and also a higher boiling temperature. This makes methane 3 times cheaper to store than hydrogen[41]. The distribution network is also already in place, since methane gas can be fed into the traditional natural gas feedstock[38]. The technology of producing methane is also quite mature. It was developed in the 70's as a result of the oil crisis and the high prices of oil. The power output for a methane energy storage system is of the same order as for hydrogen.

Some of the drawbacks with methane as a energy storage option, besides the previously mentioned low round-trip efficiency, is the fact that is is competing with traditional natural gas, the need for a carbon dioxide source and the fact that it is expensive [38].

4.3 Electro-chemical energy storage (batteries)

Batteries store electrical energy, through a reversible chemical reaction, as chemical energy. The main building blocks of a battery are the electrodes (anode and cathode), the electrolyte and the container. In this section three types of batteries will be presented; Lithium-ion, Sodium-Sulfur and Flow batteries. In a traditional battery the electrolyte is acting as medium to transfer ions between the electrodes to generate electricity. In a flow battery however, the electrolyte is the medium in which the chemical energy is stored [23].

4.3.1 Lithium-ion battery

Lithium-ion batteries are one of the most common batteries used in fine electronics such as computers and mobile phones. But they are also used in some smaller energy storage systems. The main advantage with these batteries is the high energy density they offer and the high round-trip efficiency which lies in between 80-98 %. The number of recharges is also high and lies in between 1000 and 10000[20]. The discharge rate is around 80 % [23]. Due to a low weight and a fast response time, down to milliseconds, they can be used for frequency regulation and in system where weight is a concern[24]. The power output is between 1 kW to 1 MW and a discharge time of 1-4 hours [23].

One of the major disadvantages with lithium-ion batteries is connected to safety concerns. They require additional and expensive protecting circuits in order to prevent overcharging [42, 20]. The lifetime is also severely reduced when deeply discharged or exposed to high temperatures. These are problems that needs to be handled before lithium batteries can be used in large scale operations[23].

4.3.2 Sodium-sulfur battery

A Sodium-sulfur battery consist of molten sulfur and molten sodium at the electrodes separated by a solid electrolyte[23]. For the sodium and sulfur to be molten, or liquid, the temperature of the battery lies in the range of 300 and 350°C. One of the main advantages of this battery is its fast response time. It can react in milliseconds, and are therefore capable of being used in grid stabilization. The round-trip efficiency is around 75 %, with a lifespan of 2500-4500 recharges and a charge time of 6-7 hours [20], and there is no self-discharge. Normally power output varies from 1 to 10 MW for 4 hours [40].

One of the major drawbacks of the Sodium-Sulfur battery is the need for a heat supply to reach the required operating temperature of 300-350°C[42]. However, once operational, the heat produced during discharge or charge is enough to keep the process running. Another drawback is the high investment cost(1,420-2,500 EUR/kW)[23].

4.3.3 Flow battery

The basic components of a flow battery are two storage tanks containing two electrolytes, two pumps and a power cell. The two electrolytes are pumped trough the power cell where

the chemical energy stored in the electrolytes are converted to electrical energy. This can be seen in Figure 4.6.

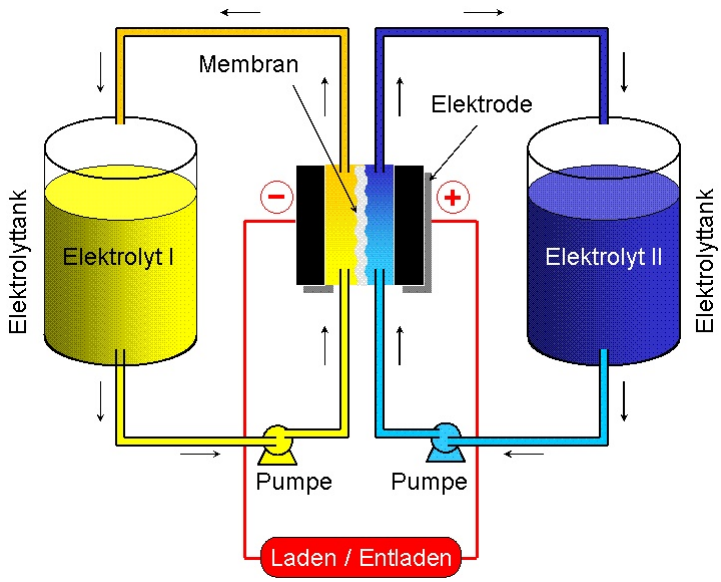

Figure 4.6: Schematic of a flow battery [vi]

[vi] Source, isea: http://www.isea.rwth-aachen.de/en/energy_storage_systems_technology_redox_flow_batteries/, accessed October 2014

For a flow battery the energy stored is defined from the size of the electrolyte storage tanks, while the deciding criteria for power is the size of the cell [20]. The technology is not yet fully commercial, but the energy efficiency is said to be up to 85 % and the power output from 50 kW to 10 MW[23]. One of the major advantages of the flow battery is the fast recharge time, which is achieved through replacing the old electrolytes with a new charged ones [20].

Possible ways of using flow batteries includes frequency regulation, peak shaving and increased security for an intermittent energy system. However, the capital cost are estimated quite high, and lies between 2300-3200 EUR/kW [23].

4.4 Electrical energy storage

4.4.1 Superconducting magnetic energy storage – SMES

In a superconducting magnetic energy storage (SMES) System electrical energy is stored in the electromagnetic field generated by circulating a direct current (DC) in a superconducting electromagnetic coil [20, 24]. The DC is able to circulate the coil due to the superconducting properties of the wires used in the coil. The super conductance is achieved by cooling the wire down to a temperature where the material becomes superconducting. Current can then flow through the wires without any considerable losses due to the frictional forces[24]. The main components of a SMES unit, as can be seen if Figure 4.7, are the superconducting coil, a refrigerator system, DC/AC converter and a vacuum-insulated vessel.

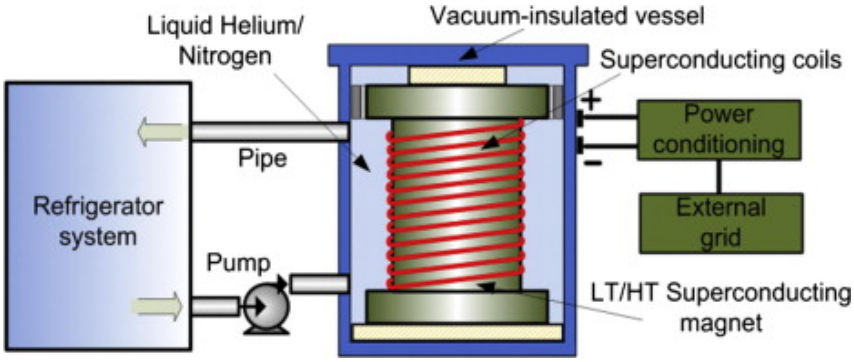

Figure 4.7: Schematic of a superconducting magnetic energy storage system [vii]

[vii] Source: [24]

There are two forms of SMES; low temperature and high temperature. The low temperature SMES operates at temperatures around ≈ 5 K, and the high temperature SMES at ≈ 70 K [24]. However, the technology is by today not yet commercial.

Some of the advantages of the SMES are the high power density, fast response time (down to milliseconds) and a long lifetime (30 years) with a high number of discharges without any significant degradation of the performance [24]. The round-trip is as high as 95 %, the maintenance cost is low and operation safety is high since there are no moving parts in the main system. Power output is typically in between 1 and 10 MW. Due to the fast response time SMES is well suited for improving grid stability and to ensure power quality [23].

Some of the drawbacks are connected to the fast self discharge rate, around 10-15 % a day, high capital cost (7200 USD/kW) [24] and environmental concerns due to the effect of the strong electromagnetic fields generated [23]. In current development increased current density and a higher mechanical strength of the wire are of interest [20].

4.4.2 Supercapacitor

A supercapacitors main components are the two electrodes and the porous membrane that separates them, see Figure 4.8. Electric energy is stored by separating the charge on the surface between the electrodes and the electrolyte. When one electrode is charged an opposite charge is induced in the other electrode [23, 24]. Today supercapacitors are mostly used in finer electronics such as cellphones and computers[20].

The round-trip efficiency of a supercapacitor are in the area of 70-80 %. They operate in a way similar to both traditional batteries and capacitors, but their energy density is lower and their power density is higher than that of batteries [20]. The high power density is a result of a high surface area due to porous material used in the electrodes. A supercapacitor also has a fast self discharge, making them unsuited for long term energy storage. However, their high power density and a fast response time makes them well suited for frequency regulation. Normal values of power output is 100 to 250 kW [23]. One of the major adevantage with the supercapacitor is their long lifetime, due to the small degradation they experience in deep discharge, and they should be able to handle more than than 100.000 cycles[23]. However,

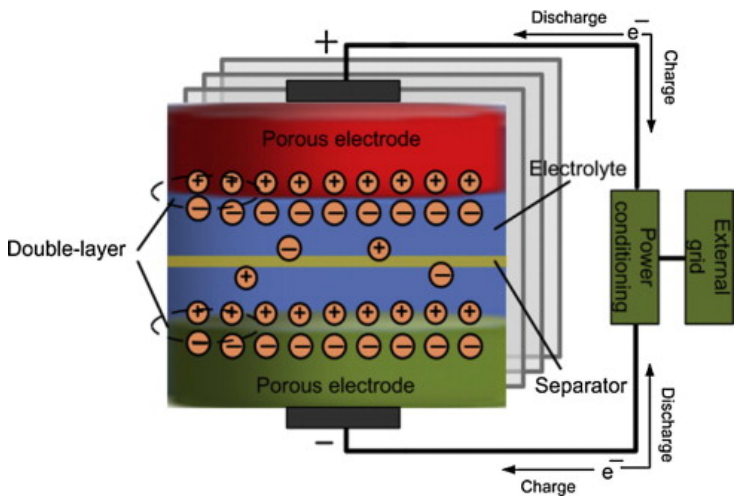

Figure 4.8: Schematic of a supercapacitor [viii]

[viii] Source: [24]

the cost of a supercapacitor lies around 6000 USD/kWh[24], making them too expensive for large scale applications today.

4.5 Summary of different storage technologies

Table 4.2: Summarization of different storage technologies[x]

Technology	Energy Storage Status	Investment cost	Round-trip efficiency	Scale	Storage periods	Usage
PHS	OP	500-4600 USD/kW	70-85 %	Large scale	Long	Load following, frequency regulation, non-spinning reserve, time-shifting and peak shaving
CAES	OP	500-1500 USD/kW	42-54 %	Large scale	Long	Load following, frequency and voltage regulation, spinning reserve, time-shifting and peak shaving
ACAES	R & D	n.a.	70 %	Large scale	Short	Load following, time shift
ICAES	R & D	1000-1500 EUR/kW	80 %	Small scale	Short	Load following, time shift

Table 4.2: Continued

Technology	Energy Storage Status	Investment cost	Round-trip efficiency	Scale	Storage periods	Usage
Flywheel	OP	130-500 USD/kW	80-85 %	Small scale	Short	Frequency regulation and black start
Hydrogen	R & D	1000-2000 USD/kW	20-45 %	Large scale	Long	Load following, time shift, fuel, heating
Methane	R & D	n.a.	20-30 %	Large scale	Long	Load following, time shift, heating
Litium-ion battery	OP	n.a.	80-98 %	Small scale	Short/ long	Frequency regulation
Sodium-Sulphur battery	OP	1420-2500 EUR/kW	75 %	Small scale	Short	Grid stabilisation, load following, black start
Flow battery	R & D	2300-3200 EUR/kW	85 %	Small scale	Short/ long	Peak sheaving, frequency regulation
SMES	R & D	7200 USD/ kW	95 %	Small scale	Short	Grid stabilisation and load following
Super-capacitor	R & D	6000 USD/ kW	70-80 %	Small scale	Short	Frequency regulation
Sensible heat	OP	n.a.	n.a.	All scales	Short/ long	Heat
Latent heat	OP	n.a.	n.a.	All scales	Short/ long	Heat

[x]based on data presented in Chapter 3 and 4

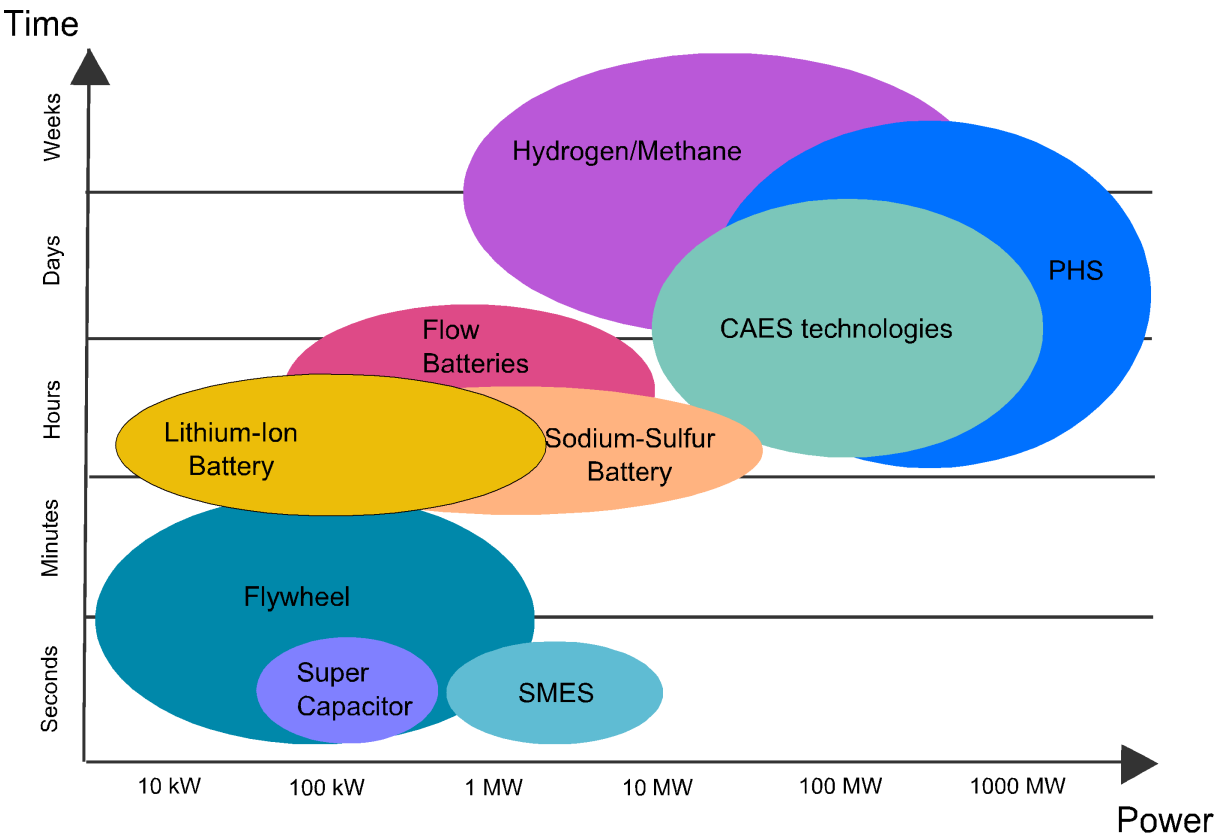

Figure 4.9: Sketch of generation time and power output [ix]

[ix] Made from data presented in Chapter 3 and 4

Chapter 5

Thermodynamics

The purpose with this chapter is to give a short introduction to the most fundamental thermodynamic concepts that creates the foundation needed to understand the operation of an ACEAS power plant. For further study of these concepts it is referred to [44] and [45].

5.1 The first law of thermodynamics

One of the fundamental rules of thermodynamics is the conservation of energy, or the first law of thermodynamics. The conservation of energy states that the total energy in an isolated system remains constant. For a closed system experiences change in energy, the change of system energy, ΔE_{sys}, must equal the energy transferred across the system boundary in the form of work and heat. This relation is expressed in Equation (5.1). Heat is here defined as positive into the system, while work is defined positive when done by the system [44].

$$\Delta E_{sys} = \Delta E_{kin} + \Delta E_{pot} + \Delta U = Q - W \tag{5.1}$$

The principal difference between an open and a closed system is the fact that in an open system mass can be transferred across the system boundaries. The conservation law of mass (5.2) must then be applied[44].

$$\frac{dm_{cv}}{dt} = \dot{m}_i - \dot{m}_o \tag{5.2}$$

Equation (5.2) states that the change in the open system control volume mass must equal the rate of change in mass in and out of the control volume. The closed system energy balance (5.1) can together with the conservation of mass be modified to create the open system energy rate balance. Here the terms of potential, kinetic and internal energy are also written out[44].

$$\frac{dE_{cv}}{dt} = \dot{Q} - \dot{W} + \dot{m}_i\left(u_i + \frac{C_i^2}{2} + gz_i\right) - \dot{m}_o\left(u_o + \frac{C_o^2}{2} + gz_o\right) \tag{5.3}$$

The term for work in (5.3) can be divided into two entities (5.4). One entity associated with the work done by the fluid pressure at system inlets and outlets and the other entity associ-

ated with all other forms of work denoted $\dot{W}_{cv}$ [44].

$$\dot{W} = \dot{W}_{cv} + \dot{m}_o(p_o v_o) - \dot{m}_i(p_i v_i) \tag{5.4}$$

The expression for work can be inserted to Equation (5.3), and together with the relation between internal energy and enthalpy in Equation (5.5), Equation (5.6) can be derived. The equation is here written in a general form, with mass flow entering and exiting at several locations through the boundary [44].

$$h = u + pv \tag{5.5}$$

$$\frac{dE_{cv}}{dt} = \dot{Q}_{cv} - \dot{W}_{cv} + \sum_i \dot{m}_i\left(h_i + \frac{C_i^2}{2} + gz_i\right) - \sum_o \dot{m}_o\left(h_o + \frac{C_o^2}{2} + gz_o\right) \tag{5.6}$$

The use of enthalpy is here mostly for convenience, simplifying the algebraic balance and due to the fact that enthalpy is given in most tables together with other properties. Equation (5.6) is a general form of the energy rate balance stating that the change in energy within a control volume equals the rate of energy transfer across the boundary [44].

If the system operates in steady state, the left-hand side of Equation (5.6) is zero, this is however not the case for ACAES-systems that behave transiently. Adiabatic systems operate without heat transfer between the system and its surroundings. For an ACAES system the change of energy can be obtained by integrating the energy rate balance (5.6) over the given time. Information is then needed about time dependence of work transfer rates, mass flow rates and mass flow states at control volume inlet and outlet [44]. In the total system energy rate balance the heat transfer rate would be cancelled since the system is adiabatic. However, different components of the ACAES plant are not undergoing an adiabatic process. To find the rate of energy change over these components, such as the heat exchangers, the rate of heat change over these components boundaries are needed. Heat losses will also always occur in all real system, so it should be made clear that a perfect adiabatic system only is possible in theory. But with good insulation resulting in small enough heat losses it is possible to come close to an adiabatic system.

5.2 The second law of thermodynamics

The second law of thermodynamics allow us among other to predict the direction of processes, establish conditions for equilibrium and determine the theoretical performance of cycles. There are several alternative statements of the second law, the Clausius-statement proclaims:

> *"It is impossible for any system to operate in such a way that the sole result would be an energy transfer by heat from a cooler to a hotter body."* [44]

The Clausius-statement says that heat cannot be transferred from a cooler body to a hotter body by itself. The heat transfer needs to be carried out by some other effect within the

system.

5.2.1 Irreversible and reversible processes

Irreversible processes

As mentioned above, is one of the most useful applications of the second law of thermodynamics to determine the theoretical performance of a system, allowing insight to potential areas of improvement in real systems. In all real systems losses will always occur, these losses are referred to as irreversibilities. A process is irreversible if it cannot be returned to its initial state without inflicting change to its surroundings. Change to its surroundings can here mean the need of applying work to restore the system. The second law can be used to minimize irreversibilities. Typical examples of irreversibilities can be; spontaneous heat transfer, spontaneous chemical reaction, spontaneous mixing of matter, unrestrained expansion of a gas and friction [44].

Reversible processes

The opposite of an irreversible process is a reversible processes. Reversible processes are theoretical, and does not occur in reality. The Carnot efficiency, Equation (5.7), expresses the efficiency of a reversible process operating between two thermal reservoirs.

$$\eta_{max} = 1 - \frac{T_C}{T_H} \tag{5.7}$$

T_C and T_H represent the temperature of the cold and hot thermal reservoir respectfully. The Carnot efficiency is the maximum possible efficiency for a power cycle operating between the two thermal reservoirs. From Equation (5.7) it becomes clear that the Carnot efficiency increases with an increase in T_H or a decrease in T_C. A gas turbine can be seen as a power cycle operating between the two thermal reservoirs. T_H and T_C, the two thermal reservoirs, can then be represented by the gas turbine inlet and outlet temperature respectfully.To minimize the thermal losses, the temperature difference between the two reservoirs must be as big as possible. The only practical way to do this is to increase T_H, since T_3 is restricted to the temperature of the surroundings. It should be mentioned that the Carnot efficiency does not include the internal losses such as flow and friction losses, nor the mechanical losses such as bearing friction [44].

5.2.2 Entropy and the entropy rate balance

Entropy

The second law of thermodynamics can better be understood by introducing the property entropy, denoted S. For any system undergoing a process from one state to another, there is a change in entropy. Entropy can be explained as a measurement to describe distribution of energy. An example of this can be the spontaneous heat flow between two thermal reservoirs.

This process can occur until the two reservoirs are at the same state. The thermal energy has been equally distributed between the two [44]. The definition of entropy change can be seen in Equation (5.8):

$$S_2 - S_1 = \left(\int_1^2 \frac{\delta Q}{T} \right)_{\substack{int \\ rev}} \tag{5.8}$$

The subscript in Equation (5.8) stands for internal reversible. Internal reversible systems don't have internal irreversibilities. Entropy is a property, meaning that the change in entropy is the same from state 1 to state 2 for both internal reversible and irreversible systems. The change in entropy can never be a negative. Negative entropy would violate the second law of thermodynamics, allowing heat to flow from the cold reservoir to the hot reservoir. If the change in entropy is zero there are no irreversibilities within the system, the process is then isentropic [44].

Entropy balance

Entropy, like mass, is an extensive property, meaning that it can be transported across a system boundary. The entropy rate balance for a control volume can be seen in Equation (5.9).

$$\frac{dS_{cv}}{dt} = \sum_j \frac{\dot{Q}_j}{T_j} + \sum_i \dot{m}_i s_i - \sum_o \dot{m}_o s_o + \dot{\sigma}_{cv} \tag{5.9}$$

If the system operates in steady state, the left-hand-side of the equation is zero. The term $\dot{\sigma}_{cv}$ is the rate of entropy production, created by irreversibilities. $\dot{Q}_j / T_j$ is the rate of entropy accompanying the heat transfer across system boundaries. The last two terms represent entropy accompanying the mass flow across system boundaries [44].

5.2.3 Isentropic efficiencies

Isentropic efficiencies are used to compare the difference between real and isentropic (ideal) performance of a component, such as turbines, compressors and pumps. The isentropic efficiency for a turbine can be seen in Equation (5.10). It is defined as the real work divided by isentropic work. Typical values for the isentropic turbine efficiency range from 0.7 to 0.9 [44].

$$\eta_{t,is} = \frac{\dot{W}_{cv}/\dot{m}}{(\dot{W}_{cv}/\dot{m})_{is}} \tag{5.10}$$

The isentropic efficiency for a compressor and a pump can be seen in Equation (5.11) and (5.12) respectfully. They are defined as the isentropic work divided by real work. Typical values for compressor isentropic efficiency range from 0.75 to 0.85 [44].

$$\eta_{c,is} = \frac{(-\dot{W}_{cv}/\dot{m})_{is}}{(-\dot{W}_{cv}/\dot{m})} \tag{5.11}$$

$$\eta_{p,is} = \frac{(-\dot{W}_{cv}/\dot{m})_{is}}{(-\dot{W}_{cv}/\dot{m})} \tag{5.12}$$

5.3 Ideal gas and polytropic process

5.3.1 The ideal gas model

The ideal gas law, given in Equation (5.13), are the equation describing a theoretical ideal gas.

$$pV = n\Re T \tag{5.13}$$

It can be used as an approximation for gases where the pressure is small relative to the critical pressure, or when the temperature is high relative to the critical temperature. When a gas is assumed ideal, the enthalpy and internal energy only depends on temperature [44].

Specific heats of an ideal gas

The specific heat tells how much heat is needed to raise the temperature of a given mass by one degree Celsius. c_v is the specific heat capacity for heat added at constant volume, can be seen in Equation (5.14). The specific heat when heat is added at constant pressure, c_p, can be seen in Equation (5.15). As mention are the internal energy and enthalpy for ideal gasses only dependent on temperature, thus are the specific heats only a function of temperature[44].

$$c_v(T) = \frac{du}{dT} \tag{5.14}$$

$$c_p(T) = \frac{dh}{dT} \tag{5.15}$$

In Equation (5.16) is the relation between the specific heat shown.

$$c_p(T) = c_v(T) + \Re \tag{5.16}$$

The specific heat ratio is defined as:

$$k = \frac{c_p(T,p)}{c_v(T,p)} \xrightarrow[gas]{ideal} k = \frac{c_p(T)}{c_v(T)} \tag{5.17}$$

5.3.2 Polytropic process

A polytropic process follows the relation $pv^n = constant$, where n is a constant defined for the specific process. A polytropic process is often referred to as a quasi-stationary process, meaning that changes in the process taking place at small stages all reaching equilibrium. A polytropic process between two states can be written as [44]:

$$p_1 v_1^n = p_2 v_2^n \tag{5.18}$$

where v is the specific volume. Equation (5.18) can be rearranged:

$$\frac{p_2}{p_1} = \left(\frac{v_1}{v_2}\right)^n \tag{5.19}$$

If ideal gas properties are assumed for the medium, using Equation (5.17), Equation (5.19) changes to the polytropic pressure-temperature relation:

$$\frac{T_2}{T_1} = \left(\frac{p_2}{p_1}\right)^{\frac{n-1}{n}} \tag{5.20}$$

Polytropic exponent

In Figure 5.1 different values of the polytropic exponent can be seen. The special case where n equals the specific heat ratio k, the specific heats are constant and the process is isentropic. When $n = 0$ the process is taking place at constant pressure. For $n = 1$ the process is isothermal, meaning pressure increasing at constant temperature. Values of $n = \pm\infty$ correspond to a constant volume process[44].

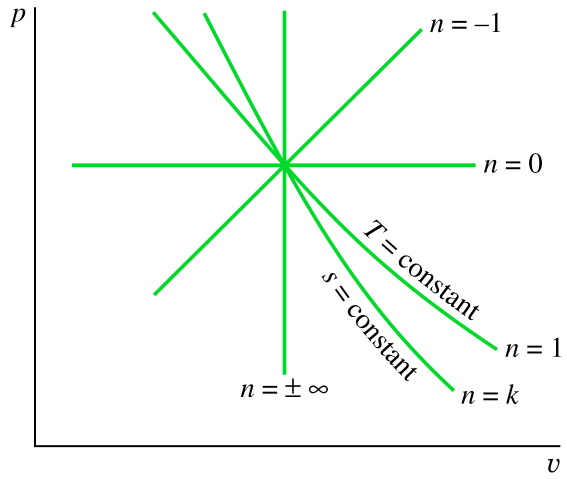

Figure 5.1: P-v diagram of a polytropic process [i]

[i] Source: [44]

Equation (5.18) can be rearranged to find an expression for the polytropic exponent.

$$n = \frac{ln\left(\frac{p_1}{p_2}\right)}{ln\left(\frac{v_2}{v_1}\right)} \tag{5.21}$$

5.3.3 Polytropic efficiency

In a temperature-entropy diagram, it can be seen that the vertical distance between the constant pressure lines increases with an increase in entropy. This change in vertical distance gives an increase in the isentropic efficiency for an increase in designed turbine pressure ratio. It has the opposite effect for compressors. When a system operates over a range of pressure ratios, such as compressors and turbines, it is common to use the polytropic efficiency instead of the isentropic efficiency. The polytropic efficiency is defined to be the isentropic efficiency of an infinitely small stage in a process. The polytropic efficiency then remains constant for each stage throughout the process[45].

An expression for the polytropic efficiency for a compressor and a gas turbine can be seen in equations (5.22) and (5.23) respectfully [45].

$$\eta_{p,c} = \frac{n}{n-1}\frac{k-1}{k} \tag{5.22}$$

$$\eta_{p,t} = \frac{n-1}{n}\frac{k}{k-1} \tag{5.23}$$

5.3.4 Real gas behavior

When working with real gas the traditional approach of performance calculation for turbomachinery, based on specific heats, may result in major deviations. It is then a need to distinguish between the polytropic temperature exponent n_T and the polytropic volume exponent n_v defined as [46]:

$$n_T = \frac{1}{1 - \frac{p_1}{T_1}\left(\frac{\delta T}{\delta p}\right)_{\eta_p}} \tag{5.24a}$$

$$n_v = -\frac{v}{p}\left(\frac{\delta p_1}{\delta v_1}\right)_{\eta_p} \tag{5.24b}$$

For ideal gas $n = n_T = n_v$

With the new definitions of n_T and n_v one then needs to separate Equation (5.19) and (5.20) which becomes:

$$\frac{p_2}{p_1} = \left(\frac{v_1}{v_2}\right)^{n_v} \tag{5.25}$$

$$\frac{T_2}{T_1} = \left(\frac{P_2}{P_1}\right)^{\frac{n_T-1}{n_T}} \tag{5.26}$$

The polytropic exponents vary throughout the expansion or compression process. An approximation of the polytropic exponent for a process can be found through an iterative procedure, i.e. Schultz method for compression.

Analytically the polytropic head is defined as:

$$H_p = \int_1^2 v dp \tag{5.27}$$

Since the polytropic exponent varies throughout the process is it impossible to calculate an exact polytropic head[46].

An approximation to the polytropic head for a compressor is given in Equation (5.28):

$$H_{p,c} \approx f \frac{n_v}{n_v - 1} \frac{Z_1 \Re_0 T_1}{MW} \left[\left(\frac{p_2}{p_1} \right)^{\frac{n_v - 1}{n_v}} - 1 \right] \tag{5.28}$$

For an expansion process the polytropic head becomes:

$$H_{p,t} \approx \frac{n}{n-1} \frac{Z_1 \Re_0 T_1}{MW} \left[1 - \left(\frac{p_2}{p_1} \right)^{\frac{n-1}{n}} \right] \tag{5.29}$$

The expression for turbine and compressor fluid power is then:

$$\dot{W}_{fluid,t} = \dot{m} H_{p,t} \eta_p \tag{5.30}$$

$$\dot{W}_{fluid,c} = \dot{m} H_{p,c} \eta_p \tag{5.31}$$

For electric power generated/consumed:

$$\dot{W}_{el,t} = P_t \eta_{mech} \eta_{gen} \tag{5.32}$$

$$\dot{W}_{el,c} = P_c \eta_{mech} \eta_{motor} \tag{5.33}$$

5.4 Ideal gas turbine cycle

The main difference between a traditional gas power plant and a CAES power plant is the fact that CAES does not operate both compressor and turbine at the same time, but rather uses electricity from the grid to compress and store air. This means it doesn't need to use any turbine work for compression. However, the main components and operation of the two are similar. For an ideal gas turbine cycle, such as the ideal Joule-Brayton cycle, some assumption are given below [45]:

1. The compression and expansion process are adiabatic and reversible.
2. Change in kinetic energy of fluid in each component is negligible.
3. No pressure losses in the components.

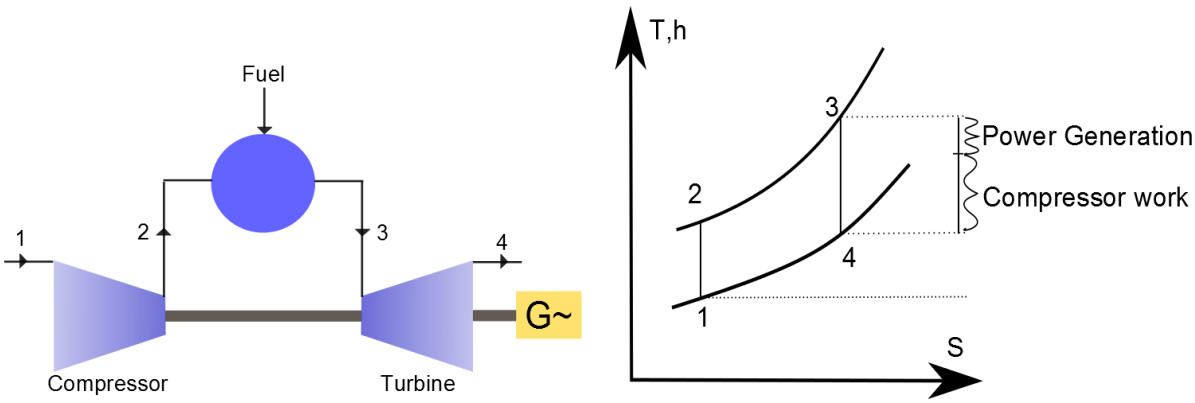

(a) Components map (b) T(/h)-S Diagram

Figure 5.2: Joule-Brayton cycle

4. The working fluid have a constant composition throughout the cycle and is an ideal gas.
5. The mas flow of gas throughout the cycle is constant.
6. Complete heat transfer in a heat exchanger, meaning that the temperature rise on cold side is at maximum level and equal to the temperature drop on hot side.

Figure 5.2 shows an open Joule-Brayton gas turbine cycle. Air is drawn into the compressor at atmospheric pressure, and then compressed isentropically to a higher pressure before entering the combustion chamber. In the combustion chamber the air is mixed with fuel before ignition. The warm exhaust gas leaves the combustion chamber and expands isentropically through the gas turbine. Some of the work produced by the turbine are used to drive the compressor, while the rest can be utilized for electricity generation [44].

Using Equation (5.6) together with the assumption of an ideal gas cycle, gives the steady flow energy equation:

$$\dot{Q} = \dot{m}_1(h_2 - h_1) + \dot{W} \tag{5.34}$$

This is the general equation of the cycle, with subscript 1 denoting the inlet of cycle and subscript 2 the outlet. For the Joule-Brayton cycle, the componential equation system becomes [45]:

$$\dot{W}_{1,2} = -\dot{m}_1(h_2 - h_1) = -\dot{m}_1 c_p(T_2 - T_1) \tag{5.35a}$$

$$\dot{Q}_{2,3} = \dot{m}_3(h_3 - h_2) = \dot{m}_3 c_p(T_3 - T2) \tag{5.35b}$$

$$\dot{W}_{3,4} = \dot{m}_3(h_3 - h_4) = \dot{m}_3 c_p(T_3 - T_4) \tag{5.35c}$$

The cycle efficiency is defined as:

$$\eta = \frac{\text{net work output}}{\text{heat supplied}} = \frac{\dot{m}_3 c_p (T_3 - T_4) - \dot{m}_1 c_p (T_2 - T_1)}{\dot{m}_3 c_p (T_3 - T_2)} \tag{5.36}$$

One of the deciding factors when it comes to the size of the power plants is the specific work. The specific work is dependent on both the pressure ratio and the maximum cycle temperature T_3. T_3 is the inlet temperature to the turbine, which is limited by the material properties of the turbine blades. The equation for specific work is:

$$\frac{\dot{W}}{\dot{m}} = \dot{m}_3 c_p (T_3 - T_4) - \dot{m}_1 c_p (T_2 - T_1) \tag{5.37}$$

The highest specific work possible is given when the compressor and turbine outlet temperature are equal [45].

5.5 CAES Evaluation Criteria

The energy ratio shows the difference between electric energy consumed and electric energy generated.

Energy rate [47]:

$$ER = \frac{W_c}{W_t} \tag{5.38}$$

The heat rate, only valid for DCAES power plants, gives the heat input [kJ] required to generate a given amount of energy [kWh].

Heat rate [45]:

$$HR = \frac{Q_f}{W_t} \tag{5.39}$$

The overall efficiency or the round-trip efficiency [47]:

$$\eta_{round-trip} = \frac{W_t}{Q_f + W_c} \tag{5.40}$$

For a ACAES and ICAES power plant, no external heat is added and the round-trip efficiency equals:

$$\eta_{round-trip} = \frac{W_t}{W_c} \tag{5.41}$$

From the expression of the round-trip efficiency, can it be seen that it is the inverse of the energy ratio, ER. The thermal efficiency of the TES can be defined using the first law of thermodynamics:

$$\eta_{th,TES} = \frac{Q_o}{Q_i} \tag{5.42}$$

An estimate of the additional price of CO_2 emissions for diabatic CAES power plants can be

found by finding the average of allowance price, Π_{CO_2}.

$$\Pi_{CO_2} = 7.06 \frac{€}{10^3 \text{kg}} \frac{\text{kg}_{CO_2}}{\text{MWh}} \left[\frac{€}{\text{MWh}} \right] \tag{5.43}$$

The price used here,7.06 €/tonne CO_2 , is the average auction price of CO_2-allowances in the period 8/1 to 15/6 in 2015 at the EEX [9]:

Chapter 6

Components

6.1 Compressor

6.1.1 Radial versus axial

The two major configurations for turbomachinery are axial and radial design. In the radial compressor (or centrifugal compressor) air is being sucked into the compressor in the axial direction, and then exits perpendicular to the axial. In an axial compressor, the air enters and exits in the axial direction. For a given frontal area, the axial compressor has the possibility of a much larger flow rate than a radial compressor, and the pressure ratios can also be significantly higher. This results in axial compressor being used where high power is needed, while the radial compressor is used for smaller mass flows and pressure ratios [45].

6.1.2 Compressor characteristics

The performance of a compressor can be described by plotting curves of the stagnation pressure and temperature ratio separately versus the non-dimensional mass flow. The curves are plotted for several fixed values of the non-dimensional rotational speed, creating two sets of curves. Using these two sets of curves and the relation (6.1), the isentropic efficiency can be plotted for constant speed curves versus the non-dimensional mass flow. The resulting plot can be seen in Figure 6.1 [45].

$$\eta_c = \frac{T_{02,is} - T_{01}}{T_{02} - T_{01}} = \frac{\frac{p_{01}}{p_{02}}^{\frac{k-1}{k}} - 1}{\frac{T_{02}}{T_{01}} - 1} \tag{6.1}$$

The surge region is located at the left hand side of the surge line which can be seen in Figure 6.1. Surge occurs when the pressure after the compressor is higher than the pressure delivered by the compressor. Meaning the compressor can no longer maintain a forward flow. If driven into surge, a back flow of air, and some time fuel from the combustion chamber, can find its way in reverse through the compressor. The back flow of air causes pressure downstream to fall, giving the compressor the opportunity to catch up. If the compressor is still in the surge area the process repeat itself, this creates violent aerodynamic pulsation

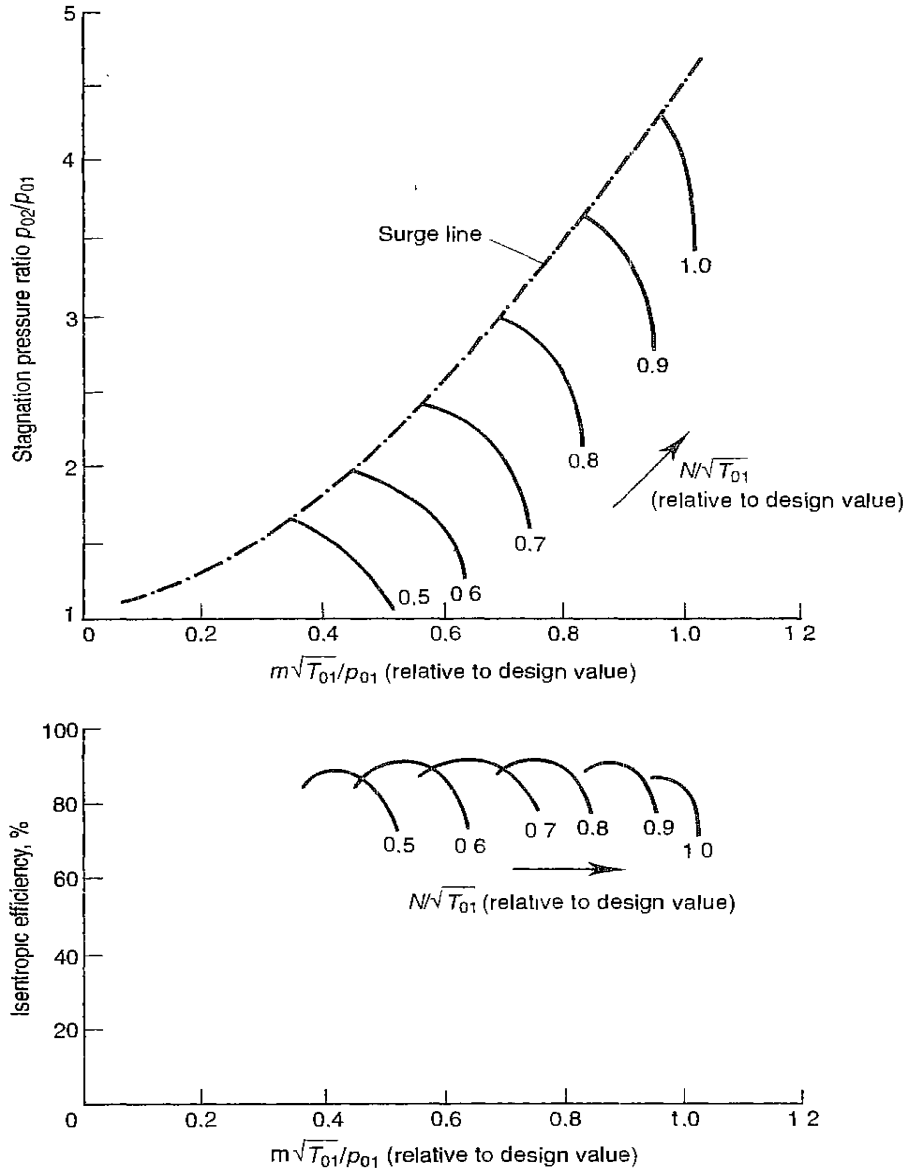

Figure 6.1: Axial compressor characteristics [i]

[i]Source: [45]

that extends through the entire machine [45]. On the right hand side of the speed lines in Figure 6.1 is the choke point. If a line where drawn between the choke points of all the different speed lines, it would create a choke line. Choke occur when the maximum mass flow through the compressor is reached. Operation on the right hand side of the chock line is impossible, since no more mass flow can pass through the compressor. The maximum volume flow rate through the compressor is limited by the inlet cross section area [45]. When designing a compressor, it should be design for the highest possible pressure ratio, minimizing the risk of surge operation.

6.2 Gas turbine

6.2.1 Radial versus axial

As for the compressors there are two main categories of turbines; axial flow and radial flow. The axial flow turbine is the most common used today. However, for small flows through an axial turbine, the blade height becomes so small that it becomes difficult to maintain a small clearance to the turbine housing inner wall. There is then a significant drop in the efficiency. Radial flow turbines are much better at handling smaller flows and are used for smaller power ranges. For higher power the cost and size of the radial turbine increases and the efficiency becomes similar to that of the axial turbine [45].

6.2.2 Turbine characteristics

As the in the case of compressor characteristics in Section 6.1.2 it is possible to calculate the performance of a turbine over a wide range of operations. Normally this is done by plotting the isentropic turbine efficiency against dimensionless mass flow and dimensionless pressure ratio. The efficiency is quite consistent over a wide range of rotational speed and pressure ratios. The maximum value for the reduced mass flow is reached when the turbine choke. The difference between the speed lines for the reduced mass flow is very small in both the unchoked region and the choked region, and it is often presented by one independent speed line [45].

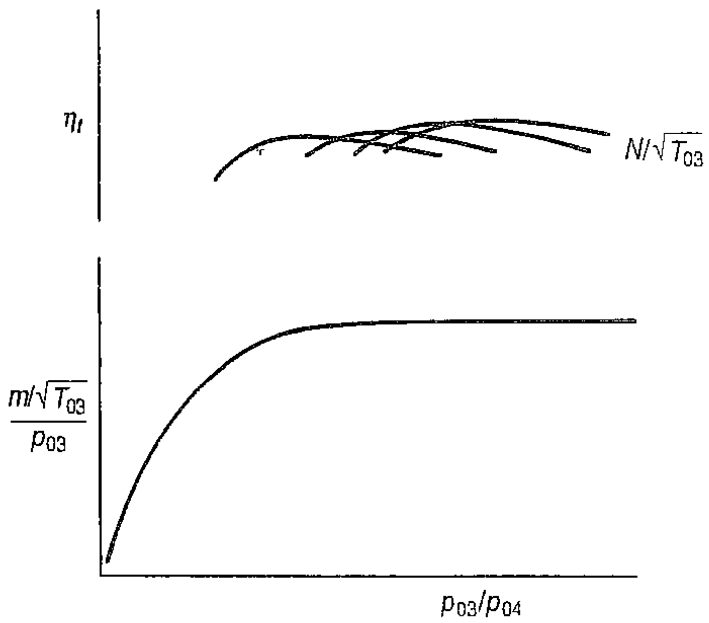

Figure 6.2: Gas turbine characteristics [ii]

[ii] Source: [45]

6.3 Thermal storage tank

6.3.1 Heat transfer mechanisms

As discussed in Section 5.2 will heat only transfer from the high to the low temperature reservoir unless energy is added to reverse the process. For any thermal storage tank, there will be a loss of heat driven by the temperature difference between the thermal storage medium and the surroundings. The heat loss occurs through three mechanisms; convection, conduction and radiation.

Convection

Convection heat transfer can be expressed through Newton's law of cooling. Convection heat transfer occurs between solid and fluid, or fluid and fluid. It is a result of diffusion and bulk motion of the fluid [48].

$$Q = \mathrm{h}(T_s - T_\infty) \tag{6.2}$$

Conduction

Conduction is a form of heat transfer taking place through a body or in between two stationary bodies. The heat transfer trough a solid wall can be expressed with Fourier's law [48].

$$Q = -\mathrm{k}A\frac{dT}{dx} \tag{6.3}$$

k is the thermal conductivity. The thermal conductivity is specific to the material the heat flows through.

Radiation

Radiation is a form of heat transfer where energy is transmitted through electromagnetic waves. Equation (6.4) is a balance of the thermal energy increased from absorption and decreased due to emission from the body.

$$Q = \epsilon\sigma(T_s^4 - T_\infty^4) \tag{6.4}$$

ϵ is the surface emissivity, and σ is the Stefan-Boltzmann constant ($\sigma = 5.67 \cdot 10^{-8} W/m^2$) [48].

6.3.2 Thermal losses

For an ACAES power plant the thermal losses from the thermal energy storage tanks plays a crucial role for the system round-trip efficiency. The thermal losses from the tanks depend on the insulation, storage medium and geometry of the tank. The general equation for the thermal loss is:

$$Q_{loss} = \mathrm{U}A\Delta T \tag{6.5}$$

Here U is the overall heat transfer coefficient, A is the surface are over which the heat transfer mechanism take place and ΔT is the temperature difference between the inside of the tank and the surroundings. The overall heat transfer coefficient is defines as [48]:

$$\mathrm{U}A = \sum \frac{1}{R_{tot}} \tag{6.6}$$

R_{tot} is the total thermal resistance of the body. The total thermal resistance is a sum of resistance caused by all heat transfer mechanisms taking place.

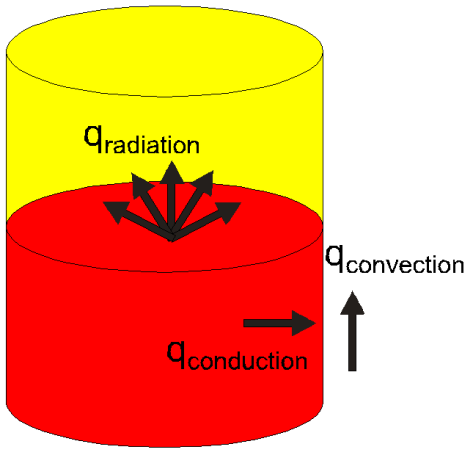

Figure 6.3: Thermal storage tank heat transfer mechanisms

Figure 6.3 shows a thermal storage tank half full of some thermal storage medium. When the tank is half-full, heat transfer by radiation between the thermal medium and the storage tank inner wall takes place. Heat is conducted through the storage medium and the tank wall and convection takes place at the outside. If the tank is well insulated may the outside radiation losses be neglected. If the storage medium is entering or exiting the storage tank, heat transfer by convection also takes place at the inner wall. When the tank is full there is no more mass entering the storage tank, therefore no more convection heat transfer on the inside wall. Inside radiation losses can also be neglected.

The thermal resistance for heat transfer taking place through a wall are given in Equation (6.7) [48]:

$$R_{conv} = \frac{1}{\mathrm{h}A} \tag{6.7a}$$

$$R_{cond} = \frac{L_w}{\mathrm{k}A} \tag{6.7b}$$

$$R_{rad} = \frac{1}{\mathrm{h}_{rad}A} \tag{6.7c}$$

6.4 Heat exchanger

A heat exchanger transfer heat between two fluids without the fluid mixing. Heat transfer between the fluids takes place through conduction, convection and radiation. When designing a heat exchanger there are two requirements, energy vs. economy, in conflict. The goal of the heat exchanger is to recycle as much heat as possible, but to do so the heat exchanger needs a large surface area. A large surface increases the volume of the heat exchanger, increasing building and operation cost [49]. There are many different designs for heat exchangers and they are classified by the arrangement of the flow. In a parallel flow design are the fluids entering the heat exchanger at the same direction flowing parallel to each other. In a counterflow design are the fluids flowing in the opposite direction. The third configuration is cross-flow, where the fluids flow perpendicular [48].

The heat transfer can be expressed as a function of the overall heat transfer coefficient (U), heat transfer surface area (A) and the log mean temperature (ΔT_{lm}) , see Equation (6.8):

$$Q = \mathrm{U} A \Delta T_{lm} \tag{6.8}$$

The a counterflow heat exchanger the ΔT_{lm} is higher than for parallel flow. This means that for a given overall heat transfer coefficient, the heat transfer surface area, A, is smaller for counterflow than for parallel flow heat exchangers [48].

The log mean temperature is expressed in Equation (6.9):

$$\Delta T_{lm} = \frac{(T_{1,i} - T_{2,o}) - (T_{1,i} - T_{2,o})}{ln\left(\frac{T_{1,o}T_{2,i}}{T_{1,i}T_{2,o}}\right)} \tag{6.9}$$

index 1 and 2 are here used to extinguish the two flows, and i and o for inlet and outlet respectfully [49].

6.5 Combustion chamber

The compressor is one of the most critical components for a gas turbine, as well for a CAES power plant. It must be able to operate at high temperatures, deliver the correct temperature to the turbine as well as create the minimum amount of pollutants over its lifetime. Pressure losses are normally in the area of 2-8 %, while the combustion efficiency is as high as 99 % [45].

6.5.1 Stability limits

To a combustion chamber there is both a rich and lean (or weak) limit of the air/fuel ratio for which within the combustion process can take place. The limits are in general defined for the air/fuel ratios where the flame is blown out. However, instabilities may occur long before bow-out of the flame. Operation in the instability areas is undesirable since the instabilities

may create aerodynamic vibrations that can shorten the life of both the combustion chamber and turbine blading. The stable flame area decreases with an increase in air velocity [45].

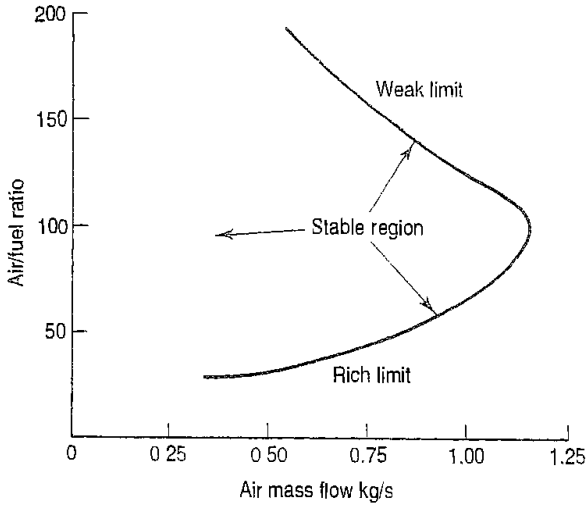

Figure 6.4: Combustion stability limits [iii]

[iii] Source: [45]

When designing a combustion chamber different operating conditions needs to be accounted for such as acceleration or deceleration. When a gas turbine is accelerated, there is a rapid increase in fuel mass flow; while the air fuel flow is lagging behind until the engine has reached is new speed. This causes a lower air/fuel ratio [45].

6.5.2 Emissions

The equation for a stoichiometric combustion is given in Equation (6.10).

$$C_xH_y + (x + \frac{y}{4}O_2 \rightarrow xCO_2 + \frac{y}{2}H_2O) \tag{6.10}$$

Equation (6.10) assumes a complete combustion of fuel and air, resulting in CO_2 and H_2O as the only by-products. When the combustion process is incomplete, small amounts of CO, NO_x and unburned hydrocarbons (UHC) may occur. If the fuel contains sulphur (S), SO_x will also be a by-product [45]. The by-products of an incomplete combustion; CO, NO_x, SO_x and UHC are unwanted, but quite often inevitable. In Figure 6.5 the relation between NO_X, CO and UCH can be seen. NOx emission increases greatly with rising flame temperature, which has a theoretical maximum at stoichiometric conditions, decreasing both at rich and lean mixtures. The formation of CO and UHC behaves opposite to the NOx formation, increasing at both rich and lean mixtures with a low at stoichiometric combustion [45].

It is not only the flame temperature and mixture composition that effects the formation of pollutants. The residence time of the fuel in the combustor also has a role to play. The residence time is increasing with an increased combustor cross-sectional area or volume. NOx formation slightly increases with residence time, while CO and UHC decrease [45].

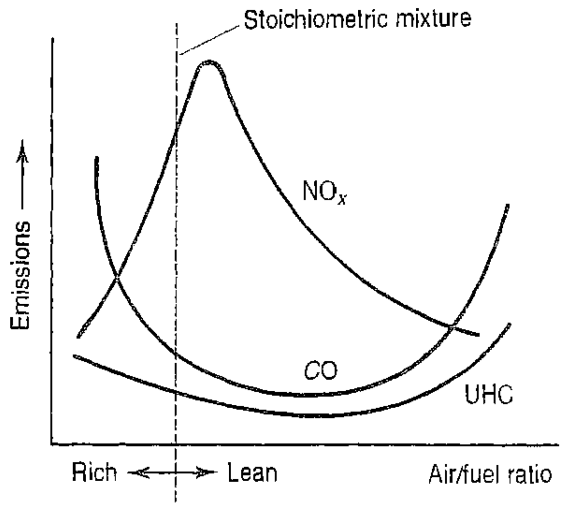

Figure 6.5: Pollution from combustion [iv]

[iv] Source: [45]

Reduction of emission

Today there are three methods for minimizing emissions: water injection, selective catalytic reduction and dry low NO_x systems [45]:

1. Water injection systems use water to decrease the flame temperature and thus reducing the formation of NO_x. However, this also increases the formation of CO and UHC emissions. The amount of water needed is also very high, and therefor unsuited for areas where water is scarce.

2. Selective catalytic reduction (SCR) uses a catalyst together with ammonia (NH_3) to convert NO_x into N_2 and H_2O. However, the catalytic reaction occurs at a low temperature and over a small temperature range (285-400°C). It can therefor only be used with a waste heat recovery system. There are a lot of problems in relation to SCR, such as increased capital costs, control of NH3 flow, and difficulties handling a variable flow.

3. Dry low NO_x methods use no water. Instead they focus on the geometry of the combustion chamber, dividing the fuel mass flow into two separate parts. The fuel mass flow is then fed into two distinct combustion zones. The first combustion zone is functioning as start-up and idling, while the second zone is the main stage of combustion and handles the bulk fuel flow.

6.5.3 Heating values

The heating value of a fuel is equal to the magnitude of the enthalpy of combustion, $\bar{h}_{RP}$. The enthalpy of combustion is defined as the enthalpy difference between products and re-

actants after a complete combustion at a given pressure and temperature[44].

$$\bar{h}_{RP} = \sum_{P} n_o \bar{h}_o - \sum_{R} n_i \bar{h}_i \tag{6.11}$$

n is the number of moles per fuel of the respective products and reactants, $\bar{h}$ is the enthalpy per mole of respective products and reactants. There are two definitions of heating values, lower and higher heating value. The lower heating value is found when all water formed during combustion is vapour, while the higher heating value is found when all water is liquid[44].

6.6 Pumps

The basic function of a pump is to change mechanical work into fluid motion. There are a waste number of different pump configurations, but they can be categorized in two main groups; momentum-change pumps and positive displacement pumps. Momentum-change pumps increases the momentum of the fluid as it passes through the impeller. When leaving the impeller, the increased velocity is converted to higher pressure through a diffusor [50]. Momentum pumps can handle large flow rates and have a steady discharge, but are bad at handling high viscosity liquids and high pressures[51]. A positive displacement pump traps a given volume of fluid at the inlet and then forces the fluid forward by changing the volume. Positive displacement pumps are good at handling high viscous liquid and high pressure ratio, but they have a lower flow rate [51].

The power needed for a pump is given in Equation (6.12)

$$\dot{W}_{pump} = \frac{\dot{m} v_{sat}(T_{in})(p_o - p_i)}{\eta_{pump}} \tag{6.12}$$

where η_{pump} is the pump efficiency.

6.6.1 Pump characteristics

Figure 6.6 shows typical pump performance curves plotted for constant rotational speed, with the discharge Q as independent variable and the head (H), break horsepower and efficiency as dependent variables[51].

If the pump head characteristic have a positive slope to the left for the best operating point it can cause pressure oscillation and back flow if the pump is operated in that area. If operated to far right for the best operating point, cavitation may occur. The horsepower steadily increases with flow rate, but could sometimes rise significantly after the best operating point, creating the need of larger motors driving the pump. When it comes to the efficiency is it desirable that the efficiency curve is as flat as possible around the best operating point, creating a wide range with efficient operation [51].

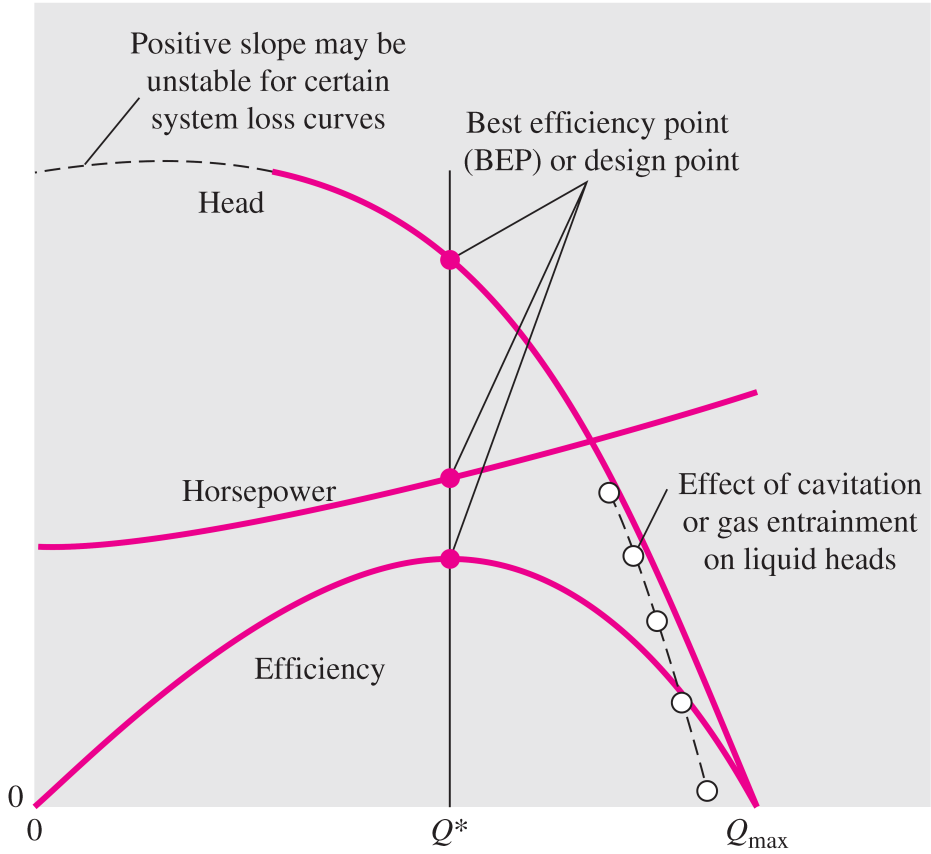

Figure 6.6: Centrifugal pump performance curve [v]

[v] Source: [51]

Chapter 7

EBSILON®Professional and model assumptions

The modeling tool used for simulating CAES and ACAES power plant configurations are EBSILON®Professional, version 10.06. The aim of this chapter is to give the reader insight in the way EBSILON®Professional work to better understand the model build up and assumptions made.

7.1 Introduction to EBSILON®Professional

EBSILON®Professional is a powerful modeling tool that can be used for system simulation and optimization. It allows the user to control and balance both individual components and entire systems. The three main features of EBSILON®Professional used are; the graphical editor, ebsScript and TimeSeries [52].

The graphical editor

The simulated models are all drawn up in the graphical editor. Here is it possible to enter each component and specify calculation options and values. It is possible to create sub-profiles from the design system to execute off-design analysis, and static simulations can be performed [52].

ebsScript

Through ebsScript is it possible to access and manipulate every variable of every component for both the main profile and its sub-profiles, and programs can be written to execute power plant operations. The programming language used is a modified version of Pascal [52].

TimeSeries

By using the TimeSeries module, is it possible to execute quasi-dynamic simulation of the system. To get the full effect of the TimeSeries module, it should be used together with

ebsScript, making it possible to simulate different operational states over time. To use the TimeSeries module, component 117 the sun, needs to be placed in the modeling area of the graphical editor [52].

7.2 Design and off-design

In EBSILON®Professional is it possible to choose between two modes for global calculation; design and off-design. The design mode is used for entering the component specific values and to perform full-load simulations. These calculations are done in the design profile. Off-design mode is used to calculate the design mode in different variations and is performed in sub-profiles of the design profile [52].

Local off-design

In many components in EBSILON®Professional is it possible to choose the option "local off-design". The local off-design option allows a component to be in off-design in the design profile. This feature becomes useful in a dynamic system where a components operation point may differ from the global design. In this work local off-design have been used on all the heat exchangers, as they need to be designed for the largest possible mass flow [52].

7.3 Possibilities and limitations in EBSILON®Professional

TimeSeries and ebsScript

The physical equations describing the components in EBSILON®Professional are only valid for steady state calculation, making non-steady-state calculations impossible. The way around this limitation is to perform series of simulation on a small timescales, making it possible to neglect the dynamic effects. By using a combination of TimeSeries and ebsScript is it possible to create and simulate such quasi-dynamic systems. The time interval and the different states of the system are calculated and simulated through ebsScript before being written into the TimeSeries document. When all system states are calculated, the TimeSeries simulation is performed [52].

Component 118

Component 118 is a direct storage tank used to simulate the thermal storage and air storage of CAES and ACAES power plants through TimeSeries. It allows for change in mass and temperature, which are calculated through a mass and energy balance. The storage pressure is by default constant throughout the simulation process. To change the storage pressure over time it needs to be calculated in ebsScript and specified in the TimeSeries document for each simulation [52].

Characteristics

Several of EBSILON®Professional components such as; pumps, motors, compressors and turbines, have their own predefined characteristic fields. But it is also possible to implement a user defined characteristic field [52].

Controllers

There are several types of controllers in EBSILON®Professional and many components with control capabilities. The controller modifies the actual value from the system, with the help of a correction value, through an iterative procedure until it reaches the scheduled vale. For all controllers the correction value and the actual value must be specified. Only basic quantities such as pressure, enthalpy or mass flow can be correction values, while the actual value can be derived quantities such as temperature, heat flow or chemical composition. The characteristic of the controller must also be specified. The controller characteristic defines the direction in which the corrected value is modified. If both values change in the same direction, it characteristic is positive. For opposite direction the characteristic is negative [52].

Libraries

EBSILON®Professional also contains several material libraries, based on standards such as REFPROP (Reference Fluid Thermodynamic and Transport Properties) and VDI (verein deutscher ingenieure) guideline 4670. By using component 33, a boundary value input component, the fluid composition can be specified [52].

7.4 General assumptions

This section present the general assumptions used in all the different design case simulation. A summary of all the general assumptions can be seen in Table 7.1. The ambient temperature and pressure of air was chosen equal to the design values of the Huntorf CAES power plant in Germany, at 15°C and 1.013 bar [53]. During the compression and expansion operation phase are the power consumption and generation assumed constant respectfully. A controller acts between the power input/output line and regulates the mass flow of air to the required power input/output level. Controllers were also used to regulate the mass flow of thermal liquid passing through the heat exchangers.

The pressure loss through the heat exchangers were chosen following the guidelines given in [54], resulting in a pressure drop of 0.4 bar on the liquid side and a 2 % drop on the gas side. The exhaust outlet pressure were chosen to 1.03 bar, slightly higher than ambient pressure, based on simular values presented in [55].

All the mechanical and electrical efficiencies used are standard component values given from EBSILON®Professional. For the compressor polytropic efficiency were there found values in the literature ranging from 80-90 % [56, 57, 58, 59]. A middle value of 85 %, equal for all compression stages was then decided. The gas turbine isentropic efficiency was selected

to 90 % [58]. The pressure ratios over both Low Pressure (LP) and High Pressure(HP) compressors were chosen equal [45]

Table 7.1: General assumptions

	Unit	Value	Source
Boundary conditions			
Ambient air temperature	[°C]	15	[53]
Ambient air pressure	[bar]	1.013	[53]
Exhaust outlet pressure	[bar]	1.03	
Air storage			
Polytropic constant	[-]	1	
Specific heat loss	[kW/kgK]	20	
Operation procedure			
Storage time	[h]	12	
Power consumption/generation	[MW]	Constant[i]	
Heat exchangers			
Lower terminal temperature difference	[°C]	10	[55]
Pressure drop liquid side	[bar]	0.4 bar	[54]
Pressure drop gas side	[%]	2	[54]
Effectiveness	[%]	80	[52]
Compressors			
LP compressors rotational speed	[rpm]	3000	[60]
HP compressors rotational speed	[rpm]	7622	[60]
Efficiencies (nominal)			
Compressor polytropic efficiency	[%]	85	[56, 57, 58, 59]
Compressor mechanical efficiency	[%]	99	[52]
Turbine isentropic efficiency	[%]	90	[58]
Turbine mechanical efficiency	[%]	99	[52]
Pump isentropic efficiency	[%]	80	[52]
Pump mechanical efficiency	[%]	99.8	[52]
Motor electrical efficiency	[%]	85	[52]
Motor mechanical efficiency	[%]	99.8	[52]
Generator efficiency	[%]	98.6	[52]

Both Huntorf and McIntosh uses underground salt caverns for storage, but the salt wall temperature was only found for the Huntorf CAES power plant. The storage time is assumed to be 12 hours for all the simulated models. Rotary speed of the compressors was also only

[i] Constant during operation

known from the Huntorf power plant, and chosen equal for the two other models.

The air storage inlet temperature is assumed constant and equal to the salt wall (or storage) temperature. Based on the theory presented in Chapter 5.3, together with a constant storage temperature, is the pressure changing process isothermal and n=1. The compressor train back pressure was chosen equal to the storage pressure.

7.5 Huntorf reference model

The Huntorf CAES power plant was modelled with a good knowledge of the different system parameters, and thus suffices as a good reference model. A picture of the model can be seen at the end if this section in Figure 7.1. Table 7.2 contains the different assumptions made to the Huntorf CAES power plant model. All the known parameter values are summarized in Table 7.3.

Table 7.2: Assumptions, Huntorf CAES power plant model

	Unit	**Value**	**Source**
Coolant			
Inlet temperature	[°C]	10	
Outlet temperature	[°C]	25	[55]
Pressure	[bar]	2	[55]
Air storage			
Volume	[m^3]	138666	
Air density at 46 bar and 50°C	[kg/m^3]	49.6	[52]
Air density at 66 bar and 50°C	[kg/m^3]	71.2	[52]
Minimum level	[kg]	6877866	
Maximum level	[kg]	9873066	

The coolant water inlet temperature is assumed to be 10°C, this is slightly higher than the recommended values from [55] which recommends a value of 8°C in Norway. The Huntorf power plant is however located in Germany, and it is a reasonable assumption that the water temperature would be slightly higher. The coolant outlet temperature was chosen in accordance with [55] to 25°C.

With the compressor power chosen constant to 60 MW showed initial simulation that mass flow varied from 108 to 100 kg/s. If both cavern storages, with a total volume of 300000 m^3 were to be filled with air from 46 to 66 bar, it would take approximately 16 hours. This is twice the time given in tabel 7.3. The charging time was instead chosen to be 8 hours. Then only one of the two cavern storages would be filled. To get 8 hours charging time of the air storage cavern, the volume was calculated using Equation (7.1).

$$V = \frac{\bar{m} \cdot 8h \cdot 3600\frac{s}{h}}{\rho_{66bar} - \rho_{46bar}} = \frac{\Delta m}{\Delta \rho} = 138666 m^3 \tag{7.1}$$

The densities used in the calculation, shown in Table 7.2, were taken from the gas property tables available in EBSILON®Professional. The mass flow used is the mean mass flow of approximately 104 kg/s.

Table 7.3: Known data, Huntorf CAES power plant

	Unit	Value	Source
Storage			
Capacity	[MWh]	1160	[19]
Charging hour	[h]	8 [ii]	[60]
Discharge hours	[h]	4	[19]
Cavern wall temperature	[°C]	50	[60]
Volume	[m^3]	2 x 150 000	[60, 61]
Pressure min/max	[bar]	42/72	[19, 60]
Compressors			
Power	[MW]	60	[60, 62]
Mass flow	[kg/s]	108	[60]
Stages	[-]	2	[60]
LP compressor rotational speed	[rpm]	3000	[53]
HP compressor rotational speed	[rpm]	7622	[53]
Intercooler/recuperator			
Outlet temperature of aftercooler	[°C]	50	[60]
Intercoolers/aftercoolers	[-]	3/1	[60]
Aftercooler exitpressure min/max	[bar]	46-66 [iii]	[60, 62]
Coolant type	[-]	Water	[53]
Gas turbines			
Power	[MW]	300	[60]
Mass flow	[kg/s]	417	[60]
Fuel	[-]	Natural gas	[53]
HP expander inlet temperature	[°C]	550	[60]
HP expander inlet pressure	[bar]	42 [iv]	[63, 64]
LP expander inlet temperature	[°C]	825	[60]
LP expander inlet pressure	[bar]	11	[60]

[ii] (Pressure range: 46-66 bar)
[iii] Maximum pressure 72 bar
[iv] Pressure throttled down

The expansion process also takes place over a constant power generation of 300 MW. The inlet pressure and temperature of the turbine were specified according to values given in Table 7.3. The mass flow of air is regulated by a controller to maintain the required power output. Two regulators also control the mass flow of fuel, assumed methane, to maintain the required turbine inlet temperature. The fuel stream inlet pressure equals the combustion chamber inlet pressure. The ambient fuel temperature was chosen to 10°C.

According to the theory presented in Chapter 6 should the compressors be design for the highest possible pressure ratio, thus minimizing the possibility for surge. When doing so initial simulation showed the compressor operating outside its characteristic lines at low pressures. Through simulations were the compressors chosen in local off design at a compressor train back pressure of 56 bar. Operation within the available compressor characteristics were then ensured for all simulated pressure ratios.

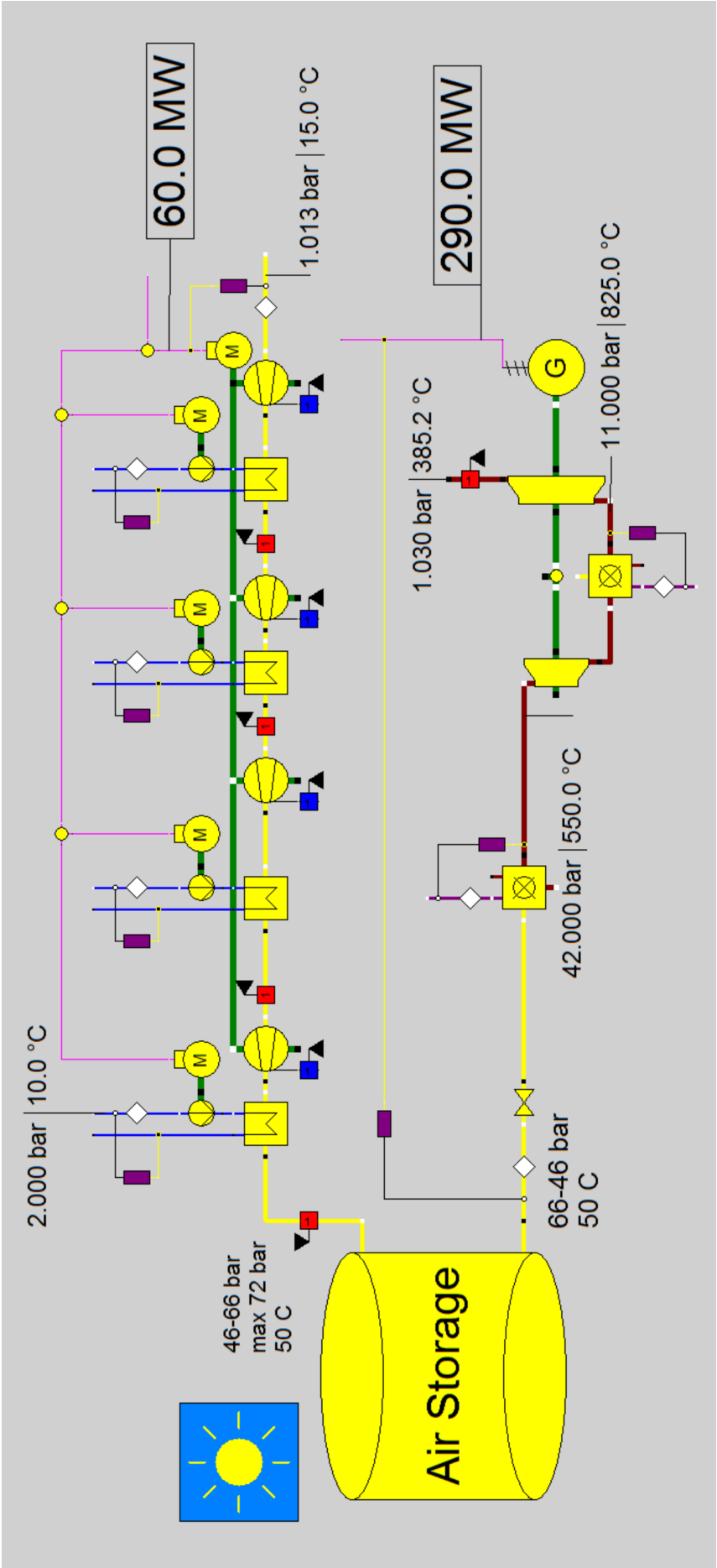

Figure 7.1: Huntorf model

7.6 McIntosh reference model

The second reference model is based upon the McIntosh CAES power plant. A picture of the model can be seen in Figure 7.2 at the end of this section. All model specific assumptions made are available in Table 7.4 and the known component specification are summarized in Table 7.5.

Table 7.4: Assumptions, McIntosh CAES power plant model

	Unit	Value	Source
Coolant			
Coolant		water	
Inlet temperature	[°C]	10	
Outlet temperature	[°C]	25	[55]
Pressure	[bar]	2	[55]
Air storage			
Salt wall temperature	[°C]	35	
Air density at 45 bar and 35°C	[kg/m^3]	50.9	[52]
Air density at 76 bar and 35°C	[kg/m^3]	85.9	[52]
Minimum storage level	[kg]	28249500	
Maximum storage level	[kg]	47674500	

Power consumption was put to the known design value of 50 MW. The type of coolant used at McIntosh CAES power plant was not found, and thus assumed water. The upper and lower coolant temperature was chosen equal to those used in the Huntorf reference model.

The salt wall temperature (ambient cavern temperature) of the air storage cavern was not found in the literature. Therefor were the temperature chosen equal to the recuperator inlet temperature of air, at 35°C. This assumption seems valid as the McIntosh power plant operates similar to the Huntorfor power plant, in which the air is cooled down to ambient cavern temperature from the aftercooler. The densities of 50.9 and 85.9 kg/m^3, at 35°C, 45 and 76 bar respectfully, were taken from the gas property table available in EBSILON®Professional. The storage volume was chosen equal to the known volume of the McIntosh power plant. Together with the densities were the storage upper and lower mass limit calculated.

The expansion process takes place over a constant power generation of 110 MW. The inlet pressure and temperature of the turbine were specified according to values given in Table 7.5. The mass flow of air is regulated by a controller which maintain the required power output. Two regulators also control the mass flow of fuel, assumed methane, to maintain the required turbine inlet temperature. The fuel stream inlet pressure equals the combustion chamber inlet pressure. The ambient fuel temperature was chosen to 10°C.

As in the case of the Huntorf reference model did the compressors, when design for highest possible pressure ratio, operate outside the characteristic lines at lower pressures. Through simulations were the compressors chosen in local off design at a compressor train back pressure of 60 bar. Operation within the available compressor characteristics were then ensured for all simulated pressure ratios.

Table 7.5: Known data, McIntosh CAES power plant

	Unit	Value	Source
Air storage			
Capacity	[MWh]	2860	
Charging hours	[h]	42 (45-76 bar)	[65]
Discharge hours	[h]	26	[65]
Volume	[m^3]	555 000	[65]
Pressure min/max	[bar]	45/90	[61, 65]
Compressors			
Power	[MW]	50	[66]
Mass flow	[kg/s]	94	[65]
Stages	[-]	4	[65]
Intercoolers/recuperator			
Intercoolers/aftercoolers	[-]	3/1	[19]
Aftercooler exitpressure min/max	[bar]	45-76	[61]
Gas turbines			
Power	[MW]	110	[65]
Mass flow	[kg/s]	154.4	[65]
Fuel	[-]	Natural gas	[65]
HP expander inlet temperature	[°C]	540	[65]
HP expander inlet pressure	[bar]	42.5 [v]	[67]
LP expander inlet temperature	[°C]	870	[65]
LP expander inlet pressure	[bar]	15	[65]
Recuperator			
Recuperator air in/out	[°C]	35/285	[65]
Recuperator exhaust in/out	[°C]	368/145	[65]

[v] Pressure throttled down

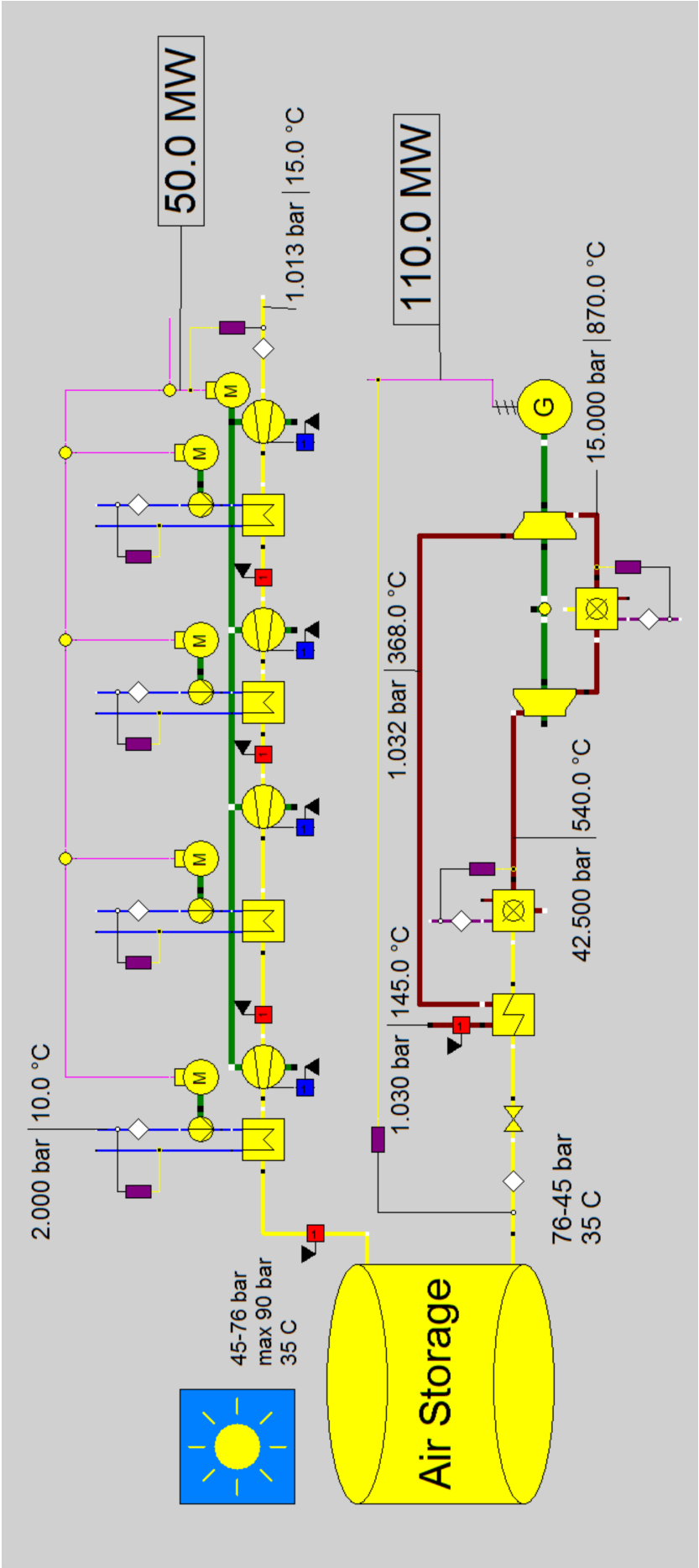

Figure 7.2: McIntosh model

7.7 ACAES model

The ACAES model build during this work, is based on the two CAES power plants in existence (Huntorf and McIntosh) as well as data known from the two ACAES projects under planning of today (ADELE and ALACAES). All four power plants were described in Section 3. A picture of the model can be seen in Figure 7.3, and the assumed values are summarized in Table 7.7.

For the ACAES model the air storage ambient temperature was chosen equal to that of McIntosh CAES power plant, at 50°C. The air storage temperature of 50°C also equals that of the ADELE project. The compression power consumption and turbine generation were chosen to 60 and 110 MW respectfully. The plant was to be modelled over about 8 hours charge, 12 hours storage and 2 hours discharge. Both the ADELE and ALACAES project uses solid sensible heat storage for storing the compression heat. This option is however not available in EBSILON®Professional. Instead offers EBSILON®Professional a variety of different heat transfer fluids, mainly aimed at solar thermal power plants. Values for the different possible thermal heat transfer fluids can be seen in Table 7.6.

Table 7.6: Heat transfer fluids available in EBSILON®Professional[vi]

Name	**Temperature**		**Density (kg/m^3)**	**Heat conductivity (W/mK)**	**Isobaric specific heat (kJ/kgK)**	**Mol weight (kg/kmol)**
	Cold (°C)	**Hot (°C)**				
HITEC Heat Transfer Salt	150	525	1865	0.3963	1.5617	10000
Jarytherm DBT	0	380	836	0.1051	2.4768	10000
Jarytherm AX320	-20	340	786	0.1076	2.6375	10000
Jarytherm BT06	-40	380	805	0.0947	2.4309	10000
Jarytherm CF	-80	340	619	0.0691	2.8782	10000
60 % $NaNO_3$ + 40%KNO3	200	600	1898	0.4926	1.4990	91.438
Dowtherm A	0	400	806	0.0939	2.3562	166
Therminol VP1	0	400	817	0.0965	2.3093	165.97

Due to simplicity a system with one thermal fluid was decided. The heat transfer fluid (HTF) should be able to stand temperatures near ambient temperatures, making it possible to cool down the air to the required storage temperature of 50°C. Based on the available HTFs in EBSILON®Professional, the minimum temperature was chosen to be 0°C, resulting in a maximum allowed temperature of 400°C. If any higher temperatures were to be chosen the lower temperature limit would be higher than 150°C, resulting in the need of a secondary

[vi]Values taken at 300°C and 2 bar. Source: [52]

cooling or heat transfer system. Therminol VP1 was chosen as heat transfer fluid for the model. Some of the advantages of Therminol VP1 are its low liquid viscosity, low toxicity, a high thermal stability and exceptional temperature control. One of the drawbacks with Terminol VP1 is that when hot fluid is leaked into cold air, it can form an explosive vapour mist [68].

As can be seen in Figure 7.3 does the ACAES model contain a four stage compression train and a two stage expansion train. This configuration was based on the two reference models. The pressure ratio over the gas turbines were chosen equal, based on theory presented in [45]. The air storage pressure range of 70-100 bar, were chosen equal to the known values of the ADELE project. The number of intercoolers and their air outlet temperature was found through trial and error, keeping in mind the temperature restrain of the HTF of 0-400°C. An air temperature of 120°C with two intercoolers were decided, resulting in an average temperature of the high temperature storage of approximately 300°C. The cold thermal storage temperature was chosen to 40°C, thus ensuring an aftercooler air outlet temperature of 50°C into the air storage.

The required air storage volume, of 62338 m^3, was calculated using Equation (7.1), with an average compression mass flow of 70 kg/s and 8 hours compression. The densities, at 50°C and 70-100 bar, were taken from EBSILON®Professionals gas tables. The mass limits of the thermal storage tanks were chosen so that the upper limit would not be reached after one cycle. Both thermal storage tanks are assumed to be over ground storage, and thus have an ambient temperature of 15°C. A HTF pressure of 6 bar was needed to avoid two-phase operation. The inlet temperatures of the gas turbines are given from two controllers that regulate the temperature with HTF mass flow. The temperature difference between the two fluids is sat equal to the heat exchanger terminal temperature difference of 10°C presented in Section 7.4.

Specific heat loss of the low temperature thermal storage and the air storage was elected to 20 kW/kgK. The air entering the storage is cooled down to cavern ambient temperature. The thermal loses of the cavern are then negligible and the heat loss coefficient is thought assumed to have no effect. Initial simulation showed HTF entering the cold storage tank at a temperature higher than the chosen initial temperature. The high specific heat loss was thus chosen to faster cool down the HTF to around 40°C after a completed cycle. For the hot thermal storage, the temperature loss is desired as small as possible. Initial simulation showed the storage temperature varied with only a few degrees over operation when the specific heat loss was chosen to 1 kW/kgK.

The compressors were chosen in off design for a pressure of 100 bar, giving the highest possible pressure ratio. The heat exchangers were chosen in local off design for the highest possible mass flow of both air and HTF. The highest mass flow of both air and HTF was achieved when the pressure is at 70 bar. The gas turbines were chosen in local off design for the highest mass flow possible [52].

The model were also to be simulated for ideal conditions. The ideal assumptions, based on similar work from Hartmann et al. [58], were a 92.5 % isentropic efficiency of the gas turbine and a 87.5 % isentropic compressor efficiency. The motor and pump efficiency, all

mechanical and electrical efficiencies and the effectiveness of the heat exchangers were chosen to 1. Pressure losses throughout the model were neglected. For the thermal storages and the air storage tanks were there no heat loss meaning the specific heat loss coefficient were chosen to zero.

Table 7.7: Assumptions, ACAES power plant model

	Unit	Value	Source
Air Storage			
Charging hour	[h]	8	
Storage Hours	[h]	12	
Discharge hours	[h]	2.3	
Volume	[m^3]	62338	
Minimum level	[kg]	4704000	
Maximum level	[kg]	6720000	
Pressure min/max	[bar]	70/100	
Density (70 bar, 50°C)	[kg/s]	75.5	[52]
Density (100 bar, 50°C)	[kg/s]	107.8	[52]
Cavern wall temperature	[°C]	50	
Specific heat loss	[kW/kgK]	20	
Cold thermal storage			
Minimum level	[kg]	500000	
Maximum level	[kg]	3100000	
Pressure	[bar]	6	
Initial temperature	[°C]	40	
Ambient temperature	[°C]	15	
Specific heat loss	[kW/kgK]	20	
Hot thermal storage			
Minimum level	[kg]	500000	
Maximum level	[kg]	3100000	
Pressure	[bar]	6	
Initial temperature	[°C]	300	
Ambient temperature	[°C]	15	
Specific heat loss	[kW/kgK]	1	
Compressors			
Power	[MW]	60	
Average mass flow	[kg/s]	70	
Stages	[rpm]	4	
HP compressor 1 inlet temperature	[°C]	120	
HP compressor 2 inlet temperature	[°C]	120	

Table 7.7: Continued

	Unit	Value	Source
Intercooler/recuperator			
Outlet temperature of aftercooler	[°C]	50	
Intercoolers/aftercoolers	[n.a.]	2/1	
Coolant type	[n.a.]	Terminol VP1	
Gas turbines			
Power	[MW]	110	
Average mass flow	[kg/s]	240	
HP expander inlet (nominal) pressure min/max	[bar]	68/98	
LP expander inlet (nominal) pressure min/max	[bar]	8.25/ 9.9	

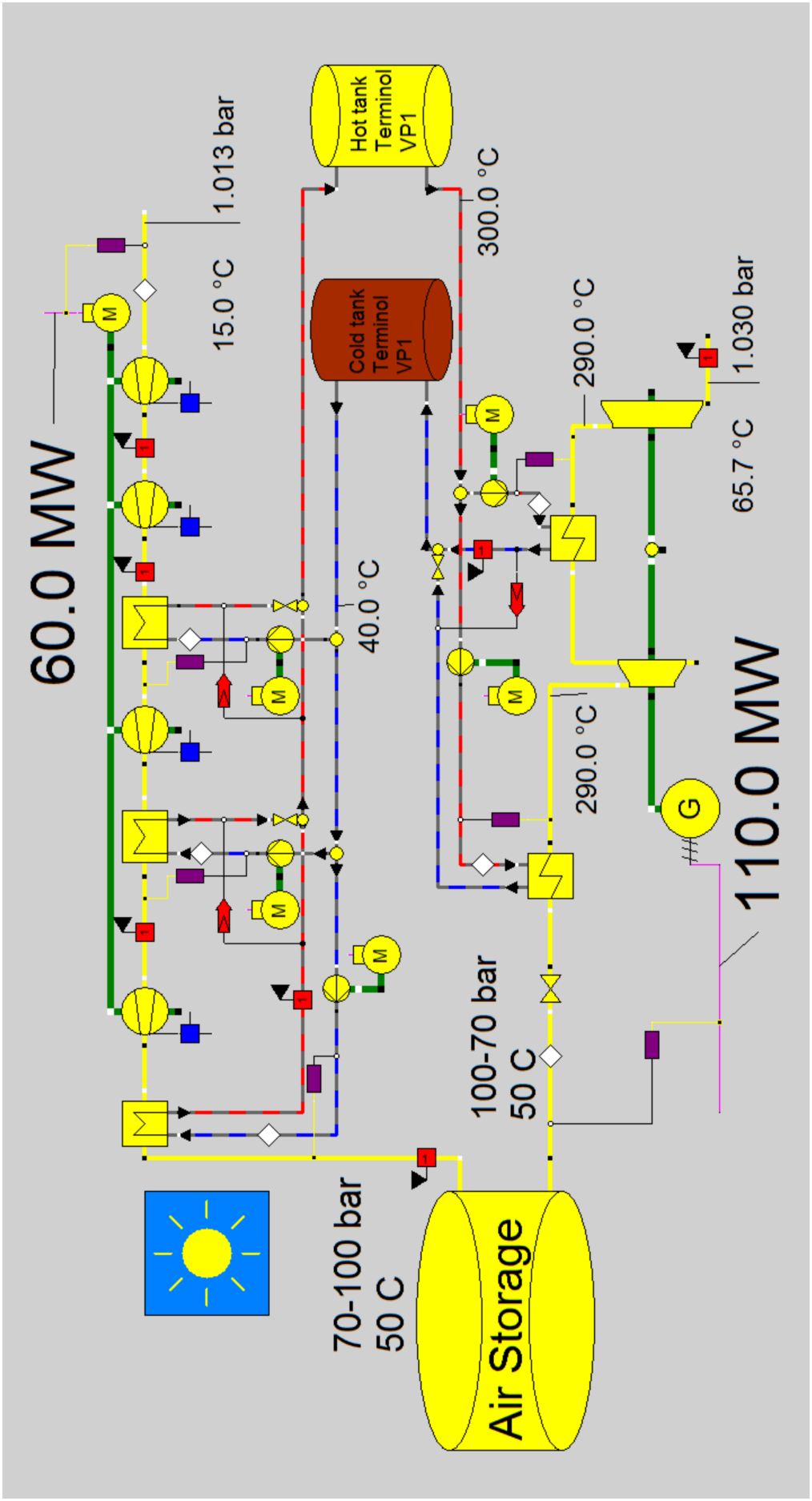

Figure 7.3: ACAES model

7.8 Code

As mentioned in Chapter 3 have a CAES power plant three modes of operation; compression, storage and expansion. The ebsScript code written for the different models can be seen in the appendix A. The intention of this section is to give an overview of the scripts work which all follows the same logic.

Figure 7.4 shows a flowchart of the code logic. Three logical constants decide the state of operation; compression, storage and expansion. Initially compression equals true, while storage and expansion equals false. After initialisation of the variables, the time and time interval are specified and written into the TimeSeries document. For every time step the model is simulated. Depending on the state of operation the intercoolers, aftercooler and heat exchangers are switched on or put in bypass mode. The controllers are turned on or off. By doing so, the mass flows in the inactive parts of the model equals zero and the components are left stationary.

In Section 7.3 was it mentioned that component 118 not automatically allow a transient change in pressure. To get a changing pressure is it necessary to calculate and wright the pressure into the TimeSeries document for every time step. The pressure was calculated by using the polytropic relation (5.18). Specific volume for the next time step, v_2, was calculated using the mass flow of air, $\dot{m}$, and the time step, Δt_{step}. The iteration procedure can be seen in Equation (7.2). It was found trough initial simulations that 30 seconds would suffice as time step, resulting in small changes for temperatures, pressures and mass flow. Typical changes between time intervals are 0.007 K for temperature and 0.007 kg/s for mass flow. A relative short simulation time was also achieved, with the entire simulation taking place from 15 minutes to an hour.

$$m_2 = m_1 + \dot{m}\Delta t_{step} \tag{7.2a}$$

$$v_2 = \frac{V_{storage}}{m_2} \tag{7.2b}$$

$$p_2 = p_1\left(\frac{v_1}{v_2}\right)^n \tag{7.2c}$$

During compression is the compressor train back pressure equal to the air storage tank pressure. When the plant is stationary or generating power is the back pressure specified equal to the ambient pressure. When all iterations have been performed, are all values for the air storage pressure written into the TimeSeries document, as well as operating status for heat exchangers and controllers. Then the TimeSeries simulation is performed, and all component values are written into the TimeSeries document. The simulation results, stored in the TimeSeries document, have to be manually transferred to an excel document for analysis, as no calculations are allowed in the TimeSeries document.

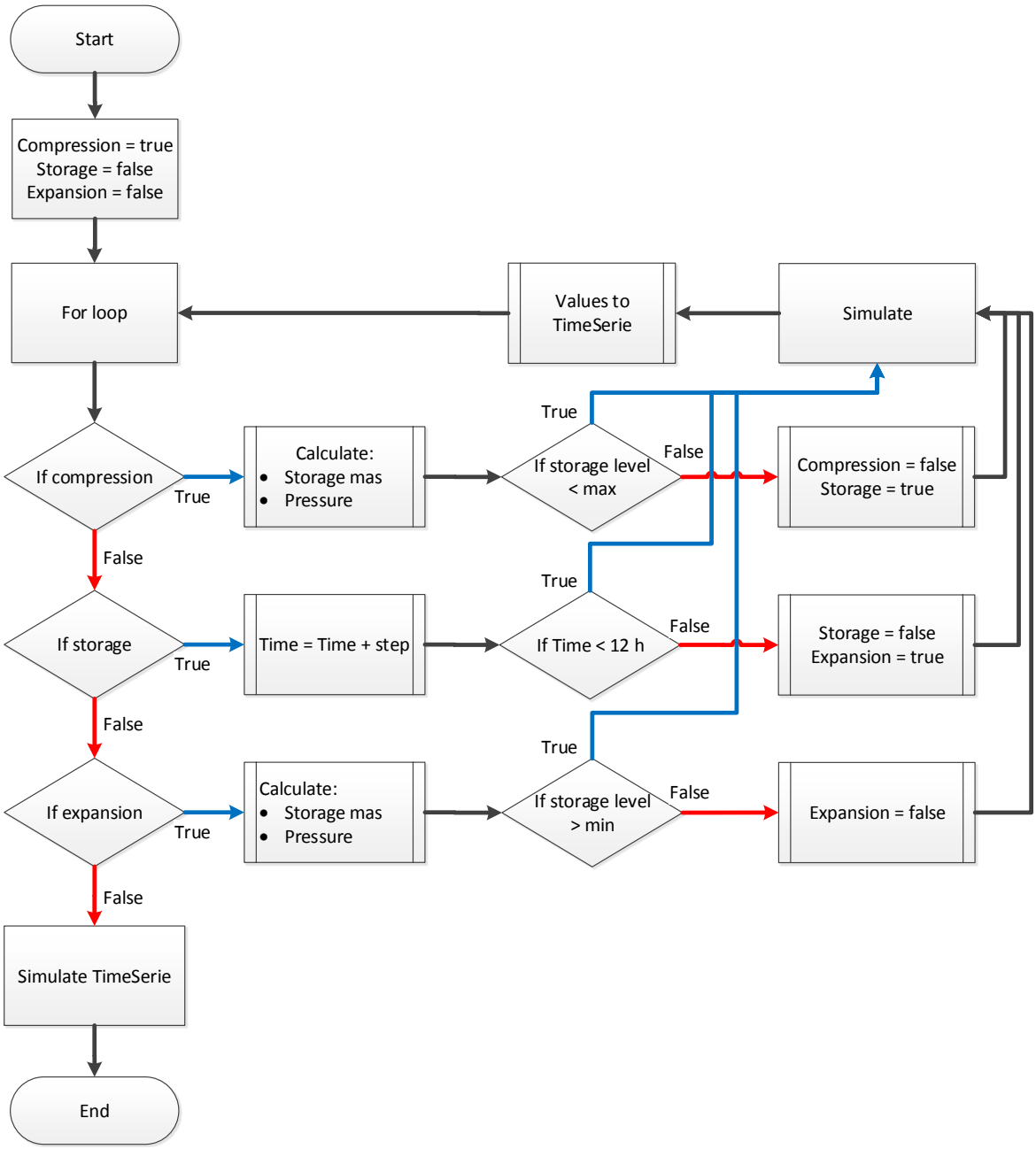

Figure 7.4: Flowchart of ebsScript code

Chapter 8

Results

In this chapter are the results of the two reference models presented together with known values of the real power plants. The ACAES model results are presented together with a critical discussion. The ACAES model together with the validity of the reference models will be further discussed in Chapter 9.

8.1 Results - Huntorf reference model

The major results found for the Huntorf CAES reference model can be seen in Table 8.1. The simulated round-trip efficiency was found to be 44 %, slightly higher than the known efficiency of 42 %, resulting in a difference from known value of 5 %. The heat rate, with a simulated value of 5480, also differs from the known value with approximately 5 %. The lower heat rate suggests that the simulated model needs less fuel than the real power plant. An energy rate of 0.75 means that 75 % of the electricity generated equals the electricity needed for storage. The remaining energy comes from the heat added by combustion of fuel. As seen in Table 8.1 is the simulated capacity about half that of the real Huntorf power plant.

Table 8.1: Results Huntorf CAES Power Plant model

	Unit	**Real power[i] plant**	**Simulated results**
Round-trip efficiency, $\eta_{Round-Trip}$	[%]	42	44
Energy rate, ER	[kWh/kWh]	n.a.	0.75
Heat rate, HR	[kJ/kWh]	5800	5480
Hours compression pr. expansion	[-]	n.a.	3.57
Capacaty	[MWh]	1160[ii]	633.16
CO_2 emissions	[kg CO_2/MWh]	n.a.	299.8
Cost of CO_2 emission	[€/ MWh]	n.a.	2.11

[i]Source of known values: [53]
[ii]For total storage volume(both caverns) of 300000 m^3. For one cavern is it approximately 580 MWh

A major factor influencing the simulated capacity is the fact that only one cavern storage volume was simulated, leaving only half the storage capacity. But even if half the capacity, 580 MWh, is used as a reference, is the simulated result, of 633 MWh, 9 % higher. Hours of compression per hours of expansion is not known for the reference plant, but the calculated number, using a compression time of 7.8 hours and expansion time of 2.2 hours, is 3.57. A lower number means less time is spent compressing air relative to expanding.

The cost of CO_2 emission, using the estimated formula (5.43) in Chapter 5, is 2.11 €/MWh. According to The United States Environmental Protection Agency [69] the average CO_2 emissions from gas power plants in the United States are 1135 Iibs/MWH or roughly 515 kg/MWh. This means the simulated CO_2, of 299.8 [kg/MWh] emission is 42 % less than the emissions of a conventional gas power plant. The calculated amount of fuel, methane, used per MWh generated electricity is 109.3.

8.1.1 Transient operation of the Huntorf model

Figure 8.1 shows different plots of the simulated operation. Figure 8.1a and Figure 8.1b shows the change in pressure and mass in air storage, respectfully, over the entire range of operating. It can be seen that during compression is the increase in both pressure and mass almost linear. During the 12 hour storage period are both constant. For the expansion process is pressure and mass changing linearly.

Figure 8.1c shows the change in coolant and air mass flow during the compression time, while Figure 8.1d shows the outlet temperatures of the compressors. The outlet temperature of the first LP compressor is lower than for the three others. This seems reasonable as the inlet temperature is lower for the first compressor than for the rest, which have an inlet temperature of 20°C. For the first LP compressor is the temperature varying from 125 to 134°C. The second LP compressor and two HP compressors outlet temperature varies from 134 to 143°C. The need for cooling, and hence the coolant mass flow, is lower for the first intercooler. The coolant mass flow through the intercooler is even lower for the aftercooler, which cools the air down to 50°C. Although the compressor outlet temperature increases over operation, is the change in coolant mass flow small. Air mass flow decreases during the compression, from 110.2 to 101.8 kg/s, as the power consumption is constant and the pressure ratio increases.

The amount of energy, in the form of heat, removed during the compression can be seen in Figure 8.1e. Total heat removed is showed by the red line and is 389.5 MWh. The heat removed by the first intercooler is 98.4 MWh. Intercooler 2 and 3 removes the same amount of heat of 105.8 MWh, while the aftercooler removes 79.4 MWh. Figure 8.1f shows the total energy balance for the system. After 7.8 hours of compression is the total amount of energy consumed by the compressors 468 MWh. After 2.2 hours of expansion is the total amount of energy added by combustion 961 MWh. The amount of energy generated equals 633 MWh.

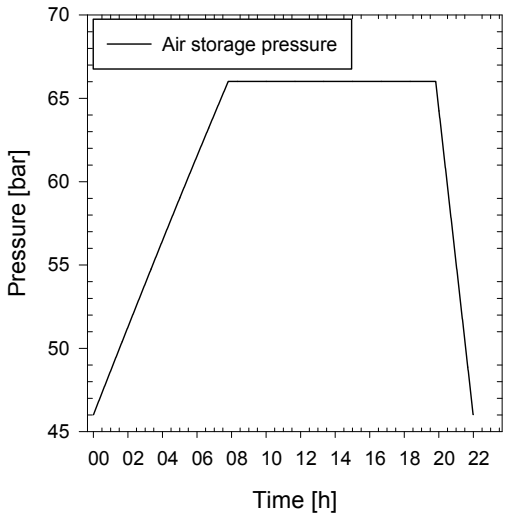

(a) Change in air storage pressure

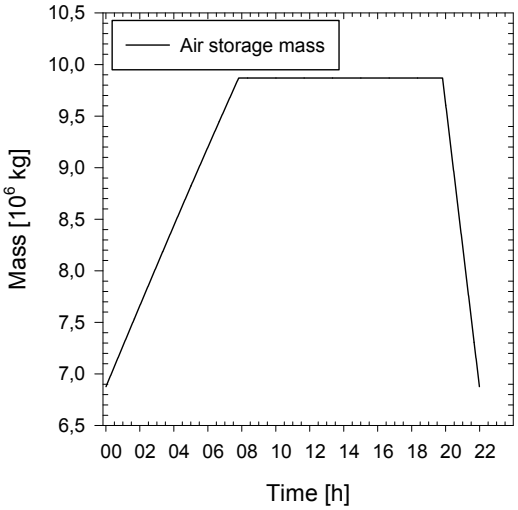

(b) Change in air storage mass

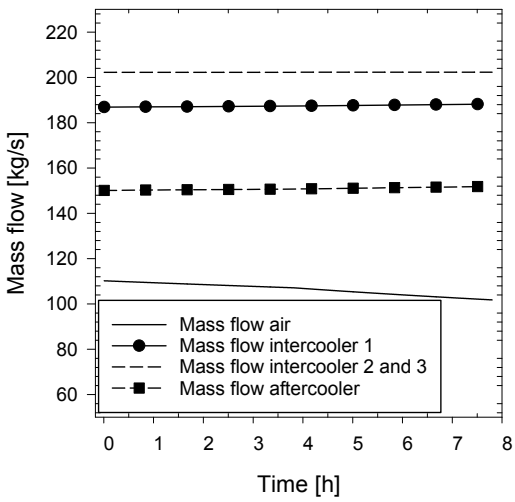

(c) Mass flow of air and cooling water through compressor train

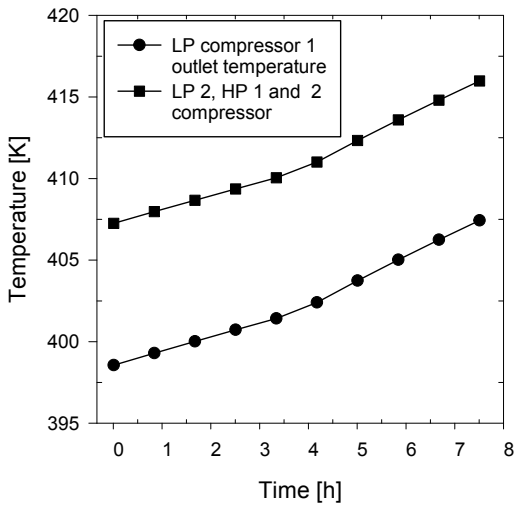

(d) Outlet temperatures of compression stages

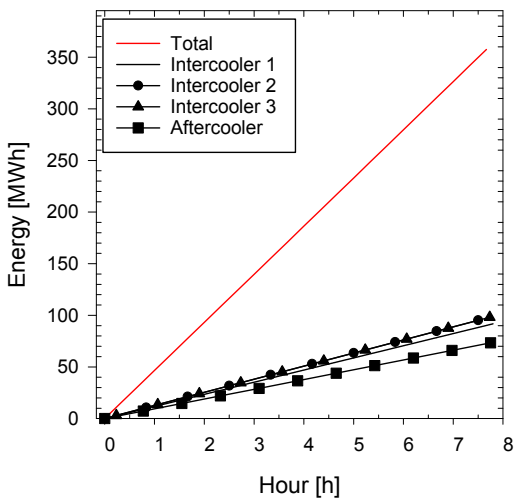

(e) Energy removed from compressor train by heat exchangers

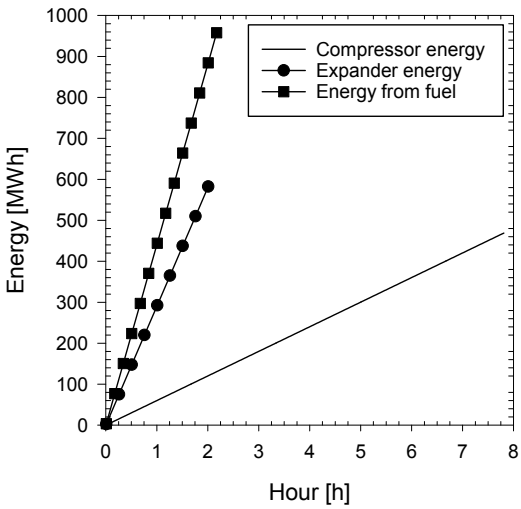

(f) Energy from fuel and energy consumed/-generated by compressor/expander

Figure 8.1: Results from simulation of Huntorf CAES power plant model

8.2 Results - McIntosh reference model

The major results found for the McIntosh reference model can be seen in Table 8.2. The simulated round-trip efficiency was found to be 51.3 %, slightly lower than the known efficiency of 54 %, resulting in a difference from known value of 5 %. The heat rate, with a simulated value of 4242 differs from the known value with a little more than 1 %. The small deviation in heat rate suggests that the simulated model have approximately equal fuel consumption as the real power plant. An energy rate of 0.77 was achieved, giving a deviation of 3.8 % from the reference value. The lover value means that less energy is used on compression relative to energy generated through expansion.

Table 8.2: Results McIntosh CAES Power Plant model

	Unit	**Real power[iii] plant**	**Simulated results**
Round-trip efficiency, $\eta_{Round-Trip}$	[%]	54	51.3
Energy rate, ER	[kWh/kWh]	0.8	0.77
Heat rate, HR	[kJ/kWh]	4187	4242
Hours compression pr. expansion	[-]	1.6	1.69
Capacity	[MWh]	2860	4167
CO_2 emissions	[kg CO_2/MWh]	208 [iv]	232.7
Cost of CO_2 emission	[€/ MWh]	n.a.	1.64

The simulated capacity, of 4167 MWh, is nearly twice the value known for the McIntosh power plant. Simulated compression and expansion time is 64.1 and 37.9 hours respectfully. The known times for McIntosh are 42 and 26 hours. The resulting hours of compression per hours of expansion is 1.69, which is 5.6 % higher than the known value of 1.6.

Simulated CO_2 emission is 232,7 [kg CO_2/MWh], which is 12 % higher than the real emissions for the McIntosh plant. The average CO_2 emissions from gas power plants in the USA is 515 kg/[69]. This means that the simulated CO_2 emission, of 232,7 [kg/MWh], is 55 % less than that of a conventional power plant. The cost of simulated CO_2 emission, using the estimated formula (5.43) in Chapter 5, becomes 1.64 €/MWh. The calculated amount of fuel, methane, used per MWh generated electricity is 84.8.

8.2.1 Transient operation of the McIntosh model

Figure 8.2 shows different plots of the simulated operation. Figure 8.2a and Figure 8.2b shows the change in pressure and mass in the air storage, respectfully, over the entire range of operation. It can be seen that during compression is the increase in both pressure and mass

[iii] Source of known values if nothing else stated: [65]
[iv] Source: Published raw data from [70]

almost linear. During the 12 hour storage period are both constant. For the expansion process is pressure and mass changing linearly.

Figure 8.2c shows the change in coolant and air mass flow during the compression period, while Figure 8.2d shows the outlet temperatures of the compressors. The first LP compressor outlet temperature is lower than the other three, which are equal and changes equally over time. For the first LP compressor is the temperature varying from 130 to 140°C. The second LP compressor and two HP compressors outlet temperature varies from 140 to 149°C. The need for cooling and hence the coolant mass flow, is lower for the first LP compressor and the aftercooler. The air mass flow decreases throughout the compression process, from 87.5 to 81.3 kg/s, as the power consumption is constant and the pressure ratio increases.

The amount of energy, in the form of heat, removed during the compression can be seen in Figure 8.2e. Total heat removed, after 64.1 hour, is showed by the red line and is 2584 MWh. The heat removed by the first intercooler is 629.6 MWh. Intercooler 2 and 3 remove the same amount of heat of 678.3 MWh, while the aftercooler removes 597.8 MWh. Figure 8.2f shows the total energy balance for the system. After 37.8 hours of expansion is the heat added by fuel 4911 MWh. The recuperator reuses 1322 MWh heat from the hot exhaust gas, while the generated electricity equals 4167 MWh. During the 64.1 hour long compression period is 3210 MWh of electricity used.

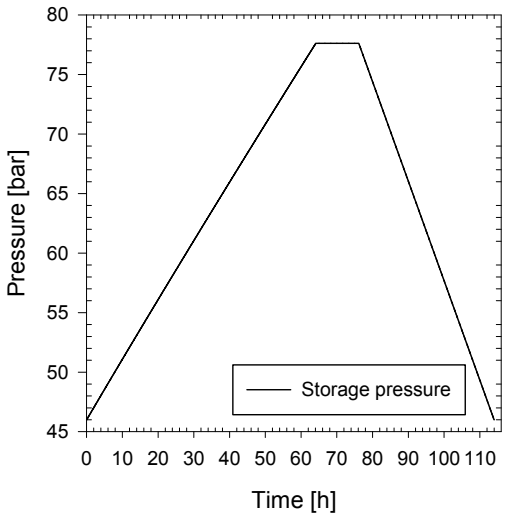

(a) Change in air storage pressure

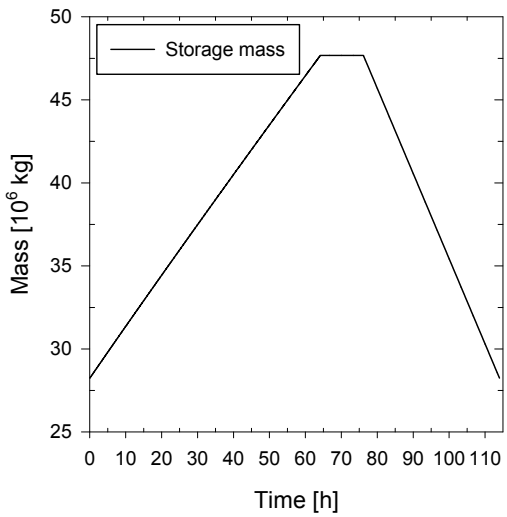

(b) Change in air storage mass

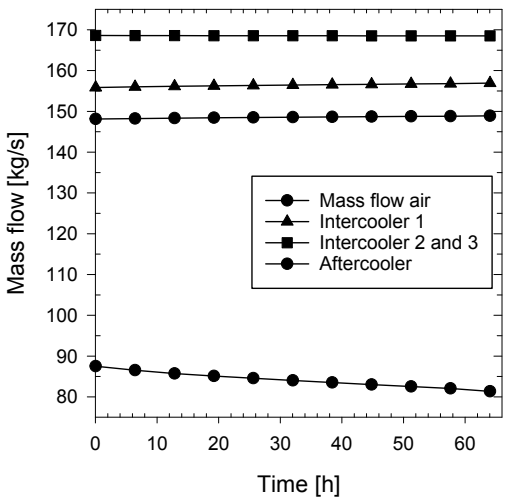

(c) Mass flow of air and water through compressor train

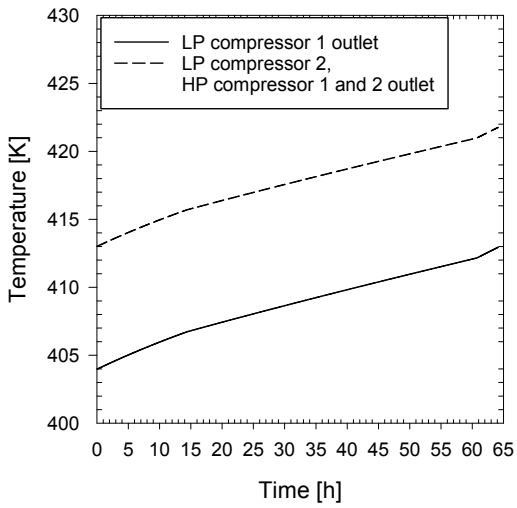

(d) Outlet temperature of compression stages

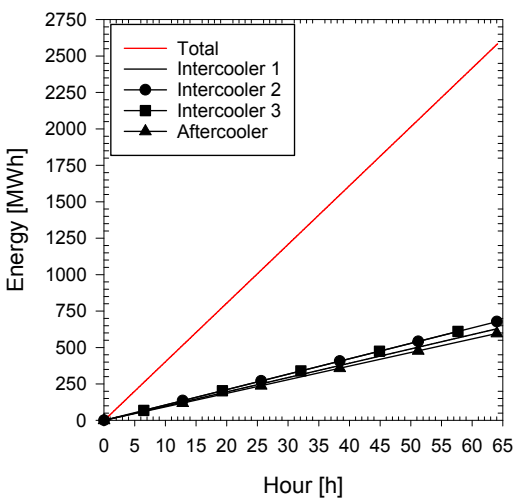

(e) Energy removed by intercoolers

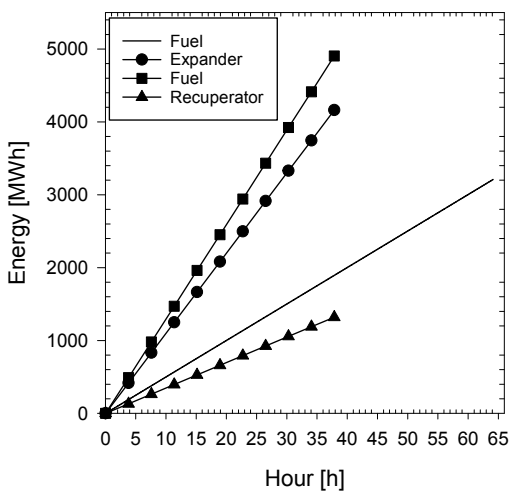

(f) Compression, expansion, fuel and recuperator energy

Figure 8.2: Results from simulation of McIntosh CAES power plant model

8.3 Results - the ACAES model

The major results found for the ACAES model can be seen in Table 8.3. The systems calculated round-trip efficiency was found to be 55.4 %, slightly higher than the efficiency known for the McIntosh power plant. The hours of compression per hours of expansion was calculated to 3.28, with a compression time of 7.78 hours and an expansion time of 2.35 hours. The expansion and compression time is thus similar to that of Huntorf CAES power plant. The calculated energy ratio, the inverse of the round-trip efficiency, were 1.8. Meaning the ACAES model returns less energy to the grid than what is consumed during compression. The electricity consumed by the compressors, during the filling state, summarized to 467 MWh. The electricity generated, during expansion, summarized to 258.6 MWh.

Table 8.3: Results of the ACAES model

	Unit	**Results**
Round-trip efficiency, $\eta_{Round-Trip}$	[%]	55.4
Thermal efficiency of hot storage $\eta_{th,TES}$	[%]	79.3
Hours compression	[h]	7.78
Hours expansion	[h]	2.28
Hours compression pr. expansion	[-]	3.28
Energy ratio, ER	[-]	1.8
Electricity consumed	[MWh]	467
Electricity generated	[MWh]	258.6
Energy into Hot tank	[MWh]	414.7
Energy out of Hot tank	[MWh]	328.9
Heat stored from compression	[MWh]	372.5
Heat delivered to turbines	[MWh]	272.6
Heat loss hot tank	[MWh]	6.3
Heat loss cold tank	[MWh]	7.9
Hot HTF left after cycle	[kg]	520890
Hot storage temperature after cycle	[°C]	289.5

The amount of compression heat stored was 372.5 MWh, while the amount of heat delivered to the expanders was 272.6 MWh. This means that 73.2 % of the stored compression heat is reused by heating the air before the turbines. The amount of heat lost to the surroundings form the hot storage was 6.3 MWh. For the cold storage was the heat loss 7.9 MWh. An energy balance then reveals that 93.6 MWh of the compression heat is not utilized by the expander train, and is either lost to the surroundings and the cold storage or remains in the hot storage. The thermal efficiency of the hot storage tank equals 79.3 %.

A simulation with different values of compressor and turbine efficiencies were performed next to the design simulation. This was done in order to see how the compressor and turbine efficiencies would affect the round-trip efficiencies. The calculated round-trip efficiencies for the different scenarios can be seen in Table 8.4. With a 97 % component efficiency, relative to design, the round-trip efficiency became 52.5 %. This result in a decline of 5.2 % from the design model. With a 103 % component efficiency relative to design, was the calculated round-trip efficiency 58.4 %. This is an increase of 5.5 % compared to the design model.

A simulation using ideal conditions was also performed. The round-trip efficiency reached by the ideal model, were 71.2 %. This means the round-trip efficiency of the model, under ideal conditions, reaches the same level as values known from the literature which were presented in Chapter 3.3. The thermal efficiency reached by the hot storage tank was 78.8 %. This is a decline of 0.5 percentage point, compared to the design model.

Table 8.4: Different compressor and turbine efficiencies

	Compressor train [v] **efficiency [%]**	**Expander train** [vi] **efficiency [%]**	**Round-trip efficiency,** $\eta_{\mathbf{Round-Trip}}$ **[%]**
97% of design	82.5	87.3	52.5
Desing	85	90	55.4
103% of design	87.5	92.7	58.4
Ideal model	87.5[vii]	92.5	71.2%

8.3.1 Transient operation of the ACAES model

The air storage pressure changes from 70 to 100 bar during the compression phase, and from 100 to 70 bar during the expansion phase. The behavior of both the air storage pressure and the air storage mass level, during compression and expansion, are equal to that of the reference models and can be seen in Figure 8.3a and Figure 8.3b.

Figure 8.4a shows the mass flow through the compressor train. The mass flow sinks from 73.3 kg/s at the beginning of the compression period to 70.5 kg/s at the end. It can be seen that the compressor train mass flow changes almost linearly over the compression time. The change in mass flow through the expander train can be seen in Figure 8.4b. A change in mass flow over time goes from 234.5 kg/s to 245.8 kg/s. The change in mass flow for both the compressor and the expander train seems reasonable, as the power consumption/generation is constant during operation and the pressure increases/decreases respectfully.

The temperature of air at the intercooler inlets are changing through the compression phase. At the first intercooler is the temperature changing from 226 to 341°C. The second

[v] Polytropic efficiency
[vi] Isotropic efficiency
[vii] Isentropic efficiency

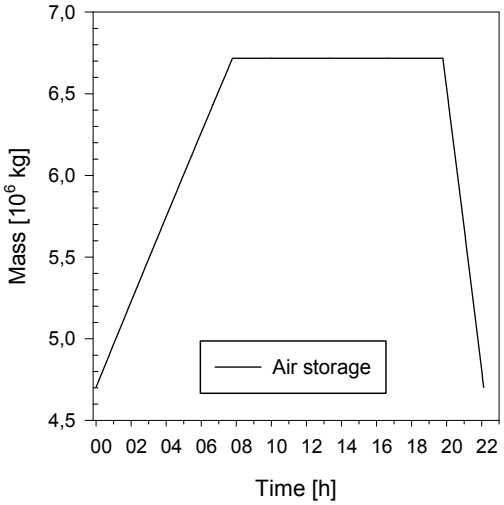

(a) Air storage mass

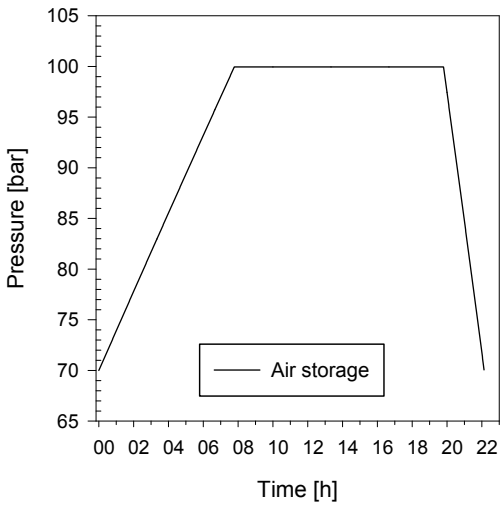

(b) Air storage pressure

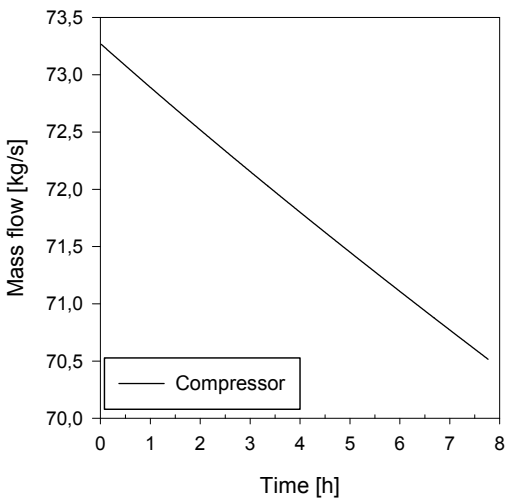

(a) Air mass flow compression

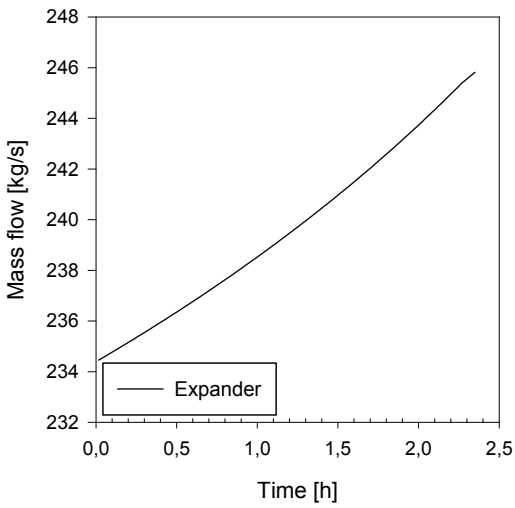

(b) Air mass flow expansion

Figure 8.4: Change in air storage mass and pressure over operation

intercooler inlet temperature is changing from 301 to 306°C, while the inlet temperature of the aftercooler is changing from 297 to 303°C.

The changes in cold storage temperature and mass, and the changes of HTF temperature in and out of the storage tank, can be seen in Figure 8.5a and 8.5b. The temperature of the cold storage, seen by the blue line, starts out at 40°C. Over the 7.78 hour compression, when HTF flows out of the storage, is the storage temperature changing to 34°C. During the storage period is the storage temperature decreasing further, to its lowest point of the cycle, to 21.7°C. Throughout the expansion phase is the cold tank temperature increasing rapidly to 54.4°C. The cold storage tank is almost emptied during the compression phase. During the expansion phase is the tank filled again, but the final mass level of the tank is only 80 % of the full state.

The HTF temperature into and out of the cold tank is plotted in Figure 8.5a. During the

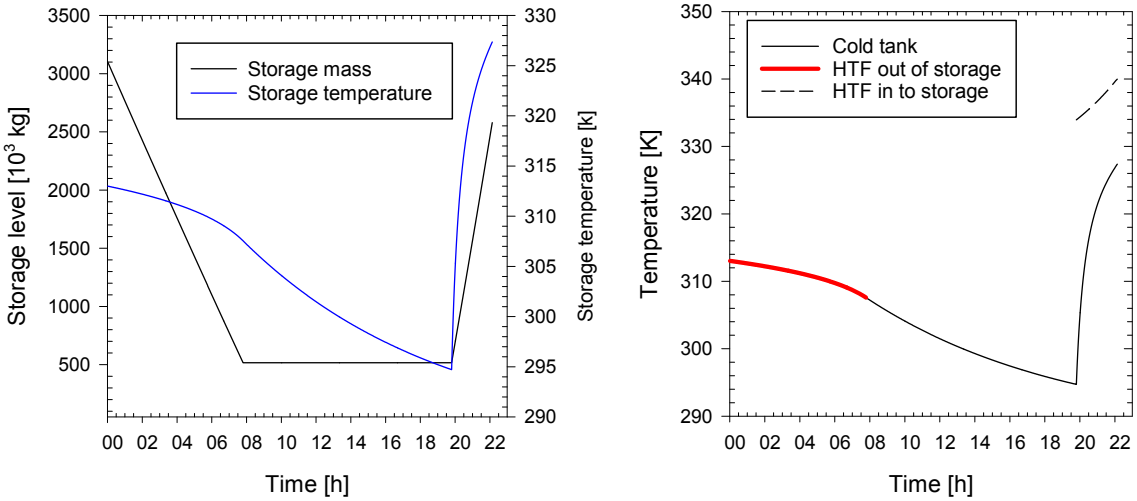

(a) Cold storage tank mass vs. temperature

(b) Cold storage tank temperature vs. HTF temperature

Figure 8.5: Changes of thermal storage mass and temperatures during operation

compression phase is the HTF temperature out of storage, plotted by the red thick line, equal to the storage temperature. Through the expansion phase is the HTF temperature, plotted by dotted line, significantly higher than that of the storage (60.9-67°C). The higher HTF temperature gives rise to the fast change in cold storage temperature.

The changes in hot storage temperature and mass, and the changes of HTF temperature in and out of the hot storage tank, can be seen in Figure 8.6a and 8.6b. The temperature of the hot storage, seen by the red line in Figure 8.6b, is at the beginning of the compression falling from 300°C to 298.5°C, before increasing again to 300.7°C at the end of the compression interval. During the storage period is the temperature decreasing to 299°C. A further decrease in temperature takes place over the compression phase were the storage temperature falls to 298.5°C. The changes in hot storage mass changes exactly opposite to that of the cold storage. This means 20 % of the HTF mass is left in the storage after the expansion phase. This is equivalent to 520.9 tonne of HTF at almost 300°C.

The HTF temperature into and out of the hot storage tank is plotted in Figure 8.6b. At the beginning of the compression phase is the temperature of HTF into the tank (dotted line) lower than the temperature of the tank. The temperature changes from 297.4 to 307.4°C. It can be seen that the HTF temperature and tank temperature are equal just before the hot tank reaches its minimum temperature. The lowest temperature in hot tank occurs when the heat added to the storage is greater than the thermal loss of the tank. During the expansion phase is the HTF temperature (red thick line) equal to the hot tank temperature.

Outlet temperature of air through the air heaters can be seen in Figure 8.7a next to the outlet temperature of the HP and LP gas turbines in Figure 8.7b. The outlet temperature is equal for both air heaters, as it is decided using the assumption of 10°C temperature difference presented in Chapter 7.4. The temperature decrease with time then follows that of the hot thermal storage, only 10 degrees lower, and changes from 289°C to 288.5°C. The out-

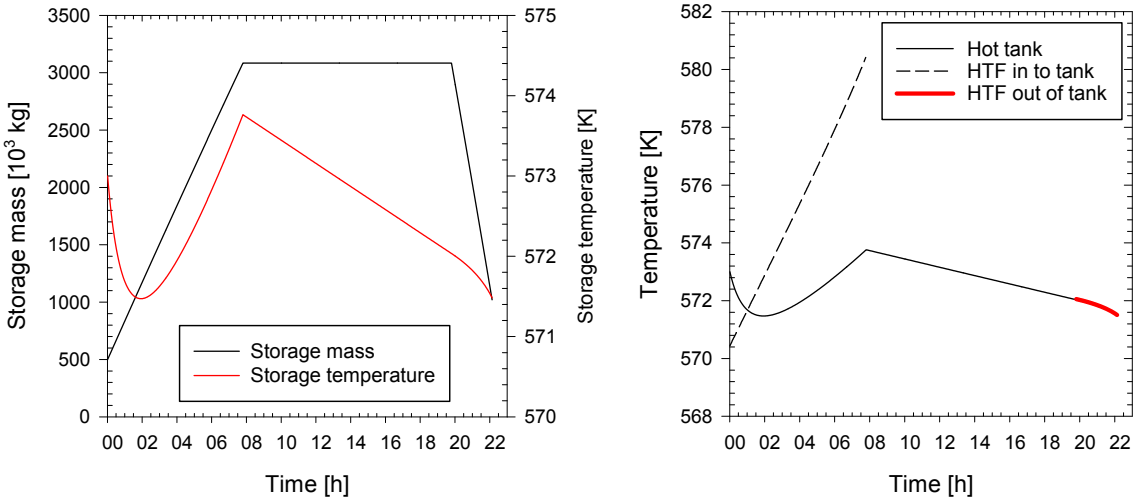

(a) Hot storage tank mass vs. temperature

(b) Hot storage tank temperature vs. HTF temperature

Figure 8.6: Changes of hot thermal storage mass and temperatures during operation

let temperature of the HP gas turbine increases from 51.5°C to 64.1°C, while the LP turbine outlet temperature increases from 56.1°C to 64.5°C.

The increase in gas turbine outlet temperature seems reasonable as; the pressure ratios over the gas turbines decrease over time as the air storage is depleted. At the same time is the hot thermal storage temperature almost constant, thus leaving the gas turbine inlet temperature, or the air heater outlet temperature, almost constant. It can also be seen from the figure that the temperature difference between the two gas turbine outlets gets closer over time and is almost equal at the end of the expansion process.

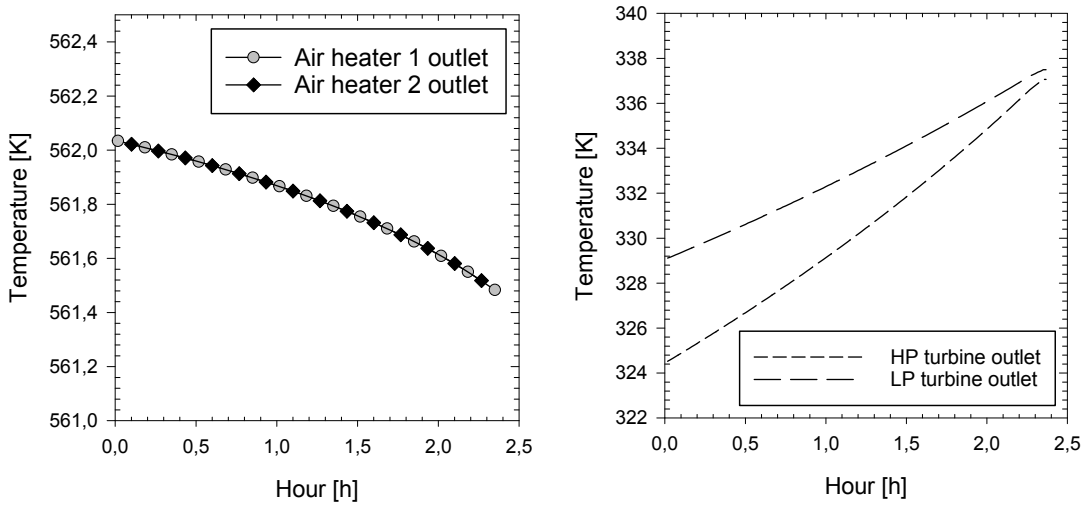

(a) Outlet temperature from air heaters

(b) Gas turbine outlet temperature

Figure 8.7: Outlet temperatures of air preheater and gas turbine

Figure 8.8 shows different plots of energy transfers taking place over the simulated oper-

ation. Figure 8.8a and Figure 8.8bshows the amount of heat transferred in the compression and expansion train respectfully. The amount compression heat transferred by the intercoolers and the aftercooler to the hot HTF is 372.5 MWh. The aftercooler removes the most heat, with a total of 143.1 MWh. The first intercooler removes 123.5 MWh while the second intercooler removes 105.9 MWh. Total amount of heat delivered to the compressor train is in total 272.6 MWh. The first airheater delivers a total of 138.4 MWh, while the second delivers slightly less of 134.2 MWh.

The amount of energy consumed and generated, by the compressor and expander train, can be seen in Figure 8.8c. It should be noted that the energy-axis is higher in this plot than for Figure 8.8a and 8.8b. Thermal losses for the hot and cold storage tank can be seen in Figure 8.8d. The thermal loss of the hot storage tank (red line) is almost constant over the entire range of operation. For the cold storage tank is the thermal losses higher than for the hot storage tank. Through the compression phase is the loss close to constant. For the 12 hour storage period is however the loss declining, before increasing again during the expansion phase.

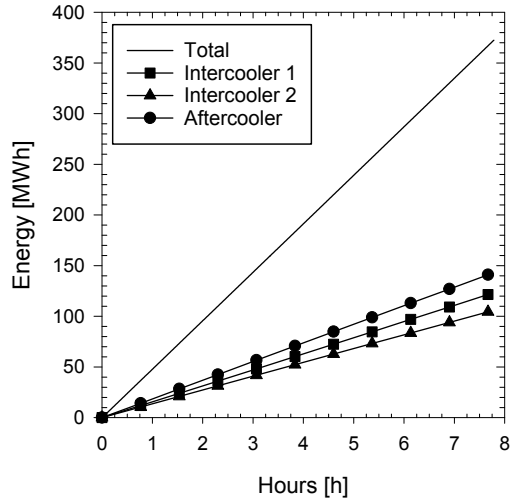

(a) Thermal energy extracted from compressor train

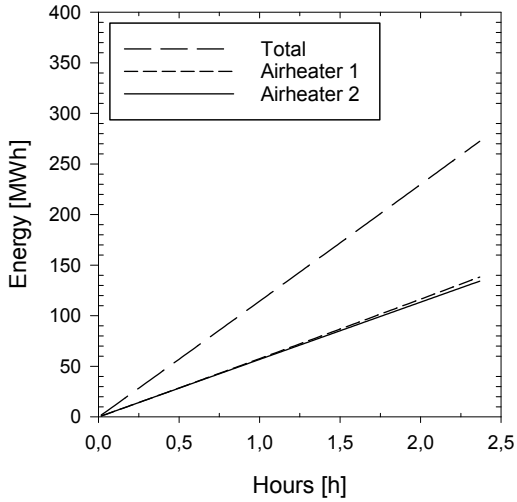

(b) Thermal energy injected to expander train

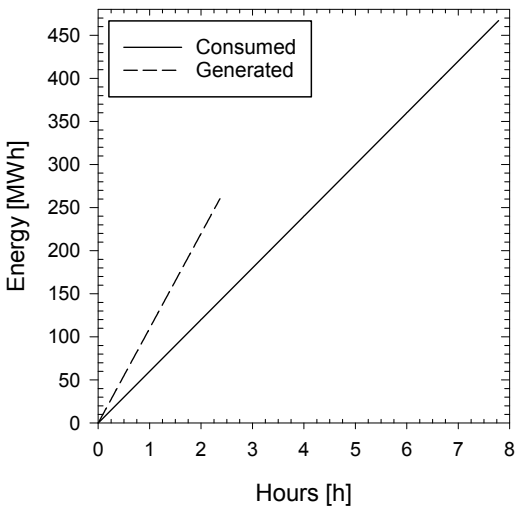

(c) Energy consumed/generated from compressor/expander

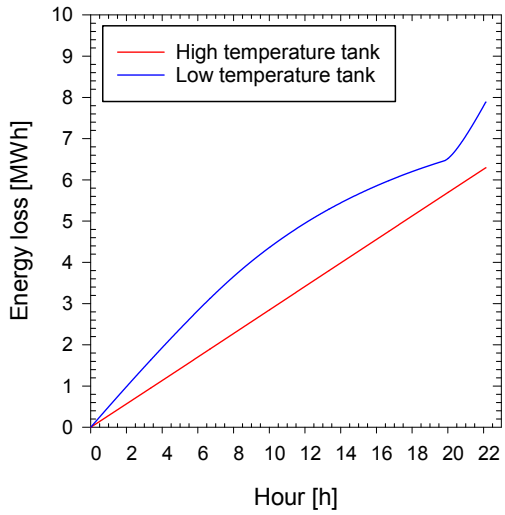

(d) Heat loss from storage tanks

Figure 8.8: Plots of energy transfers

8.4 Sensitivity analysis

There is always a lot of uncertainty when it comes to simulated models. The main focus of this chapter is to describe how different assumed parameter values affect the models round-trip efficiency. A sensitivity analysis has been performed on different components in the ACAES model where the assumed values are insecure, or when the assumed values could experience a change over time. Manual work was needed to transfer the result of each simulation. As a result were the sensitivity analysis performed for selective values only. It should also be noted that the range of change varies as the values do not have a common scale.

8.4.1 Ambient conditions

The values of the models ambient temperature were chosen to temperatures assumed typical for Europe throughout a year. Figure 8.9 shows the effect ambient temperatures from -5°C to 20°C has on the round-trip efficiency. Over the temperature range is the round-trip efficiency changing from 56.2 % to 55.2 %.

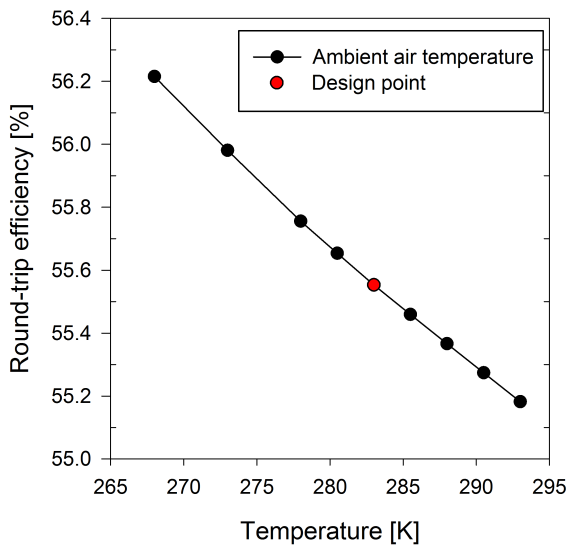

Figure 8.9: Change of ambient air temperature

The round-trip efficiency decreases steadily with increasing temperature until 20°C. At higher temperatures is the cold storage tank emptied before the air storage tank is full. Due to the logic of the script which only controls the air storage level, will the simulation still run, but the results will be wrong.

A lower ambient temperature also affected the thermal storage temperatures. As shown in Table 7.6 is the lower temperature limit of Therminol VP1 0°C. The minimum temperature reached in the cold tank during design simulation were 21.7°C, thus above the minimum temperature. In the sensitivity, when the ambient air temperature fell down to -5°C, the cold tank storage temperature was as low as 8.5°C.

8.4.2 Thermal storages

The hot and cold thermal storage temperatures vary through the simulation. Simulations were performed with different initial storage temperatures. The cold tank initial temperatures were changed from 30°C to 45°C. The resulting round-trip efficiencies can be seen in Figure 8.10a. For initial temperatures lower than design is the round-trip efficiency increasing slowly. In the case of temperatures higher than design, is the round-trip falling. An upper temperature limit of 45°C was given by the model. This was caused by the aftercooler outlet temperature assumption of 50°C, which have a minimum allowed temperature difference of 5°C.

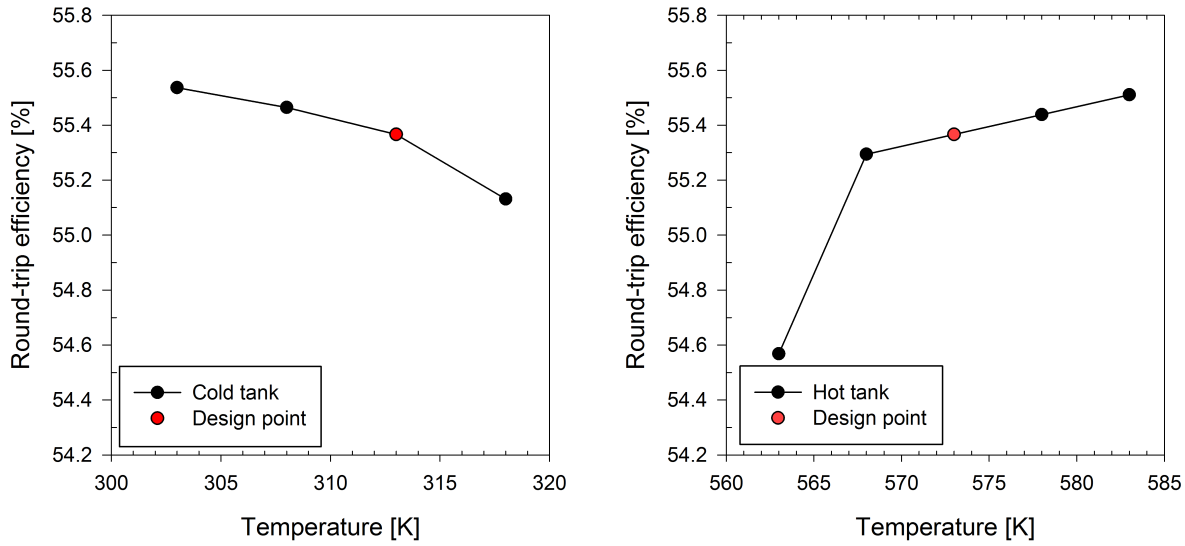

(a) Change of cold storage tank start temperature (b) Change in hot storage tank start temperature

Figure 8.10: Change of initial temperatures in hot and cold thermal storage

The effect of changing initial temperatures in the hot tank can be seen in Figure 8.10b. The range of temperatures goes from 290°C to 310°C. These temperatures were chosen based on the known temperatures of the HTF into the storage tank, which was presented in Chapter 7. For temperatures higher than design is the efficiency increasing slowly. A small change in temperature, lower than design, results in a small change in the round-trip efficiency. If the initial temperature is lower than 295°C, is there however in a larger drop in efficiency. It should also be noted that temperatures lower than 290°C, resulted in an increased HTF mass flow to the hot tank during compression. The increase in mass flow made the hot tank fill up faster, creating a situation similar to that presented for low ambient air temperatures where air is compressed without being cooled down.

The effect of changing the specific heat loss coefficient of the thermal storage tanks can be seen in Figure 8.11. The effects of changing specific heat loss in the cold tank can be seen in Figure 8.11a. For a wide range, 11 to 30 kW/kgK is the change in round-trip efficiency less than 1 percentage point from design.

For the hot storage tank is the changes in thermal coefficient shown in Figure 8.11b. With no losses, meaning a specific heat loss coefficient of 0 kW/kgK, is the round-trip efficiency

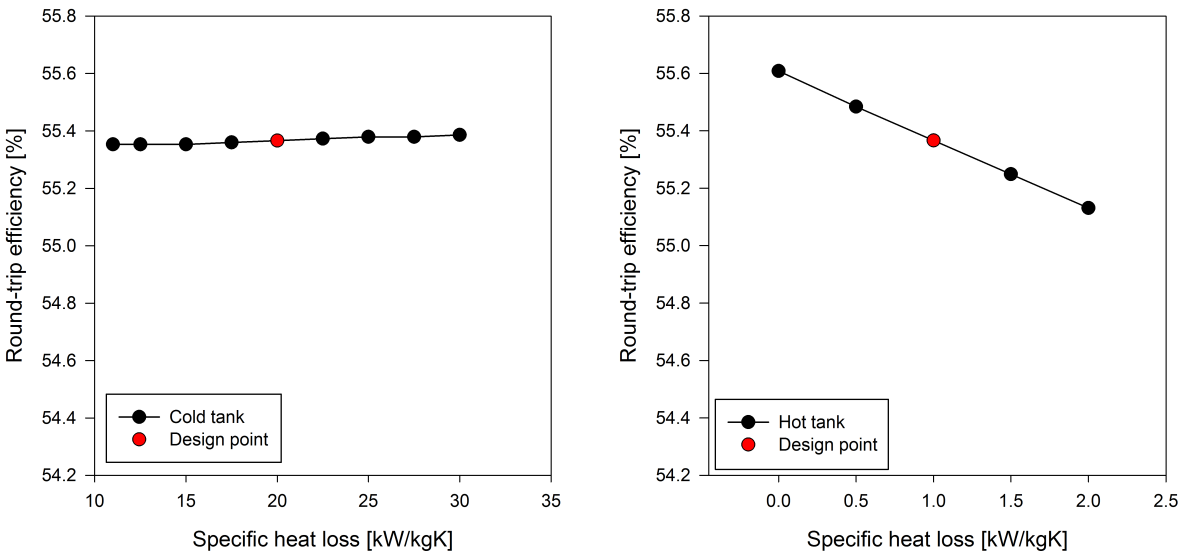

(a) Change of cold storage tank specific heat loss (b) Change in hot storage tank specific heat loss

Figure 8.11: Change of specific heat loss coefficient of cold and hot tank

55.6 %. The round-trip efficiency falls steady with the increasing specific loss coefficient until 2 kW/kgK, where the round-trip efficiency is 55.1 %. Any further increase in specific heat loss coefficient resulted in component warnings and a new design simulation would be necessary.

8.4.3 Power consumption and generation

One of the major advantages with energy storage technologies is their ability to store energy and stabilize the electrical grid. The available electricity for storage and the need of stored electricity might vary through operation.

Figure 8.12a shows the round-trip efficiency for different compressor power consumptions. The compressor power consumption was changed from 50 to 70 MW. The figure shows that the round-trip efficiency increases for lower compressor power input. At 50 MW is the round-trip efficiency 56.3 %, almost one percentage point higher than for design. At 70 MW have the round-trip efficiency fallen down to 53.8 %. An increase above 70 MW and a decrease lower than 50 MW both resulted in warnings saying the compressor were operating outside its characteristic lines.

Figure 8.12b shows the round-trip efficiency is increasing with higher electricity generation. At 120 MW power output is the round-trip efficiency 57.1 %. For lower power output is the round-trip efficiency decreasing. For a 100 MW power output is the round-trip efficiency down to 53.7 %. An increase above 110 MW and a decrease lower than 100 MW both resulted in warnings saying the turbine were operating outside its characteristic lines.

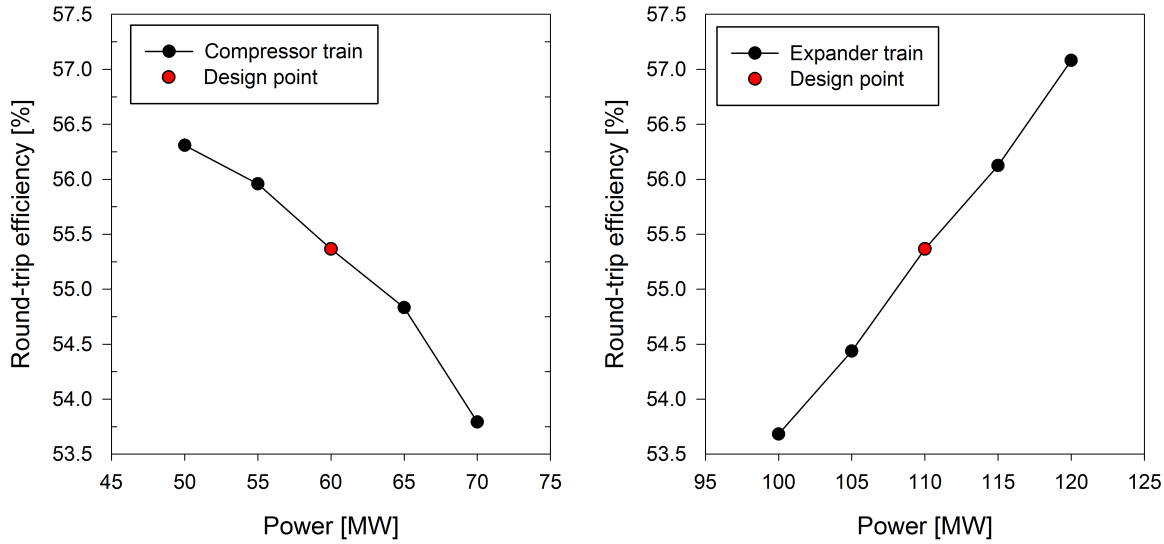

(a) Change in compressor train power consumption

(b) Change in expander train power generation

Figure 8.12: Change of compression and expansion power consumption/generation

8.4.4 Intercoolers outlet temperature

A fouled intercooler cooling surface may have the effect of reducing the effectiveness and reducing the flows cross section area. The reduction in cross sectional area increases the pressure loss through the component. Another possible outcome is an increase in intercooler outlet temperature [49, 71]. As Equation (6.8) and (6.9) shows will a reduction in surface area and an increased outlet temperature reduces the transferred heat in the intercooler. To try model the effects of fouling, were the outlet temperature of the intercoolers changed.

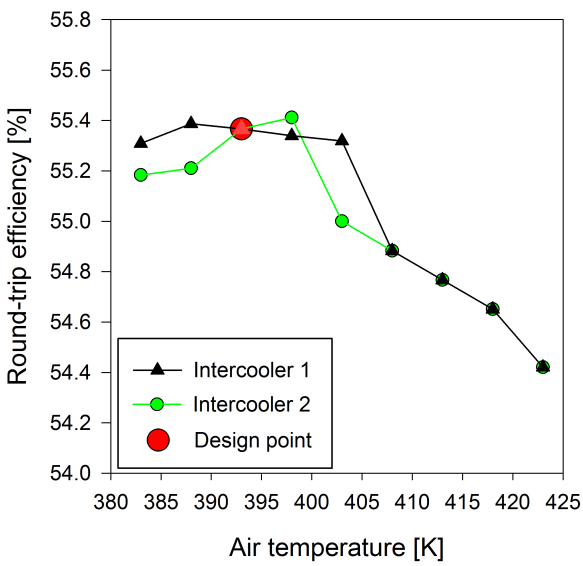

Figure 8.13: Change in intercooler air outlet temperature

The effects of different outlet temperatures of air in the intercoolers can be seen in Figure

8.13. The figure shows that a small change in temperature creates a larger fall in round-trip efficiency for the second intercooler than for the first. The round-trip efficiency is however equal for both intercoolers when the temperature is higher than 135°C. A small increase in round-trip efficiency can also be seen for the first intercooler at 115°C, and for the second intercooler at 125°C. For outlet temperatures lower than 110°C did the mass flow of HTF through the intercoolers become too high, and the simulation failed.

8.4.5 Summary of sensitivity analysis

Figure 8.14 shows all the different variables changed in the sensitivity analysis, plotted for percentage change. The change was calculated from design values. Since some of the parameters have different units which not is on a definitive scale, these figures cannot be directly used for comparison on the effect of change. It does however work as an indication. For the temperatures were Kelvin used as temperature scale as a change in Celsius would be much larger in percent.

Figure 8.14a indicates that a 2 % change in temperature in the hot storage tank has a higher influence on the round-trip efficiency than the cold storage tank and ambient air temperature. A 2 % change in cold tank and ambient air temperature seems to affect the round-trip efficiency the same way and opposite to the hot storage tank temperature. The change caused by the ambient air temperature is however larger.

Figure 8.14b indicates that the round-trip efficiency is more vulnerable to a change in power input than power output. The effects of storage tank specific heat loss, Figure 8.14c, seems to be small.

Figure 8.14d indicates that 2 % change in outlet temperature of air have a larger negative effect on the roundtrip efficiency in intercooler 2 than 1. More than 4 % increase in temperature seems to result in a similar and negative effect on the efficiency for both intercoolers.

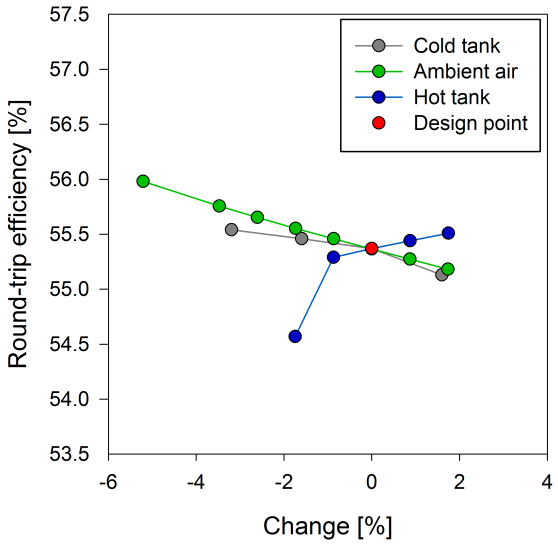

(a) Change of ambient air and storage tank temperatures

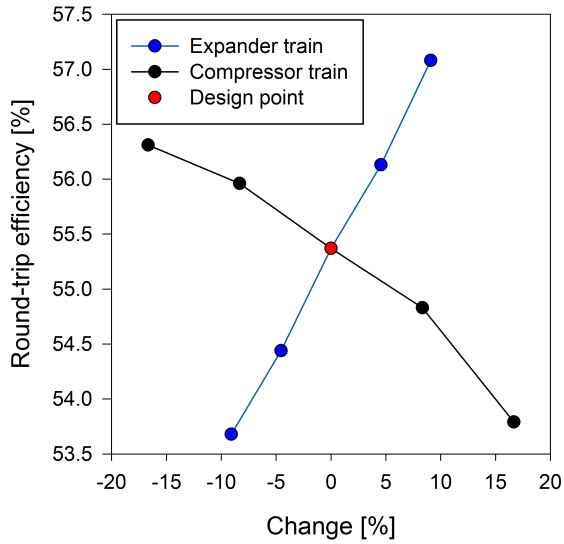

(b) Change in power consumption/generation

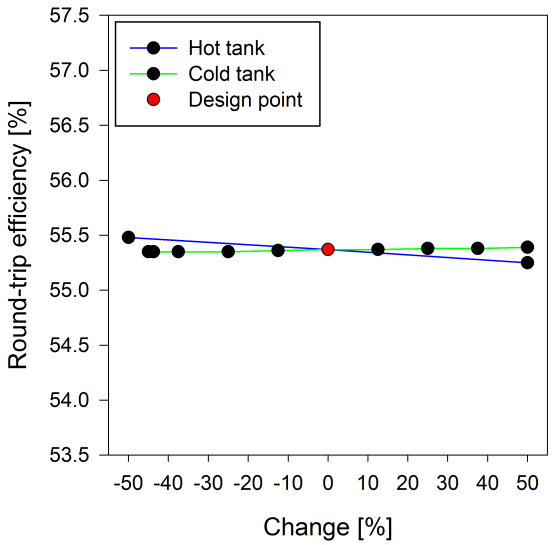

(c) Change of specific heat loss

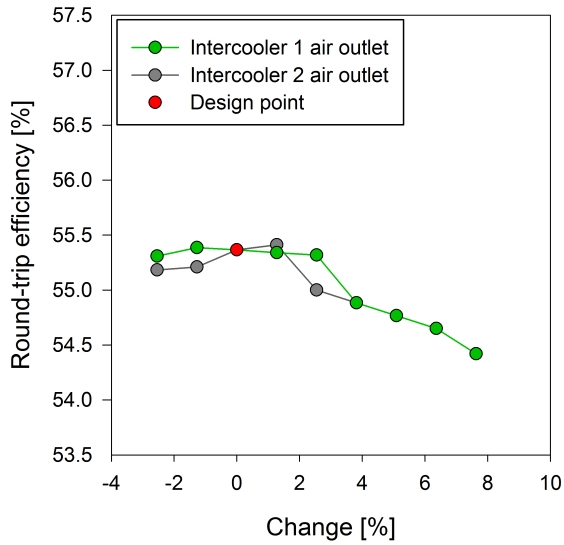

(d) Change in air outlet temperatures of intercoolers

Figure 8.14: Percentage change of all analyzed parameters

Chapter 9

Discussion

9.1 Discussion of the reference models

9.1.1 Round-trip efficiency and other key parameters

The round-trip efficiency and the heat rate of the simulated reference models are close to the known values of the respective power plants. In the case of the Huntorf reference model was the simulated round-trip efficiency 5 % higher and the heat rate 5 % lower than that of the real power plant. For the McIntosh reference model the round-trip efficiency was 5 % lower and heat rate 1 % higher than the known values. Interestingly are these values better than those of the Huntorf power plant, while in the case of the McIntosh is the opposite. The Huntorf power plant was built in 1978 and the McIntosh power plant was built in 1991. One possible explanation for the difference in round-trip efficiency and heat rate might be that the compressor and gas turbine efficiencies used in the simulations were wrong. For the Huntorf model the values might be to high, while to low for the McIntosh model. This seems reasonable, as the power plants are 13 years apart.

As mentioned in Chapter 7 were the time interval for each simulation chosen to be 30 seconds. The value was chosen as a result of a wish to minimize the compilation time, without affecting the results. It could however be a source of uncertainty, even though the effect on round-trip efficiency was negligible. Typical results from initial simulation showed a change in round-trip efficiency of 0.7 % when reducing the time interval from 60 to 30 seconds. A further reduction in time step lead to an even smaller difference in round-trip efficiency.

The energy rate was not found for the Huntorf power plant, but the calculated value was 0.75. For the McIntosh model the value was calculated to 0.77, which is 3.8 % lower than the reference value. The small deviation in energy rate suggests that the relation between energy generated by the expanders and energy consumed by the compressor train is equal. It does however not tell anything about the relation of compression and expansion time.

The compression time per expansion time for the Huntorf power plant were not found in the literature, but an estimate could be made by using the approximate values of operation given in [60] of 8 hours compression and 2 hours expansion. This gives a compression time per expansion ratio of 4. The value calculated for the simulated model was 3.57. For the

McIntosh power plant is the compression time per expansion time 5.6 % higher.

The mass flow of air is in general smaller for the simulated models than those of the real power plants. For the Huntorf model is the compression and expansion mass flow 108 and 417 kg/s respectfully [60]. And for the McIntosh power plant the values are 94 and 154.4 k/s [65]. The maximum value of the simulated compression mass flow is then 2 % higher for the Huntorf model and 6.9 % lower for the McIntosh model compared to power plant. For expansion mass flow are the amount 8.1 % and 7.7 % lower respectfully.

The storage capacity varies a lot for the McIntosh model compared to the known values of the power plant. The large capacity difference is a result of the long compression and expansion time reached in the simulations. One possible reason for the large deviation could be that the storage volume used in the simulation is not correct. The value have however been found in several published papers [65, 25, 28], and it is assumed to be correct. The mass flow through the compressor and expander train, as explained above, is lower. With a lower mass flow through both will the changes in compression time per expansion time remain small, while change in the capacity increases when the storage volume is held constant. It is uncertain what causes the lower mass flow through the compressor and expander train, but one explanation could be that to low values were being used for the efficiencies. In the case of the compressor train, is the intercooler outlet temperature not known, and if the air were to be cooled down more than to 20°C, would the mass flow increase as a result of less work needed by the compressors and a constant power consumption.

Another parameter influencing the mass flows and the storage capacity is the air storage temperature. The air storage temperature were not known for the McIntosh power plant, and assumed to be 35°C. If however the temperature were to increase to 50°C, would the storage capacity decrees, as higher temperature means a lower density. Calculating the available mass difference in storage, Δm, using Equation (7.1) and densities from the available gas tables in EBSILON®Professional, yields a reduction of 4.6 % of storage mass capacity. The assumption of a fixed rotary speed might also be a source of deviation. As the compressor and expander train would be locked to one operating line in the compressor/turbine characteristic. This gives a smaller area of operation and could be a reason for the big change in mass flows through the compressor train.

9.1.2 Carbon emissions

The amount of heat, 1322 MWh, transferred from the exhaust gas in the recuperator equals 32 % of the generated electricity. This is energy that would need to be supplied through combustion of natural gas if no recuperator were fitted. According to Luo et al. [24] does a recuperator reduce the fuel consumption of a diabatic CAES power plant of 22-25 %. The amount of fuel used in the McIntosh model was calculated to be 22.4 % of the Huntorf power plant.

According to Mason and Archer [27] is the CO_2 emission for a diabatic CAES power plant roughly 68 % of the emissions from a conventional gas power plant. For the Huntorf model were the emissions 42 % less and for the McIntosh simulation was it 55 % less. The difference

in CO_2 emission of the two models becomes the same as the difference in fuel consumption, 22.4 %, by combusting methane. The price of CO_2 emissions together with the different round-trip efficiencies result in different operating conditions for the two power plants. The Huntorf model would require a higher difference between consumption and generation electricity price, as it have a higher fuel cost per MWh and a larger cost of emissions.

9.1.3 Waste heat

The major energy loss for the diabatic CAES models, showed in Figure 8.1e and Figure 8.2e, gives rise to the question; is the cooling water outlet temperature assumption, of 25°C, the most efficiency utilization of energy? In the time between 11.00-12.00 in 2010 did Hafslund district heating in Oslo, Norway, produced 586 MWh heat [72]. In comparison does the compression heat for one simulated hour of the Huntorf model equivalent to 45.6 MWh. This equals around 8 % of the district heating demand for that time period in Oslo.

As mentioned in Chapter 2 is the price of power fluctuating throughout the day. The fluctuation of the electricity price creates the foundation for energy storage, making it possible to earn money on price difference by storing energy. If the compression heat were to be used for district heating could the fluctuating nature of CAES operating cause problems for the overall operation of the district heating system. Situations where too much or too little heat is produced could occur, resulting in less profitable operation.

9.1.4 The effect of local off-design

In the assumptions made for the Huntorf and McIntosh models, was the design point of the compressors chosen to be at 56 and 60 bar compressor train back pressure respectfully. There is uncertainty with the validity of this assumption, as it is based on initial simulation results as discussed in Chapter 7. In the resulting plots, of compressor train mass flow, Figure 8.1c and outlet temperatures of air Figure 8.1d, for the Huntorf model a change in gradient can be observed. The gradient change occurs at the same time as the storage pressure, and hence the compressor back pressure is 56 bar. This change might be related to the crossing of the compressors design point. At pressures lower than 56 bar, is the change of air mass flow and temperature lower than for pressures above 56 bar. For the McIntosh model however does the air mass flow and the temperature change increase more rapidly during the first 14 hours of compression. The temperature change and the mass flow also increase faster the last 4 hours of compression.

9.2 Discussion of the ACAES model

9.2.1 Round-trip efficiency

The modelled ACAES system reached a round-trip efficiency of 55.4 %, which is slightly higher than the known value of the McIntosh diabatic CAES power plant of 54%. The calculated round-trip efficiency is a lot lower than those used in the literature of around 70 % [23, 21] and the ALACAES project have an estimated value of 72 % [30]. The values used in the literature are however calculated using ideal assumptions.

The round-trip efficiency reached in the ideal model simulation was 71.2 %. Similar work, done by Hartmann et al. [58], reached a round-trip efficiency of about 70 % using ideal assumptions. Here it was also discussed that a more realistic ACAES efficiency would be 60 % achieved through the use of polytropic efficiencies and account of component losses. It should here be noted that the compressor and turbine efficiencies used by Hartmann et al. [58] in their real model equals the efficiencies used in the 103 % AACAES simulation, which achieved a round-trip efficiency of 58.4 %. The round-trip efficiency of the 97 % simulation only reached a round-trip efficiency of 52.5 %. The large difference in round-trip efficiency of the 97 %, 103 % and the ideal simulation illustrates the importance of choosing realistic efficiencies for the compressor and gas turbines.

9.2.2 Power consumption and generation

The sensitivity indicated a strong dependency of the round-trip efficiency on the compressor and gas turbine power consumption/generation. The increase in round-trip efficiency for lower compressor power consumption seems reasonable. The compressors inlet temperatures and rotational speeds are held constant. As the power consumption is lowered, is the mass flow through the compressor train reduced. In the compressor characteristic, Figure 6.1, one can see that for a constant speed line, a reduction in mass flow will lead to an increase in compressor efficiency as the point of operation is moved closer to the surge line. Increased power consumption would have the opposite effect.

The increase in round-trip efficiency for an increased power generation from the gas turbine also seems reasonable. The gas turbines inlet temperatures and rotational speed are held constant. As the power generation increases, is the mass flow through the gas turbines increasing. In the turbine characteristic, presented in Figure 6.2, one can see that for a constant speed line, an increase in mass flow will lead to an increase in turbine efficiency as the point of operation moves towards the choke. Moving in the opposite direction, lowering the power generation, the efficiency falls.

The sensitivity also indicated that changing the outlet temperature of the intercoolers affected the round-trip efficiency. The change in efficiency might be explained by the increased inlet temperature to the following compressor. As the intercooler outlet temperature increases, will the power consumption of the following compressors increase. The effect will then follow the same pattern as described above. The effect of changing ambient air temper-

atures can also be explained using the same theory.

9.2.3 Thermal efficiency

The thermal efficiency of the TES also influences the round-trip efficiency of the ACAES model. For the ACAES model was the thermal efficiency of the storage tank calculated to 79.3 %. In comparison is the thermal efficiency of the ALACAES project 95 %. The large difference in thermal efficiency presents the question; is the calculated thermal efficiency realistic? According to IEA-ETSAP and IRENA [36] is the thermal efficiency of a sensible TES in the area of 50-90 %. The thermal storage efficiency reached by the model is well inside this range, but it is still a lot lower than the efficiency of the ALACAES project.

A possible explanation to the low thermal efficiency of the hot storage tank could be the low storage temperature. In Chapter 5 was it mentioned that a gas turbine can be seen as a power cycle operating between two thermal reservoirs. The maximum efficiency is then given by the Carnot efficiency (5.7). The efficiency of the gas turbine can then be increased by increasing the temperature difference between the two thermal reservoirs. This can be done for an ACAES power plant by increasing the thermal storage temperature.

Both the ADELE and the ALACAES project are planned for storage temperatures above 600°C. Temperatures up to 600°C is possible in EBSILON®Professional by using a combination of molten salt and thermal oil, see Table 7.6. Storage temperatures higher than 600°C is however not directly possible. A possible way around this limitation is to create an independent component using the Kernel Scripting component available in EBSILON®Professional [52]. The component could be based on a solid sensible storage design, thus removing the constrained given by the thermal fluids.

Another potential reason for the lower thermal efficiency could be the large amount of HTF left in the storage tank at the end of the simulation. A total of 520.9 tonne of HTF was left in the hot tank with a temperature of 290°C. This amount of hot HTF represents a large amount of the stored compression heat, and should ideally be used. For simulations of several cycles in a row, the hot storage tank mass of HTF would accumulate. This is problematic as the result would be less and less available HTF in the cold storage tank. Eventually would there be no available HTF in the cold storage tank at beginning of compression. A possible solution would be to cool down and transfer the HTF from the hot tank to the cold. This is however not energy efficient, as the mass represents a large amount of compression heat. Another alternative could be to utilize the compression heat in a district heating system or other industry using heat at around 300°C.

There could be several reasons for the unused heat. One reason could be the uneven number of heat exchangers in the compressor and expander train. The outlet temperatures of the gas turbines are however higher than the air storage temperature at all times. Another heat exchanger and gas turbine could be added to the expander train. This could possibly result in more HTF being used from the hot storage, and thus give a higher thermal efficiency. The increased air temperature would also lead to an increased round-trip efficiency of the model.

The gas turbines outlet temperatures, shown in Figure 8.7a, are larger than the cold HTF storage temperature at all times. Adding another heat exchanger and a gas turbine could increase the usage of hot HTF. It would also increase the cold tank temperature. As shown in Figure 8.5b is the temperature of the HTF, entering the cold tank during the expansion phase, increasing the tank temperature by almost 33°C. A potential effect of an extra heat exchanger could be an increase in gas turbine outlet temperature, which again increases the HTF temperature into the cold tank.

Interestingly was the resulting hot tank thermal efficiency of the ideal ACAES configuration 78.8 %, thus yielding a small reduction from the design case. The small difference between the simulation could indicate that the thermal efficiency of the tank have a small effect on the round-trip efficiency. This could be explained by the small heat loss in the design model hot storage tank, resulting in small temperature differences between design and ideal model gas turbine inlet temperature.

As the hot tank thermal efficiency varies little, for both ideal and design model, another possible explanation to the low efficiency presents itself. The temperature difference above the heat exchangers, results in an imperfect heat transfer between the hot air and cold HTF, and from hot HTF to cold air. The 10°C temperature differences, over each heat exchanger in the compressor train, means more HTF is needed to cool down the air to its required temperature. In the expander train the effect would be opposite, meaning less HTF is needed. The end result could then be HTF left in the hot tank after a completed cycle. Another possible improvement might be achieved by increasing the hot tank temperature. This would make the temperature difference smaller relative to the storage temperature, thus make the energy lost by the temperature difference relatively smaller.

9.2.4 Storage tanks assumptions

The effect of a higher cold tank initial temperature where investigated in the sensitivity analysis. It was there found a small effect on the round-trip efficiency. An upper HTF temperature limit of 45°C was found on the aftercooler inlet. This was enforced by the fixed air storage inlet temperature. It is also the minimum temperature difference allowed by EBSILON®Professional. The assumption of a constant air storage inlet temperature thus seems to limit the model. An alternative model assumption, that could be considered, is a changing air storage temperature. This would however induce a change in the models fundamental assumptions. A polytropic exponent of 1 would no longer be valid, and the calculation of storage pressure, which sets the compressor train back pressure, would have to be changed.

An important question when it comes to the storage tanks is; are the specific heat loss coefficients, chosen for the thermal storage tanks, realistic? The specific heat loss coefficient for the cold and hot HTF storage tanks were not found in the literature. They were instead selected based on initial simulations and the resulting temperature variations inside the thermal tanks. As mentioned in Chapter 7 was the cold tank specific heat loss coefficient chosen to 20 kW/kgK. The results from the sensitivity analysis suggest that changing the specific loss coefficient, and thereby the thermal loss of the tank, will lead to small changes in

round-trip efficiency. The effect of multiple cycles of compression, storage and expansion is not considered in this case. If the cold tank temperature were to rise further, is it possible that the selected heat loss coefficient will not lead to a sufficient temperature loss. This could again lead to a higher cold tank temperature and the effects discussed above.

From the sensitivity analysis, it was found that an increase in ambient air temperature increases the need of HTF through the intercoolers. At temperatures higher than 20°C the cold tank would empty before the air storage was filled. The script would still compile and produce wrong results. A possible solution would have to choose the chosen mass limits of the cold and hot storage tanks higher. Then they would not have emptied as fast, and simulations could have been made at higher ambient temperatures.

The results from the sensitivity analysis suggest that the round-trip efficiency is more dependent on the specific heat loss coefficient in the hot tank than for the cold. This result fit well with the dependency on hot storage temperature, as previously discussed. A larger specific heat loss would lead to a larger heat loss, which in turn would lower the hot storage temperature.

The thermal losses occurring in the hot and cold storage tanks were 6.3 and 7.9 MWh respectfully. These values are decided by the specific heat loss coefficient and the ambient storage temperatures. The ambient storage temperatures were chosen equal to the ambient air temperature. For the coldest temperature used in the sensitivity analysis, the cold tank temperature was as low as 8.5°C. This is close to the lower temperature limit of the HTF. A specific heat loss coefficient higher than 20°C would reduce the storage temperature further and increase the risk of cold storage temperatures lower than what is allowed.

9.2.5 Other key values

The hours of compression per hours of expansion was calculated to 3.28. The Energy ratio for an ACAES power plant is as mentioned in Chapter 3 be the inverse of the round-trip efficiency. This results in an energy ratio of 1.8. An energy ratio larger than 1 means as previously stated that more electric energy is used for compressing the air than what is generated during the expansion phase. The ACAES model does however not get any extra energy added by fuel.

The compressor power consumption for the ACAES model were chosen equal to the known value of the Huntorf power plant, while the generated power were chosen equal to that of the McIntosh power plant. The resulting behaviour of the ACAES model is similar to that of the Huntorf model, with compression time of about 7.8 hours and expansion time of about 2.3 hours. However, the resulting capacity is 258.6 MWh which represents 41 % of the Huntorf model capacity (633.16 MWh). A potential explanation to the large difference may be the lack of extra heat added by fuel in the ACAES model. This limits the gas turbines to operate at the temperature offered by the thermal storage. As previously mentioned is the maximum efficiency of a gas turbine limited by the Carnot efficiency. For the ACAES model is the Carnot efficiency approximately 50 % for both gas turbines. In comparison is the Carnot efficiency 74 % (HP turbine) and 65 % (LP turbine) for the Huntorf model.

The round-trip efficiency achieved for the ACAES model was higher compared to the diabatic CAES reference models. The ACAES model does not use any fuel to increase the turbine inlet temperature, this means the ACAES system have no CO_2 emissions during operation. With no fuel consumption the operational cost becomes lower, as no money is spent on fuel and CO_2 allowances/taxes. With a lower cost of operation and a higher round-trip efficiency, the ACAES model would be able to operate over greater variations in electricity price than the two diabatic CAES designs.

9.3 Summary of discussions

Both of the reference models achieved a round-trip efficiency close to known value of their respective power plant. The major cause of deviation is believed to be the chosen compressor and turbine efficiencies. The simulations with different efficiencies of the ACAES model also showed the importance of choosing right values of the compressor and turbine efficiency. The reference models also achieved heat rates and energy rates close to what was known for the real power plants, and are therefore assumed to be good references for the ACAES model.

The round-trip efficiency reached by the ACAES model, was higher than for the diabatic CAES reference models. The ACAES model does however not use any fuel, thus have no carbon emission and lower operating costs. When modeled ideally the round-trip efficiency became as high as values known from literature.

The compressor train power consumption and the expander train power generation have a strong impact on the models round-trip efficiency. Ambient temperature and intercooler outlet temperature also indicated notable effects on the round-trip efficiency. An increased thermal storage temperature would increase the turbine inlet temperature, thus increase the round-trip efficiency of the ACAES model.

The ACAES model achieved a lower hot thermal storage thermal efficiency than what is expected from planned ACAES power plants. The ideal ACAES configuration also showed little change in thermal efficiency compared to design. The amount of heat left, after one simulated cycle, is a major weakness of the ACAES model. The result is a lower thermal efficiency and possibly a lower round-trip efficiency. The amount of HTF in the hot tank will, for simulations over longer periods of time, accumulate until the tank is filled. The model can then no longer operate. Possible solutions could be to remove the HTF or reuse it for other applications. Possible usage could be district heating or industry that utilizes heat at around 300°C.

Chapter 10

Conclusions & further work

The main objective of this work was; to build and simulate a process model of adiabatic compressed air energy (ACAES) design and to calculate and analyse its round-trip efficiency. As no ACAES power plant exists of today, the models design was based upon the two existing diabatic compressed air energy storage (DCAES) power plants, Huntorf and McIntosh. These power plants were also modelled and used as reference for the ACAES model. The process models were built and simulated using EBSILON®Professional.

The results show that adiabatic compressed air energy storage, with a thermal storage temperature of 300°C and realistic component assumption, can achieve a round-trip efficiency of 55.4 %. The round-trip efficiency, using ideal assumptions for all components, can be as high as 71.2 %. The Huntorf reference model reached a round-trip efficiency of about 44 %, while the McIntosh reference model reached a round-trip efficiency of about 51 %. Both values are close to the known values of their respective power plants.

The simulation results suggest that several component parameters have a strong impact on the calculated round-trip efficiency. The choice of compressor and turbine nominal efficiencies had the strongest impact. With an increase of 3 %, the round-trip efficiency of the ACAES model changed from about 55.4 to 58.4 %. For an equivalent decrease the round-trip efficiency fell to about 52.5 %. Results from the sensitivity suggested that changing power consumption and generation away from design had a strong impact on the round-trip efficiency. The ambient temperature and intercooler outlet temperature, as well as thermal storage temperature, made a considerable impact on the resulting efficiency.

Therminol VP1 was used as both heat transfer fluid and storage medium stored at 300°C. The thermal efficiency of the thermal storage was found to be 79.3 %, within the range known from the literature (50-90 %). A large amount of heat transfer fluid was found to be left in the hot storage tank after one simulation, and a usage of the left over heat should be considered. Ideal assumptions were found to have little effect on the thermal efficiency of the storage. The author believes that a higher thermal storage temperature will increase the round-trip and thermal storage efficiency.

The calculated round-trip efficiency of the ACAES model is 16 percentage points lower than for the ideal configuration. It is however believed to be a good result, as it show that the round-trip efficiency of an ACAES system can be as high as that of a conventional DCAES sys-

tem. For a ACAES power plant there is no fuel consumption and accordingly no greenhouse gas emissions. As no fuel is needed, is there no extra cost of fuel or emission during operation. With an equal round-trip efficiency, and lower operational cost, the ACAES system can compete with conventional DCAES. It is therefore believed that the simulated ACAES model shows that ACAES is a viable option for energy storage, in a future intermittent electrical system.

There are several areas of interest for a further study of the model. The *price of electricity* could be added into the model as a criterion of operation. This would allow for analysis of power plant operation over longer periods of time, and possibly give insight to the long term dynamic of the system. *Ambient temperature data* could also be implemented in the model, as the ambient air temperature affects the round-trip efficiency of the model.

As previously mentioned is the amount of heat transfer fluid, left in the hot tank after a simulated cycle, one of the models biggest weaknesses. This mass should either be minimized or utilized in some way. A possible solution, as mentioned in the discussen, could be integration of the ACAES power plant with a *district heating system* or industry that utilizes heat at temperatures of 300°C.

Integration of the ACAES model with other renewable energy technologies could be interesting. The timeSeries module in EBSILON®Professional was originally designed for simulation of *solar thermal power plants*. All the available heat transfer fluids in EBSILON®Professional are intended for solar power plants. Several possibilities then can be imagined. Solar heat could be used directly to increase the storage temperature of the ACAES plant. Another possibility could be shared heat storage, and the interaction between the two power plants could be studied. A shared thermal storage could perhaps solve the problem of left over mass in the thermal storage.

Performing an *exergy destruction analysis* could possibly reveal which components that are the weak links in the model. This information could be valuable both for selecting the right assumptions, as well as considering new designs. *Different ACAES design* simulations in EBSILON®Professional is limited by the heat transfer fluids available, see Table 7.6. A possible design, using two thermal storages, could store heat at temperatures of around 600°C and 300 °C.

The ACAES model expands air for around 2 hours. As the expansion time is so small, could effects of *start-up and shut-down* have an influence on the round-trip efficiency. This should be implemented if further work on the model is decided. There was also some uncertainty to the *heat loss* of the heat storage. A further study is therefore desired, in order to model the losses accurately.

For both the reference models, the compressor design point were chosen to fit the available characteristics in EBSILON®Professional, and not chosen for the highest possible pressure ratio. It is possible to create and implement own *compressor and turbine characteristics* to the model. If possible, implementing a *variable speed drive* could also make the model more sturdy, as it would increase the compressors operation area.

Bibliography

[1] OECD and IEA. Key world energy statistics. Report, International Energy Agency, 2014. URL http://www.iea.org/publications/freepublications/publication/KeyWorld2014.pdf. Accessed October 2014.

[2] Intergovernmental Panel on Climate Change working group 1. Climate change 2013: The physical science basis. Report, ipcc, 2013. URL http://www.climatechange2013.org/report/. Accessed November 2014.

[3] International Energy Agency. *Resources to Reserves*. IEA Publications, 2013. ISBN 978-92-64-08354-7. URL http://www.oecdilibrary.org/docserver/download/6112081e.pdf?expires=1416508233&id=id&accname=ocid42012887&checksum=A6A3724BA9BADEFE7A2406F322B4423D. Accessed November 2014.

[4] International Energy Agency, Organisation for Economic Co-operation, and Development. *World Energy Outlook 2012*. WORLD ENERGY OUTLOOK. OECD/IEA, 2012. ISBN 9789264180840. URL http://books.google.no/books?id=1PHpjwEACAAJ.

[5] *Analysis of options beyond 20% GHG emission reductions: Member State results*, 2012. URL http://ec.europa.eu/clima/policies/package/docs/swd_2012_5_en.pdf. Accessed November 2014.

[6] General Secretariat of the European Council, editor. *EUCO 169/14*, October 2014. URL http://www.consilium.europa.eu/uedocs/cms_data/docs/pressdata/en/ec/145397.pdf. Conclusion of European Council 23 and 24 October 2014. Accessed October 2014.

[7] European Commission. Eurostat, 2014. URL http://epp.eurostat.ec.europa.eu/portal/page/portal/eurostat/home/.

[8] European Commission. European commission, climate action, 2015. URL http://ec.europa.eu/clima/.

[9] European Energy Exchange. Global energy exchange, 2015. URL https://www.eex.com/en/market-data/emission-allowances/auction-market/european-emission-allowances-auction#!/2015/05/05.

[10] European Commission. *European SmarGrids Technology Platform*. Directorate-General for Research Sustainable Energy Systems, 2006. ISBN 92-79-01414-5. URL http://ec.europa.eu/research/energy/pdf/smartgrids_en.pdf. Accessed October 2014.

[11] Electricity prices in Germany for 2012 to 2014. from Professor Magnus Korpås at SINTEF.

[12] U.S. Energy Information Administration. International energy statistics, 2014. URL http://www.eia.gov/countries/data.cfm.

[13] Directorate-General for Energy, editor. *DG ENER Working Paper - The future role and challenges of Energy Storage*. URL http://ec.europa.eu/energy/infrastructure/doc/energy-storage/2013/energy_storage.pdf. Accessed October 2014.

[14] DNV GL ENERGY, Imperial College, and NERA Economic Consulting. Integration of renewable energy in europe. Report 9011-700, DNV GL - ENERGY, 2014. URL http://ec.europa.eu/energy/renewables/doc/201406_report_renewables_integration_europe.pdf. Accessed October 2014.

[15] D. Pudjianto, C. Ramsay, and G. Strbac. Virtual power plant and system integration of distributed energy resources. *Renewable Power Generation, IET*, 1(1):10–16, March 2007. ISSN 1752-1416. doi: 10.1049/iet-rpg:20060023.

[16] EEX. *At the Centre of European Energy Trading*. European Energy Exchange AG, 2014. URL http://www.eex.com/blob/68250/27b48c17c6925d18d84f5607d9a51d30/e-eex-unternehmen-februar-2014-pdf-data.pdf. Accessed October 2014.

[17] *Factors for the Success of the Energy Turnaround: Market and Europe*. European Energy Exchange AG, 2013. URL http://www.eex.com/blob/69014/15f26cca8bc6c2825b982f4b9c349209/20130618-eex-energy-policy-cornerstones-en-pdf-data.pdf.

[18] A project implemented by Consortium MVV decon/ENEA/RTE I/Terna/Sonelgaz. Paving the way for the mediterranean solar plan - state-of-play of large storage technologies: design and application consideration. Report 248-486, ENIP, 2010. URL http://www.enpi-info.eu/library/sites/default/files/attachments/Inception-Report.pdf. Accessed October 2014.

[19] I. Gyuk and S. Eckroad. Epri-doe handbook of energy storage for transmission and distribution applications. Report, U.S. Department of Energy, 2003. URL http://www.sandia.gov/ess/publications/ESHB%201001834%20reduced%20size.pdf. Accessed April 2015.

[20] Björn Sandén. Systems perspectives on renewable power, 2014, Accessed June 2015. URL http://www.chalmers.se/en/areas-of-advance/energy/Documents/Systems%20Perspectives%20on%20Biorefineries/Systems_Perspectives_on_Renewable_Power_2014_v1.1.pdf.

[21] RWE Power AG. Adele - adiabatic compressed-air energy storage for electricity supply. Report, RWE Power AG, 2010. URL http://www.rwe.com/web/cms/mediablob/en/391748/data/235554/1/rwe-power-ag/company/Brochure-ADELE.pdf. Accessed October 2014.

[22] Abraham Dayan Roy Kushnir, Amos Ullmann. Steady periodic gas flow around a well of a caes plant. 73(1):1–20, 2008. URL http://ejournals.ebsco.com/direct.asp?ArticleID=4E8AA99C430CB17C7043. Accessed October 2014.

[23] Lukas Grond, Paula Schulze, and Johan Holstein. Systems analyses power to gas: A technology review. Report, DVN KEMA, 2013. URL http://www.dnv.com/resources/position_papers/systems_analyses_power_to_gas_a_technology_review.asp. Accessed June 2015.

[24] Xing Luo, Jihong Wang, Mark Dooner, and Jonathan Clarke. Overview of current development in electrical energy storage technologies and the application potential in power system operation. *Applied Energy*, (0):–, 2014. ISSN 0306-2619. doi: http://dx.doi.org/10.1016/j.apenergy.2014.09.081. URL http://www.sciencedirect.com/science/article/pii/S0306261914010290. Accessed October 2014.

[25] International Energy Agency. Energy storage technology roadmap - technology annex. Report, IEA, 2014. URL http://www.iea.org/media/freepublications/technologyroadmaps/AnnexA_TechnologyAnnexforweb.pdf. Accessed October 2014.

[26] International Energy Agency. Technology roadmap - energy storage. Report, IEA, 2014. URL http://www.iea.org/publications/freepublications/publication/TechnologyRoadmapEnergystorage.pdf. Accessed October 2014.

[27] James E. Mason and Cristina L. Archer. Baseload electricity from wind via compressed air energy storage (caes). *Renewable and Sustainable Energy Reviews*, 16(2):1099 – 1109, 2012. ISSN 1364-0321. doi: http://dx.doi.org/10.1016/j.rser.2011.11.009. URL http://www.sciencedirect.com/science/article/pii/S1364032111005454.

[28] Xing Luo & Jihong Wang. Owerview of current development on compressed air energy storage. Report, The University of Warwick, 2013. URL http://www.cedren.no/Portals/Cedren/Overview%20of%20Current%20Development%20on%20Compressed%20Air%20Energy%20Storage_EERA%20report%202013.pdf. Accessed April 2015.

[29] Gregor-Sönke Schneider and Sabine Donadei. Long-term energy storage with compressed air storages. *ees international*, 2014. URL http://ees-magazine.com/long-term-energy-storage-with-compressed-air-storages/. Accessed April 2015.

[30] ALACAES an airlight energy company. Alaceas, 2015. URL http://www.alaceas.com.

[31] LightSail Energy. Lightsail, 2015. URL http://www.lightsail.com.

[32] Electric Power Research Institue. Caes demonstration newsletter. *EPRI Newsletter*, 2015. URL http://www.epri.com/abstracts/Pages/ProductAbstract.aspx?ProductId=000000003002003359. Accessed April 2015.

[33] M. Fatih Demirbas. Thermal energy storage and phase change materials: An overview. *Energy Sources, Part B: Economics, Planning, and Policy*, 1(1):85–95, 2006. doi: 10.1080/009083190881481. URL http://dx.doi.org/10.1080/009083190881481.

[34] S. Kalaiselvam and R. Parameshwaran. *Thermal Energy Storage Technologies for Sustainability*. Academic Press.

[35] Kamil Kaygusuz. The viability of thermal energy storage. *Energy Sources*, 21(8):745–755, 1999. doi: 10.1080/00908319950014489. URL http://dx.doi.org/10.1080/00908319950014489.

[36] IEA-ETSAP and IRENA. Thermal energy storage - technology brief. Report, IEA-ETSAP and IRENA, 2013. URL https://www.irena.org/DocumentDownloads/Publications/IRENA-ETSAP%20Tech%20Brief%20E17%20Thermal%20Energy%20Storage.pdf. Accessed June 2015.

[37] Antoni Gil, Marc Medrano, Ingrid Martorell, Ana Lázaro, Pablo Dolado, Belén Zalba, and Luisa F. Cabeza. State of the art on high temperature thermal energy storage for power generation. part 1—concepts, materials and modellization. *Renewable and Sustainable Energy Reviews*, 14(1):31 – 55, 2010. ISSN 1364-0321. doi: http://dx.doi.org/10.1016/j.rser.2009.07.035. URL http://www.sciencedirect.com/science/article/pii/S1364032109001774.

[38] SBC Energy Institute. *Electricity Storage*, 2013, Accessed October 2014. URL http://www.sbc.slb.com/SBCInstitute/Publications/~/media/Files/SBC%20Energy%20Institute/SBC%20Energy%20Institute_Electricity_Storage%20Factbook_vf.ashx.

[39] Cutler J. Cleveland. *Encyclopedia of Energy, Volumes 1 - 6*. Elsevier, 2004. ISBN 978-0-12-176480-7. URL http://app.knovel.com/hotlink/toc/id:kpEEV00001/encyclopedia-energy-volumes/encyclopedia-energy-volumes.

[40] Pengwei Du and Ning Lu. *Energy Storage for Smart Grids: Planning and Operation for Renewable and Variable Energy Resources (VERs)*. Elsevier, 1 edition, 2014. ISBN 978-0-2-410491-4. URL http://books.google.no/books?id=xiGOAwAAQBAJ&printsec=frontcover&hl=no&source=gbs_ge_summary_r&cad=0#v=onepage&q&f=false.

[41] A.G. Ter-Gazarian. *Energy Storage for Power Systems (2nd Edition)*. Institution of Engineering and Technology, 2011. ISBN 978-1-84919-219-4. URL http://app.knovel.com/hotlink/toc/id:kpESPSE001/energy-storage-power/energy-storage-power. Accessed October 2014.

[42] J. K. Kaldellis. *Stand-Alone and Hybrid Wind Energy Systems - Technology, Energy Storage and Applications*. Woodhead Publishing, 2010. ISBN 978-1-84569-527-9. URL `http://app.knovel.com/hotlink/toc/id:kpSAHWESTH/stand-alone-hybrid-wind/stand-alone-hybrid-wind`. Accessed October 2014.

[43] Frano Barbir. *PEM Fuel Cells - Theory and Practice*. Elsevier, 2013. ISBN 978-0-12-387710-9. URL `http://app.knovel.com/hotlink/toc/id:kpPEMFCTP3/pem-fuel-cells-theory/pem-fuel-cells-theory`.

[44] Michael J. Moran and Howard N. Shapiro. *Fundamentals of Engineering Thermodynamics*. John Wiley & Sons, Inc, sixth edition, 2010. ISBN 978-0-470-54019-0.

[45] Herb I.H. Saravanamuttoo, Gordon F.C. Rogers, Henry Cohen, and Paul V. Straznicky. *Gas Turbine Theory*. Pearson, sixth edition, 2009. ISBN 978-0-13-222437-6.

[46] Lars Erik Bakken. *Thermodynamics, Compression and Expansion Processes*. 2014.

[47] Wenyi Liu, Linzhi Liu, Luyao Zhou, Jian Huang, Yuwen Zhang, Gang Xu, and Yongping Yang. Analysis and optimization of a compressed air energy storage—combined cycle system. *Entropy*, 16(6):3103–3120, 2014. ISSN 1099-4300. doi: 10.3390/e16063103. URL `http://www.mdpi.com/1099-4300/16/6/3103`.

[48] Frank P. Incropera, David P. Dewitt, Theodore L. Bergman, and Adrienne S. Lavine. *Principles of Heat and Mass Transfer*. John Wiley & Sons, Inc, seventh edition, 2013. ISBN 978-0-470-64615-1. International Student Version.

[49] Erling Næss and Anders Austegard. *Kompendium i TEP-07, Industriell Varmeteknikk, Varmevekslere*. Department of Energy and Process Engineering - NTNU.

[50] Garr M. Jones. *Pumping Station Design (3rd Edition)*. Elsevier, 2006. ISBN 978-0-7506-7544-4. URL `http://app.knovel.com/hotlink/pdf/id:kt003YPEJ1/pumping-station-design-2/types-of-pumps-2`.

[51] Frank M. White. *Fluid Mechanics*. McGraw-Hill, seventh edition, 2011. ISBN 978-0-07-352934-9. International Student Version.

[52] EBSILON®Professional. *version 10.06 (patch 6)*. STEAG Energy Services Gmbh, Wetzbach 35, Zwingenberg, Germany, 2013.

[53] Dieter Hebel, Hans Hoffeins, Norbert Romeyke, and Fritz Sütterlin. Die inbetriebnahme der ersten luftspeicher-gasturbinengruppe. Report, Brown Boveri & Cie Aktiengesellschaft, 1981. URL `http://www.eon.com/content/dam/eon-content-pool/eon/company-asset-finder/asset-profiles/shared-ekk/BBC_Inbetriebnahme_Huntorf_dt.pdf`. Publication No. CH GK 1139 81 D, Accessed April 2015.

[54] Rahul Anantharaman, Olav Bolland, Nick Booth, Eva van Dorst, Clas Ekstrom Vattenfall, Eva Sanchez Fernandes, Flavio Franco, Ennio Macchi, Giampaolo Manzolini, Djordje

Nikolic, Allen Pfeffer, Mark Prins, Sina Rezvani, and Laurence Robinson. *European best practice guidelines for assessment of CO2 capture technologies.* Polit. di Milano, Shell, E.On, Univ. of Ulster, Alstom, TNO, NTNU, 2011. CAESAR, Project number 213206.

[55] Olav Bolland. *Thermal power generation.* Department of Energy and Process Engineering - NTNU, 2009. URL `http://folk.ntnu.no/lano/compendium_power_2009.pdf`. Accessed February 2015.

[56] G. Grazzini and A. Milazzo. A thermodynamic analysis of multistage adiabatic caes. *Proceedings of the IEEE*, 100(2):461–472, Feb 2012. ISSN 0018-9219. doi: 10.1109/JPROC.2011.2163049.

[57] A. R. Howell and R. P. Bonham. Overall and stage characteristics of axial-flow compressors. *Proceedings of the Institution of Mechanical Engineers*, 163(1):235–248, 1950. URL `http://pme.sagepub.com/content/163/1/235.abstract`.

[58] Niklas Hartmann, O. Vöhringer, C. Kruck, and L. Eltrop. Simulation and analysis of different adiabatic compressed air energy storage plant configurations. *Applied Energy*, 93(0):541 – 548, 2012. ISSN 0306-2619. doi: http://dx.doi.org/10.1016/j.apenergy.2011.12.007. URL `http://www.sciencedirect.com/science/article/pii/S0306261911008014`. (1) Green Energy; (2)Special Section from papers presented at the 2nd International Enery 2030 Conf.

[59] Carl R. Branan. 6 - compressors. In Carl R. Branan, editor, *Rules of Thumb for Chemical Engineers (Fourth Edition)*, pages 124 – 133. Gulf Professional Publishing, Burlington, fourth edition edition, 2005. ISBN 978-0-7506-7856-8. doi: http://dx.doi.org/10.1016/B978-075067856-8/50006-2. URL `http://www.sciencedirect.com/science/article/pii/B9780750678568500062`.

[60] Hans Hoffeins. Huntorf air storage gas turbine power plant. Report, Brown Boveri & Cie Aktiengesellschaf, 1994. URL `http://www.eon.com/content/dam/eon-content-pool/eon/company-asset-finder/asset-profiles/shared-ekk/BBC_Huntorf_engl.pdf`. Publication No. D GK 90 202 E, Accessed April 2015.

[61] BINE Informationsdienst. *Compressed air energy storage plants*, 2007. URL `http://www.bine.info/fileadmin/content/Publikationen/Englische_Infos/projekt_0507_engl_internetx.pdf`. Project number: 0329558 and 0327628, Accessed April 2015.

[62] Mandhapati Raju and Siddhartha Kumar Khaitan. Modeling and simulation of compressed air storage in caverns: A case study of the huntorf plant. *Applied Energy*, 89(1):474 – 481, 2012. ISSN 0306-2619. doi: http://dx.doi.org/10.1016/j.apenergy.2011.08.019. URL `http://www.sciencedirect.com/science/article/pii/S0306261911005150`. Special issue on Thermal Energy Management in the Process Industries.

[63] Lasse Nielsen and Reinhard Leithner. Dynamic simulation of an innovative compressed air energy storage plant - detailed modelling of the storage cavern. *WSEAS TRANSACTIONS on POWER SYSTEMS*, 4(8):253 – 263, 2008. ISSN 1790-5060. URL `http://www.wseas.us/e-library/transactions/power/2009/29-843.pdf`.

[64] *Advanced Adiabatic Compressed Air Energy Storage for he Integration of Wind Energy*, November 2004. URL `http://www.ewi.uni-koeln.de/fileadmin/user_upload/Publikationen/Zeitschriften/2004/04_11_23_EWEC_Paper_Final.pdf`. European Wind Energy Conference.

[65] Robert B. Schainker and Abhi Rao. Compressed air storage scoping study for california. Report, California Energy Commission, PIER Energy-Related Environmental Research Program, 2008. CEC-500-2008-069.

[66] Michael Nakhamkin, Madhukar Chiruvolu, and Chan Daniel. *Available Compressed Air Energy Storage (CAES) Plant Concepts*. Energy Storage and Power Corporation (ESPC), Towngas International Company LTD, 2007. URL `http://www.espcinc.com/library/PowerGen_2007_paper.pdf`.

[67] Samir Succar and Robert H. Williams. Compressed air energy storage: Theory, resources and applications for wind power. Report, Princeton Environmental Institute, 2008.

[68] Solutia. *Therminol®VP1*. Solutia, St. Louis, USA, 1999. URL `http://www.sintelub.com/files/therminol_vp1.pdf`. Technical Bulletin 7239115B.

[69] United States Environmental Protection Agency. Clean energy, natural gas, 2013. URL `http://www.epa.gov/cleanenergy/energy-and-you/affect/natural-gas.html`.

[70] Luisa Manzanares Papayanopoulos, Arturo Keer Rendón, and Emilio Manzanares Papayanopoulos. North american power plant air emissions. Technical report, Commission for Environmental Cooperation, October 2011.

[71] E. M. Talbott. Compressed air systems: a guidebook on energy and cost savings, 1993.

[72] Norsk fjernvarme. Hafslund fjernvarme satte rekord med 586 mwh, 2010. URL `http://www.fjernvarme.no/index.php?pageID=29&openLevel=4&cid=901`.

Appendix A

ACAES model ebsScript code

```
/*
Explanation of Program
#1. Declaration of moduels used and variables
#2. Creating timeSeries document and calculation profile
#3. Setting initial operation states
#4. For-Loop simulating each timeStep
#5. Calculating TimeSeries document
#6. End of Program
*/
/*
************************************************************
**************************#1.****************************
************************************************************
*/
uses @units, @TimeSeries, @Variant;
var
tID, pID, ID1:integer;
subprofilename:string;
dt,i, volume, arraylength:integer;
n:real;
tsMax, tsMin, tsStep, counter:real;
StorageLEVMAX, StorageLEVMIN:real;
StorageLevel,SpecificVolume,StoragePressure:array of real;
vStoragePressure:Variant;
compression, expansion, storage:boolean;
ePressure:ebsvar;
eAir_1, eAir_8 : ebsvar;
eHeatexchanger:array[0..4]of ebsVar;
vHeatexchanger:array[0..4] of Variant;
eController:array[0..6]of ebsVar;
vController:array [0..6] of Variant;
vCompressorPressures:array [0..3] of Variant;

/*
************************************************************
**************************#2.****************************
```

```
*************************************************************
*/
begin
clrscr;
    dt:=30;/*delta time in seconds for each iteration*/
    tsStep:=1*dt/(24*3600); /*Calculate timestep in ebsTime */
    tsMin:=41940.00000;/*StartTime, given in days from year 1900*/
    tsMax:=41941.00000;/*EndTime, given in days from year 1900*/
    counter:=1/2;/*used to calculate twelve hour storage time*/

    volume:=62337.6;/*Volume of the tank*/
    n:=1;/*Polytropic constant air storage tank*/
    arraylength:=ceil(2/tsStep)+1;/*gives the length of the arrays
                    that stores values calculated*/

    /*Needes to be calculated for the given pressure range of
    operation*/
    StorageLEVMIN:=4704000;/*storage levmin*/
    StorageLEVMAX:=6720000;/*storage levmax*/

  /*Creating calculationprifile*/
  inputBox("Enter parent ID number", ID1);/*creates box for
  specifying subprofile for calculation*/
  setParentProfile(ID1);
  setCalcProfile(ID1);

  pID := newsubprofile;/*creat subprofile from calcprofile
  to do calculations*/
  inputBox("Please enter the subprofile name: ", subprofilename);
  println (renameprofile (pID, subprofilename));

  tID := 0;/*table ID of existing TimeSeries table*/

  /*Creating timeSeries document*/
  println (tsSetName(tID, "ShowStorageLevel"));
  println (tsGenerateTimes (tID, tsMin, tsMax, tsStep, true));

/*
*************************************************************
***************************#3.****************************
*************************************************************
*/

  getEbsvar(ePressure,"Storage.PSTO");
  SetLength(StorageLevel,arraylength);
  StorageLevel[0]:=StorageLEVMIN;
  SetLength(SpecificVolume,arraylength);
  SpecificVolume[0]:=volume/StorageLevel[0];
  SetLength(StoragePressure,arraylength);
  StoragePressure[0]:=70;
  ePressure:=StoragePressure[0];
```

```
vStoragePressure:=varfromreal(StoragePressure[0]);

/*Setting Controller.FACT values if on -> 0, if off ->-2*/
getebsvar(eController[0],"Controller_1.FACT");
getebsvar(eController[1],"Controller_2.FACT");
getebsvar(eController[2],"Controller_3.FACT");
getebsvar(eController[3],"Controller_4.FACT");
getebsvar(eController[4],"Controller_5.FACT");
getebsvar(eController[5],"Controller_6.FACT");
getebsvar(eController[6],"Controller_7.FACT");
eController[0]:=0;
eController[1]:=0;
eController[2]:=0;
eController[3]:=0;
eController[4]:=-2;
eController[5]:=-2;
eController[6]:=-2;

/*Setting Heatexchanger .FFU values if on -> 1, if off ->0*/
getebsvar(eHeatexchanger[0],"Heat_Exchanger_1.FFU");
getebsvar(eHeatexchanger[1],"Heat_Exchanger_2.FFU");
getebsvar(eHeatexchanger[2],"Heat_Exchanger_3.FFU");
getebsvar(eHeatexchanger[3],"Heat_Exchanger_4.FFU");
getebsvar(eHeatexchanger[4],"Heat_Exchanger_5.FFU");
eHeatexchanger[0]:=1;
eHeatexchanger[1]:=1;
eHeatexchanger[2]:=1;
eHeatexchanger[3]:=0;
eHeatexchanger[4]:=0;

/*Turns off enthalpy flag on compressors*/
Messwert_1.FFU:=0;
Messwert_2.FFU:=0;
Messwert_3.FFU:=0;
Messwert_4.FFU:=0;

/*Setting compressor outlet pressures*/
Pressure_1.MEASM:=pow(ePressure,1/4);
Pressure_2.MEASM:=Pressure_1.MEASM*Pressure_1.MEASM;
Pressure_3.MEASM:=Pressure_1.MEASM*Pressure_2.MEASM;
Pressure_4.MEASM:=Pressure_1.MEASM*Pressure_3.MEASM;

/*Creating variant variables to wright inn values in
TimeSeries document*/
vController[0]:=Varfromreal(eController[0]);
vController[1]:=Varfromreal(eController[1]);
vController[2]:=Varfromreal(eController[2]);
vController[3]:=Varfromreal(eController[3]);
vController[4]:=Varfromreal(eController[4]);
vController[5]:=Varfromreal(eController[5]);
vController[6]:=Varfromreal(eController[6]);
```

```
  vHeatexchanger[0]:=varfromreal(eHeatexchanger[0]);
  vHeatexchanger[1]:=varfromreal(eHeatexchanger[1]);
  vHeatexchanger[2]:=varfromreal(eHeatexchanger[2]);
  vHeatexchanger[3]:=varfromreal(eHeatexchanger[3]);
  vHeatexchanger[4]:=varfromreal(eHeatexchanger[4]);
  vCompressorPressures[0]:=Varfromreal(Pressure_1.MEASM);
  vCompressorPressures[1]:=Varfromreal(Pressure_2.MEASM);
  vCompressorPressures[2]:=Varfromreal(Pressure_3.MEASM);
  vCompressorPressures[3]:=Varfromreal(Pressure_4.MEASM);

  getebsvar(eAir_1,"Air_1.M");/*Needs to be in ebsvar format to get*/
  getebsvar(eAir_8,"Air_8.M");/*calculated values for each simulation*/

  /*Writing values into TimeSeries document*/
  tsSetCell(tID,i+6,4,vCompressorPressures[0]);
  tsSetCell(tID,i+6,5,vCompressorPressures[1]);
  tsSetCell(tID,i+6,6,vCompressorPressures[2]);
  tsSetCell(tID,i+6,7,vCompressorPressures[3]);
  tsSetCell(tID,i+6,8,vController[0]);
  tsSetCell(tID,i+6,9,vController[1]);
  tsSetCell(tID,i+6,10,vController[2]);
  tsSetCell(tID,i+6,11,vController[3]);
  tsSetCell(tID,i+6,12,vController[4]);
  tsSetCell(tID,i+6,13,vController[5]);
  tsSetCell(tID,i+6,14,vController[6]);
  tsSetCell(tID,i+6,15,vHeatexchanger[0]);
  tsSetCell(tID,i+6,16,vHeatexchanger[1]);
  tsSetCell(tID,i+6,17,vHeatexchanger[2]);
  tsSetCell(tID,i+6,18,vHeatexchanger[3]);
  tsSetCell(tID,i+6,19,vHeatexchanger[4]);
  tsSetCell(tID,i+6,22,vStoragePressure);

  /*Logical values used to decide state of operation*/
  compression:=true;  expansion:=false; storage:=false;

  simulate;

/*
*************************************************************
***************************#4.****************************
*************************************************************
*/
  for i:=0 to arraylength-2 do
  begin

    if compression = true then
    begin
      StorageLevel[i+1]:=StorageLevel[i]+(Air_1.M*dt);
      SpecificVolume[i+1]:=volume/StorageLevel[i+1];
      StoragePressure[i+1]:=StoragePressure[i]*pow(SpecificVolume[i]/SpecificVolume[i
    +1],n);
```

```
      ePressure:=StoragePressure[i+1];

      eController[0]:=0;
      eController[1]:=0;
      eController[2]:=0;
      eController[3]:=0;
      eController[4]:=-2;
      eController[5]:=-2;
      eController[6]:=-2;

      eHeatexchanger[0]:=1;
      eHeatexchanger[1]:=1;
      eHeatexchanger[2]:=1;
      eHeatexchanger[3]:=0;
      eHeatexchanger[4]:=0;

      Pressure_1.MEASM:=pow(ePressure,1/4);
      Pressure_2.MEASM:=Pressure_1.MEASM*Pressure_1.MEASM;
      Pressure_3.MEASM:=Pressure_1.MEASM*Pressure_2.MEASM;
      Pressure_4.MEASM:=Pressure_1.MEASM*Pressure_3.MEASM;

      if StorageLevel[i+1]>=StorageLEVMAX then
      begin
        compression:=false;
        storage:=true;
      end;
    end;

    if storage=true then
    begin
      StorageLevel[i+1]:=StorageLevel[i];
      SpecificVolume[i+1]:=SpecificVolume[i];
      StoragePressure[i+1]:=StoragePressure[i];

      counter:=counter-tsStep;

      ePressure:=StoragePressure[i+1];

      eController[0]:=-2;
      eController[1]:=-2;
      eController[2]:=-2;
      eController[3]:=-2;
      eController[4]:=-2;
      eController[5]:=-2;
      eController[6]:=-2;

      eHeatexchanger[0]:=0;
      eHeatexchanger[1]:=0;
      eHeatexchanger[2]:=0;
      eHeatexchanger[3]:=0;
```

```
      eHeatexchanger[4]:=0;

      Pressure_1.MEASM:=1.013;
      Pressure_2.MEASM:=1.013;
      Pressure_3.MEASM:=1.013;
      Pressure_4.MEASM:=1.013;

      if counter<=0 then
      begin
        storage:=false;
        expansion:=true;
      end;
    end;

    if expansion=true then
    begin
      StorageLevel[i+1]:=StorageLevel[i]-(Air_8.M*dt);
      SpecificVolume[i+1]:=volume/StorageLevel[i+1];
      StoragePressure[i+1]:=StoragePressure[i]*pow(SpecificVolume[i]/SpecificVolume[i
    +1],n);

      ePressure:=StoragePressure[i+1];

      eController[0]:=-2;
      eController[1]:=-2;
      eController[2]:=-2;
      eController[3]:=-2;
      eController[4]:=0;
      eController[5]:=0;
      eController[6]:=0;

      eHeatexchanger[0]:=0;
      eHeatexchanger[1]:=0;
      eHeatexchanger[2]:=0;
      eHeatexchanger[3]:=1;
      eHeatexchanger[4]:=1;


      Pressure_1.MEASM:=1.013;
      Pressure_2.MEASM:=1.013;
      Pressure_3.MEASM:=1.013;
      Pressure_4.MEASM:=1.013;

      if StorageLevel[i+1]<=StorageLEVMIN then
        begin
          storage:=false;
          expansion:=false;
        end;
    end;

    if compression=false and storage=false and expansion=false then
```

```
    begin
      StorageLevel[i+1]:=StorageLevel[i];
      SpecificVolume[i+1]:=SpecificVolume[i];
      StoragePressure[i+1]:=StoragePressure[i];

      ePressure:=StoragePressure[i+1];

      eController[0]:=-2;
      eController[1]:=-2;
      eController[2]:=-2;
      eController[3]:=-2;
      eController[4]:=-2;
      eController[5]:=-2;
      eController[6]:=-2;

      eHeatexchanger[0]:=0;
      eHeatexchanger[1]:=0;
      eHeatexchanger[2]:=0;
      eHeatexchanger[3]:=0;
      eHeatexchanger[4]:=0;

      Pressure_1.MEASM:=1.013;
      Pressure_2.MEASM:=1.013;
      Pressure_3.MEASM:=1.013;
      Pressure_4.MEASM:=1.013;
    end;

    vStoragePressure:=VarFromReal(StoragePressure[i+1]);

    vController[0]:=Varfromreal(eController[0]);
    vController[1]:=Varfromreal(eController[1]);
    vController[2]:=Varfromreal(eController[2]);
    vController[3]:=Varfromreal(eController[3]);
    vController[4]:=Varfromreal(eController[4]);
    vController[5]:=Varfromreal(eController[5]);
    vController[6]:=Varfromreal(eController[6]);

    vHeatexchanger[0]:=varfromreal(eHeatexchanger[0]);
    vHeatexchanger[1]:=varfromreal(eHeatexchanger[1]);
    vHeatexchanger[2]:=varfromreal(eHeatexchanger[2]);
    vHeatexchanger[3]:=varfromreal(eHeatexchanger[3]);
    vHeatexchanger[4]:=varfromreal(eHeatexchanger[4]);

    vCompressorPressures[0]:=Varfromreal(Pressure_1.MEASM);
    vCompressorPressures[1]:=Varfromreal(Pressure_2.MEASM);
    vCompressorPressures[2]:=Varfromreal(Pressure_3.MEASM);
    vCompressorPressures[3]:=Varfromreal(Pressure_4.MEASM);

  tsSetCell(tID,i+7,4,vCompressorPressures[0]);
  tsSetCell(tID,i+7,5,vCompressorPressures[1]);
  tsSetCell(tID,i+7,6,vCompressorPressures[2]);
```

```
  tsSetCell(tID,i+7,7,vCompressorPressures[3]);
  tsSetCell(tID,i+7,8,vController[0]);
  tsSetCell(tID,i+7,9,vController[1]);
  tsSetCell(tID,i+7,10,vController[2]);
  tsSetCell(tID,i+7,11,vController[3]);
  tsSetCell(tID,i+7,12,vController[4]);
  tsSetCell(tID,i+7,13,vController[5]);
  tsSetCell(tID,i+7,14,vController[6]);
  tsSetCell(tID,i+7,15,vHeatexchanger[0]);
  tsSetCell(tID,i+7,16,vHeatexchanger[1]);
  tsSetCell(tID,i+7,17,vHeatexchanger[2]);
  tsSetCell(tID,i+7,18,vHeatexchanger[3]);
  tsSetCell(tID,i+7,19,vHeatexchanger[4]);
  tsSetCell(tID,i+7,22,vStoragePressure);

    simulate;

  end;
/*
*************************************************************
***************************#5.*****************************
*************************************************************
*/

  tsCalculate(tID,0,-1); /*Calculate timeSeries document*/

  /*Make ready for new simulation*/
  ePressure:=StoragePressure[arraylength-1];
  eController[0]:=-2;
  eController[1]:=-2;
  eController[2]:=-2;
  eController[3]:=-2;
  eController[4]:=-2;
  eController[5]:=-2;
  eController[6]:=-2;
  eHeatexchanger[0]:=0;
  eHeatexchanger[1]:=0;
  eHeatexchanger[2]:=0;
  eHeatexchanger[3]:=0;
  eHeatexchanger[4]:=0;
  Pressure_1.MEASM:=1.013;
  Pressure_2.MEASM:=1.013;
  Pressure_3.MEASM:=1.013;
  Pressure_4.MEASM:=1.013;
end;
```